Universität Bremen

Institute for Theoretical Physics

Faculty 01
Physics / Electrical Engineering

Marc Bostelmann

Generation of multipartite entanglement in coupled-cavity arrays as a resource for quantum technologies

Marc Bostelmann

Generation of multipartite entanglement in coupled-cavity arrays as a resource for quantum technologies

A dissertation submitted for the degree PhD (Dr. rer. nat.)
with permission of the Institute for Theoretical Physics
at the University of Bremen.

First examiner and supervisor:
PD Dr. Christopher Gies

Second examiner:
Prof. Dr. Michael Sentef

Submission date:
June 30, 2023

Date of oral examination:
October 11, 2023

The Art of Peace begins with you. — Morihei Ueshiba (1883–1969)

Abstract

Entanglement is an essential part of quantum mechanics and a resource for most quantum technologies. While entangled two-particle Bell states are well established, the generation and classification of entanglement in multipartite systems is much more difficult to achieve. At the same time, multipartite entanglement is the key to unlock the full advantage provided by the exponentially large Hilbert space of quantum systems. This thesis explores possibilities of entanglement generation with a specific focus on applications in quantum technologies. In systems of coupled microcavity arrays, coherent optical pulses are considered to directly drive the quantum system into multipartite entangled target states. The building block of such coupled-cavity arrays consists of a single mode cavity with a two-level emitter, whose interaction is described by the Jaynes–Cummings model. In order to gain insight into the system, a novel representation of its eigenspectrum is presented, which shows the eigenenergies and the composition of the corresponding eigenstates. Based on this, a numerical scheme, which is the central achievement of this thesis, is developed that allows to determine precise excitation parameters to generate entanglement. Finally, this scheme is used to show the generation of multipartite entanglement in the form of W and phased Dicke states with high fidelity.

Acknowledgments

First of all, I am grateful to Christopher Gies for his outstanding doctoral supervision. His dedication and his pleasing manner motivated me and made a pleasant working atmosphere in our research group possible. Speaking of our research group, which we affectionately call the *Quantum Team*, I would like to thank my colleagues for the great time I have had with them during work and beyond. These are Frederik Lohof, whom I am thankful for his valuable input to my work, and Niclas Götting, who had an answer to almost every of our questions concerning computer-related issues. We have had a nice time together sharing an office. Furthermore, there are my colleagues Steffen Wilksen, Nils-Erik Schütte, and Alexander Steinhoff-List, who were an important part of my time as a doctoral student.

I am indebted to Frank Jahnke, whose experience as a university professor were useful for our young research group. My colleagues and I had many interesting discussions with the members of his research group during work and especially during lunch time. In particular, these are Michael Lorke, Alexander Steinhoff-List, Daniel Erben, Joel Buchgeister, Ruven Hübner, Monty Drechsler, and the former members Matthias Florian and Christian Carmesin.

Besides the people in my university environment, I thank my family, who has massively supported me my way to this PhD thesis. An important part of my personal life during my studies was the training of the *Art of Peace* in the form of the Japanese martial art of Aikido with my teacher Volker. I thank him and the other participants for the nice time and all the experience I gained there.

Finally, I thank you, the reader, for your interest and I hope that you will enjoy the content of this thesis.

Contents

List of Figures

List of Tables

Chapter 1

Introduction

Quantum entanglement is an entirely non-classical correlation phenomenon that occurs in quantum systems that are composed of at least two particles. If these particles are entangled, their collective quantum state does not permit a description in terms of the separate components. Instead, predicting the behavior of one particle requires the full information about the collective state. One consequence is that the measurement of the state of one particle instantly sets the state of the others. Importantly, these correlations are set instantaneously irrespective of the distance between the particles. This is also the subject of the famous Einstein–Podolsky–Rosen (EPR) paradox [4]. This makes quantum entanglement indispensable for many tasks in quantum information theory, quantum communication [5], and quantum computing [6]. Commonly, entangled photons are used for the distribution of quantum entanglement in quantum communication networks [5], or for quantum teleportation [7, 8]. Photons are inherently non-stationary. For the local use of entanglement, e.g., for distributed quantum computation, it is more appropriate to use entangled matter qubits, like two-level atoms, nitrogen-vacancy (NV) centers, or quantum dots (QDs).

In quantum information theory many tasks rely on quantum entanglement as a resource, from which arises the potential for advantage over their classical counterparts. The point where quantum computers surpass classical computers is called *quantum supremacy* [9]. The heart of quantum supremacy lies in the use of entangled qubits instead of classical bits. Each qubit doubles the quantity of information that can be stored in a quantum system. Therefore, the amount of storable information increases exponentially. By contrast, the increase in a classical computer is just linear. Famous examples for specific tasks that theoretically exhibit quantum supremacy are Groover's algorithm for database search [10] and Shor's algorithm for finding the prime factors of large numbers [11]. To apply these algorithms to a meaningful task, quantum computers with large numbers of error-corrected qubits are needed, which are not yet available today. Nevertheless, in the last few years, reports were published claiming that quantum supremacy has been achieved by quantum processors that reduced the amount of time needed to solve particular problems by several orders of magnitude compared to the time classical state-of-the-art supercomputers would need [12, 13, 14, 15, 16, 17]. With the currently producible quantum processors with 50-100 qubits we have reached the state of quantum computing that is referred to as the noisy intermediate-scale quantum (NISQ) era [18]. This means, that NISQ quan-

tum computers are able to solve specific problems in significantly much shorter time than most powerful classical supercomputers. Furthermore, they provide new tools for exploring multipartite entanglement. However, it remains an open question of whether NISQ technologies will have useful industrial applications in the foreseeable future [18]. The current work focusses on such NISQ architectures in terms of CCAs and investigates possibilities to generate and control multipartite entanglement.

The generation of entangled qubits can be performed on a wide range of different platforms [19], where the most prominent ones include trapped ions [20, 21, 22], superconducting qubits [23, 24, 25, 26], and semiconductor QDs [27]. Another platform that has been closely investigated for this thesis is provided by coupled cavities, which are one of the research objects of cavity quantum electrodynamics (cQED) [28]. It refers to the regime, where the interaction of light and matter is modified due to the confinement of the electromagnetic field. The coupling of cavities is the result of the overlap of the corresponding field modes but can also be engineered, e.g., by using waveguides. Individual qubits inside each cavity of an array are spatially separated and do not interact directly. However, the interaction of the qubits is a necessary condition for entanglement in the system of qubits. This interaction is indirectly mediated by the light field via the cavity-cavity coupling.

The treatment of the light-matter interaction in this thesis is based on the Jaynes–Cummings model [29], which describes the interaction of a two-level atom and the quantized light field of a single cavity mode. Despite its simplicity, it is the foundation of many established concepts of generating entanglement [30, 31, 32]. Arrays of coupled cavities offer a scalable platform for the creation of quantum entanglement in a system with more than two qubits, which is referred to as multipartite entanglement (MPE).

The present thesis gives a detailed analysis on how to generate MPE in a system of coupled cavity-qubit systems. For this purpose we analyze the eigenspectrum and reveal possibilities to identify transitions from the ground state of the system to entangled target states. We discuss how to drive these transitions with optical excitation pulses and introduce a numerical approach to determine optimal system parameters for entanglement generation.

The thesis is as follows: In Chapter 2 we give an overview of current quantum technologies that harness quantum entanglement and discuss how they are related to the insights that we obtain in this thesis.

In Chapter 3 we give a formal definition of quantum entanglement and how it can be quantified in terms of suitable entanglement measures.

The building block of the extended coupled-cavity systems consists of individual microcavities with a qubit inside, whose interaction is described in terms of the well-known Jaynes–Cummings model [29]. In Chapter 4 we revisit the JC model and develop a graphical representation of the system's energy structure and discuss prerequisites for the generation of Rabi oscillations with an optical coherent pump. This is followed by an explanation of how to directly drive target states with a pump pulse. Bridging the gap to experimental realizations, we discuss how dissipative processes can be implemented.

Connecting multiple of these building blocks under the consideration of photon

hopping between the cavities is the topic of Chapter 5. Based on the insights from the previous chapter, we investigate how to generate Rabi oscillations between the ground state and different target states. We extend this discussion by harnessing an optical pulse in order to drive the system directly into entangled states with a high fidelity.

In Chapter 6 we present the generalization of the previous method using a numerical scheme for finding suitable parameters that allow us to drive a variety of entangled multipartite target states. The power of this generalized scheme is exemplarily demonstrated for arrays with three and four coupled cavities by generating W states with high fidelity. Furthermore, we discuss the symmetry of the Hamiltonian that describes the CCAs and opens the door to a wider range of entangled states by individually addressing the qubits with differently phased coherent pumps. The discussion is substantiated by demonstrating the generation of an antisymmetric tripartite W state.

In the last chapter we conclude the insights and methods, both analytic and numeric, developed in this thesis and discuss how far they can find application in future quantum technologies.

Some of the results presented in this thesis have been published in Physical Review A [33].

Chapter 2

The role of entanglement for new quantum technologies

Quantum entanglement is an essential resource for new quantum technologies. Bell states for example have a wide range of applications in quantum information protocols. Two important examples are the teleportation of quantum states [8] and quantum key distribution (QKD) using the Ekert protocol [34]. Another application for entanglement is the realization of a quantum repeater for long-range quantum communication [35]. The supremacy of quantum computers in solving specific tasks exponentially faster than classical computers would not be possible without entanglement [12]. One example of high relevance is the simulation of quantum systems. Its implementation would constitute a future milestone along the path to novel ways of studying quantum physics. Another task is to find the two prime factors of a given number obtained by their multiplication, which can be performed with Shor's algorithm. Modern cryptography uses the Rivest–Shamir–Adleman (RSA) scheme to encode data [36]. According to this scheme, products of prime numbers are generated in order to obtain large integers that cannot be factorized by classical computers within a rewarding amount of time. A quantum computer that breaks the RSA encryption by finding these prime numbers within an efficiently short period of time would be a change of paradigm in the field of encryption and secure transmission of information. The entanglement of three or more particles, which occurs for example in cluster states, is an additional step towards realizing certain quantum computing architectures, such as measurement-based quantum computing (QC) [37] and quantum reservoir computing (QRC).

The interaction between photons trapped in an optical cavity and quantum particles, like atoms, is studied in cavity quantum electrodynamics (cQED). Solid-state systems that operate in this regime are considered for many opto-electronic applications, ranging from nanolasers [38] to quantum-light sources [39] and sensors [40]. Using state-of-the-art fabrication techniques, even networks of solid-state based cQED systems can be realized, opening the door for photonic QRC [41]. The presence of a cavity allows to tailor and enhance the spontaneous emission from the particle it interacts with. This can be harnessed to increase brightness and efficiency in a wide range of material systems [38, 42, 43]. Quantum dots (QDs) are of particular interest for applications in quantum technologies due to their properties that are

precisely tunable to match the embedding resonator structure [44, 45, 46]. This makes them ideal candidates for entanglement generation [47]: Systems of fully or partially connected coupled-cavity arrays (CCAs) have already been experimentally realized [48, 49, 50]. In such experimental setups, the photonic connection between the cavities can be realized by networks of waveguides [1], as shown in Fig. 2.1, or external mirrors [51, 2], as shown in Fig. 2.2.

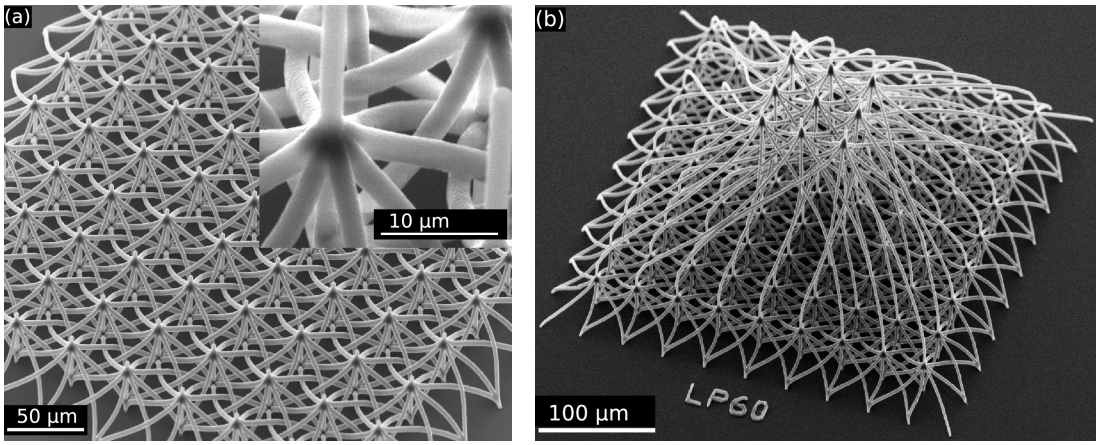

(a) Single-layer waveguide structure. (b) Two-layers waveguide structure.

Figure 2.1: SEM micrograph images of waveguide architectures reprinted from Ref. [1]. (a) Single-layer waveguide structure with 81 inputs on the top. Each input has 9 branches arranged in a square lattice, where the 8 branches that surround the one in the center are connected to the branches of the neighboring inputs. This leads to overall 121 outputs on the bottom of the whole structure. (b) Two-layer architecture with 9 inputs and 121 outputs. The 81 branches of the 9 inputs of the top layer are not connected with each other. They represent the inputs of the bottom layer.

In CCAs with spatially homogeneously distributed cavities, collective modes can form that are delocalized over the whole array [52]. In these collective modes, photons can induce correlations in the electronic degrees of freedom of the quantum emitters that are located in distant cavities. These perfectly combine an electronic system that is capable of hosting both classical and quantum correlations [53] with convenient accessibility of each individual cavity by optical excitation. For this reason, CCAs are of particular interest for several emerging technologies, such as the deterministic generation of multipartite entanglement (MPE) [54] and quantum reservoir computing [55]. A realization of an optical cavity by a micropillar and a CCA made of multiple micropillars is shown in Fig. 2.3.

In addition, CCAs have previously been considered for the generation of cluster states [54], Bell states [56], and GHZ states [57]. Another important class of entangled multipartite states are W states. They stand out due to their robustness against particle loss and their application in quantum communication protocols [58]. In general, MPE (as exhibited, e.g., by GHZ and W states) is of great interest due to its superiority over bipartite entanglement from the state convertibility perspective by local operations and classical communication (LOCC) [59]. Entangled multipartite states like W states have been generated by entangling photons [60], superconducting qubits [61], or trapped ions [62]. Different theoretical schemes for generating W

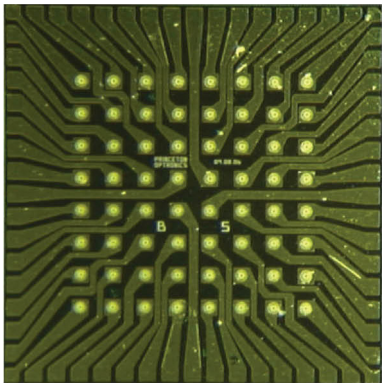

(a) VCSEL array.

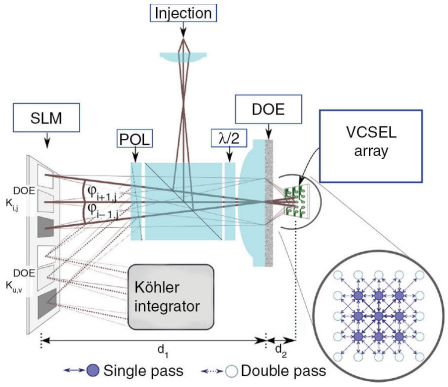

(b) Schematic of diffractive coupling.

Figure 2.2: Diffractively coupled cavities as a reservoir computer reprinted from Ref. [2]. (a) Chip hosting an 8×8 array of single-mode vertical-cavity surface-emitting lasers (VCSELs) from Princeton Optronics, arranged in a square lattice with a pitch of 250 µm [51]. (b) Schematic of the diffractive coupling of an optical array. The VCSEL array emits light that passes a diffractive optical element (DOE) and is imaged onto a reflective spatial-light modulator (SLM). The reflection of the SLM is then again imaged back onto the VCSEL array, where the overlapping orders result in coupling between neighboring emitters [51].

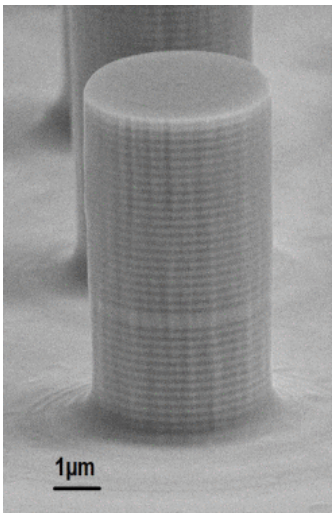

(a) Single micropillar.

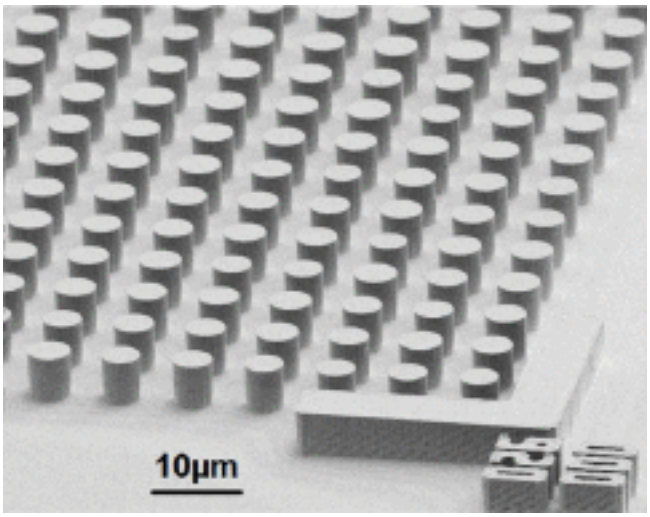

(b) Micropillar array.

Figure 2.3: SEM images of micropillars that function as optical cavities reprinted from Ref. [3]. (a) Single micropillar with a diameter of 4 µm. (b) Array of micropillar cavities with a pitch of 8.3 µm, which are coupled by diffraction optics.

states have been developed [58, 63, 64, 65, 66, 67]. Important platforms for the experimental generation of spatially distributed quantum systems are atomic qubits [68, 69], superconducting qubits [70], spins in diamonds [71], spins in semiconductor quantum dots [72], and trapped ions [73].

These examples illustrate some of the technological state of the art and underline the realizability of the concepts and methods introduced in this work. The hardware platforms and optical control over qubit and photon degrees of freedom that our methods rely on already exist in different implementations, both in atoms, superconducting circuits, and solid-state quantum emitters embedded in dielectric cavities, at least in small scale. The generation of entangled quantum states is a key ingredient towards future quantum technologies, such as quantum computers, quantum reservoir processors, and quantum sensors that rely on using entanglement as a resource to undertake specific tasks with an advantage over any classical analogue.

Chapter 3

Framework for quantifying entanglement

The main aspect of this thesis is the generation of entanglement. Two or more subsystems that form a compound quantum system are entangled if the state of one subsystem cannot be described independently of the other states. A major property of entangled subsystems is that the outcomes of measurements on each subsystem are correlated. This correlation is independent of the spatial distance between the entangled subsystems. It also persists when the measurement takes place in another basis, as it is shown schematically in Fig. 3.1.

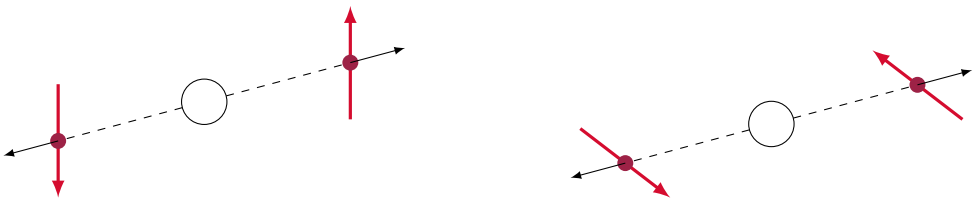

(a) Independence of spatial distance. (b) Independence of measurement basis.

Figure 3.1: Schematic picture of the properties of the entirely non-classical phenomena of entanglement. From an entanglement source (circle in the middle) two entangled particles (red dots) are emitted into different directions (indicated by black arrows). Here, the state of the particles is given by their anti-parallelly orientated spins (red arrows). The measurement of the spin of one particle immediately sets the spin of the other particle. Thus, after the spin measurement of the first particle the outcome of the spin measurement of the second particle is independent of the spatial distance of the particles (a) and the basis of the measurement (b).

Quantum entanglement is a entirely non-classical correlation. Due to its properties, entanglement is an essential resource for quantum technologies. Bipartite entangled states like the Bell states have a wide range of applications in quantum information protocols, e.g., the teleportation of quantum states [8] and quantum key distribution (QKD) [34]. Entanglement is also an important factor for creating quantum repeaters for long-range quantum communication [35]. Other important fields of research are quantum computing and quantum reservoir computing. The generation of MPE,

which occurs for example in cluster states [37], is a step towards to the realization of quantum computers that may solve specific programmable problems exponentially faster than classical computers [12].

3.1 Formal definition of entanglement

When talking about quantum states and entanglement of a compound system, one has to distinguish between pure and mixed states. In this section, we give a definition of separable pure and mixed states, respectively, for a system compound of two subsystems. The results can easily transcribed for larger systems [74].

3.1.1 Entanglement of pure states

Let $\mathcal{H}_\mathrm{A}$ and $\mathcal{H}_\mathrm{B}$ be the Hilbert spaces of two subsystems with dimensions d_A and d_B, respectively. Then the Hilbert space for the composite system made up of these two subsystems is the Hilbert tensor product $\mathcal{H}_\mathrm{A} \otimes \mathcal{H}_\mathrm{B}$. The total state $|\psi\rangle$ of the compound system is in general a superposition of the basis states $|a_i\rangle_\mathrm{A} \otimes |b_j\rangle_\mathrm{B} \in \mathcal{H}_\mathrm{A} \otimes \mathcal{H}_\mathrm{B}$ with $|a_i\rangle_\mathrm{A} \in \mathcal{H}_\mathrm{A}$ and $|b_j\rangle_\mathrm{B} \in \mathcal{H}_\mathrm{B}$:

$$|\psi\rangle = \sum_{i=1}^{d_\mathrm{A}} \sum_{j=1}^{d_\mathrm{B}} c_{ij} \, |a_i\rangle_\mathrm{A} \otimes |b_j\rangle_\mathrm{B} \in \mathcal{H}_\mathrm{A} \otimes \mathcal{H}_\mathrm{B}. \tag{3.1}$$

If we can find states $|\phi\rangle_\mathrm{A} \in \mathcal{H}_\mathrm{A}$ and $|\phi\rangle_\mathrm{B} \in \mathcal{H}_\mathrm{B}$ such that

$$|\psi\rangle = |\phi\rangle_\mathrm{A} \otimes |\phi\rangle_\mathrm{B} \,, \tag{3.2}$$

then the pure state $|\psi\rangle \in \mathcal{H}$ is called *separable*. This is the case, if $c_{ij} = c_i c_j$ such that $|\phi\rangle_\mathrm{A} = \sum_i c_i \, |a_i\rangle_\mathrm{A} \in \mathcal{H}_\mathrm{A}$ and $|\phi\rangle_\mathrm{B} = \sum_j c_j \, |b_j\rangle_\mathrm{B} \in \mathcal{H}_\mathrm{B}$. Else, if $c_{ij} \neq c_i c_j$ for at least one pair (i, j), the state $|\psi\rangle$ is called *entangled* [75]. A well-known example for bipartite entanglement are the Bell states

$$|\Phi_\pm\rangle = \frac{1}{\sqrt{2}} \left(|00\rangle \pm |11\rangle \right), \tag{3.3a}$$

$$|\Psi_\pm\rangle = \frac{1}{\sqrt{2}} \left(|01\rangle \pm |10\rangle \right), \tag{3.3b}$$

where we used the shorthand notation $|a_i\rangle_\mathrm{A} \otimes |b_j\rangle_\mathrm{B} \equiv |a_i b_j\rangle$. The states $|0\rangle$ and $|1\rangle$ are the ground state and the excited state, respectively, of a two-level system.

Entanglement can also occur in systems with more than two parties. The most important form of multipartite entanglement is the *genuine multipartite entanglement*. A given state is called genuine multipartite entangled if it is not biseparable (triseparable, etc.), i.e., partially separable. In other words, genuine multipartite entangled states cannot be separated into groups of entangled parties that are not entangled with the remaining parties of the state. One important genuine multipartite entangled state including at least three subsystems is the GHZ state named

after Greenberger, Horne, and Zeilinger [76]. For $N \geq 3$ qubits the GHZ states are defined as

$$|\mathrm{GHZ}_N\rangle = \frac{1}{\sqrt{2}} \left(|0\rangle^{\otimes N} + |1\rangle^{\otimes N} \right). \tag{3.4}$$

For three subsystems this expression simplifies to

$$|\mathrm{GHZ}_3\rangle = \frac{1}{\sqrt{2}} \left(|000\rangle + |111\rangle \right). \tag{3.5}$$

The GHZ state is a superposition of the ground state and the maximally excited state. According to many entanglement measures it is considered to be a maximally entangled multipartite state with outstanding quantum mechanical properties. This makes GHZ states interesting for the realization of quantum communication protocols such as the secret sharing protocol [77]. Another example for genuine multipartite entanglement are Dicke states [78]. For N subsystems with overall k excitations, the Dicke states are defined as

$$|\mathrm{D}_{N,k}\rangle = \binom{N}{k}^{-\frac{1}{2}} \sum_j P_j \left\{ |0\rangle^{\otimes k} \otimes |1\rangle^{\otimes (N-k)} \right\}, \tag{3.6}$$

where P_j is the j-th possible permutation. The Dicke state with three subsystems and two excitations for example is given by

$$|\mathrm{D}_{3,2}\rangle = \frac{1}{\sqrt{3}} \left(|011\rangle + |101\rangle + |110\rangle \right). \tag{3.7}$$

In the case of N subsystems with $k = 1$ excitations, the corresponding Dicke states are also known as W states:

$$|\mathrm{W}_N\rangle = \frac{1}{\sqrt{N}} \left(|0 \ldots 01\rangle + |0 \ldots 010\rangle + \cdots + |10 \ldots 0\rangle \right). \tag{3.8}$$

The tripartite W state for example is given by

$$|\mathrm{W}_3\rangle = \frac{1}{\sqrt{3}} \left(|001\rangle + |010\rangle + |100\rangle \right). \tag{3.9}$$

In contrast to the GHZ state, the entanglement of W states is very robust against the loss of qubits, i.e., the state $|\mathrm{W}_N\rangle$ remains entangled even if any $N - 2$ qubits lose the information about their particle, e.g., after a measure [79]. That means that any two out of N qubits are entangled even if they are not coupled anymore with the remaining $N - 2$ qubits. This property makes W states interesting for many applications of quantum information theory, which is they are the focus of this thesis.

3.1.2 Entanglement of mixed states

Any mixed state is represented by a density matrix. We first give a little reminder about the definition of a density matrix and discuss under which condition it is a pure or a mixed state before we return to the definition of entanglement of mixed states.

Let $\mathcal{B}(\mathcal{H})$ denote the space of bounded linear maps of $\mathcal{H}$ to $\mathcal{H}$, which is a Banach space with respect to the operator norm. An operator $\rho \in \mathcal{B}(\mathcal{H})$ is a density matrix if ρ is self-adjoint and positive-semidefinite and $\mathrm{tr}(\rho) = 1$. The expectation value Φ of an operator $A \in \mathcal{B}(\mathcal{A})$ is given by $\Phi(A) = \mathrm{tr}(\rho A) = \mathrm{tr}(A\rho)$ [80]. The orthogonal projection $|\psi\rangle \langle\psi|$ onto the span of the unit vector $|\psi\rangle \in \mathcal{H}$ is a density matrix with $\mathrm{tr}(|\psi\rangle \langle\psi| A) = \langle\psi|A|\psi\rangle$ for all $A \in \mathcal{B}(\mathcal{H})$ [80]. A density matrix $\rho \in \mathcal{B}(\mathcal{H})$ is a *pure state* if there exists a unit vector $|\psi\rangle \in \mathcal{H}$ such that

$$\rho = |\psi\rangle \langle\psi| . \tag{3.10}$$

Otherwise, it is called *mixed state*. Pure states remain pure until they interact with the environment and evolve into a mixed state. That is why mixed states play such an important role in the investigation of quantum systems.

A simple way to find out whether a given density matrix is a pure state or not is to calculate the trace of the square of that matrix, because a density matrix ρ is a pure state if and only if $\mathrm{tr}(\rho^2) = 1$. The density matrix ρ of a pure state is also idempotent, i.e., $\rho^2 = \rho$. However, there are two further criteria which can be checked. One way is to calculate the von Neumann entropy of the given density matrix. The von Neumann entropy of a density matrix ρ is defined as

$$S(\rho) = -\mathrm{tr}(\rho \ln \rho), \tag{3.11}$$

where $\rho \ln \rho$ is defined by a functional calculus and, per definition, $0 \ln 0$ is interpreted as 0 [74]. For an N-level system, this entropy reaches its highest attainable value $\ln N$ when all probabilities $p_j \equiv 1/N$. A density matrix ρ is a pure state iff $S(\rho) = 0$ [80].

In general, one has no information on the exact state of a quantum system but, if any, on the probability p_i for the system to be in the pure state $|\phi_i\rangle \in \mathcal{H}$. This situation is described by the density matrix

$$\rho = \sum_i p_i |\phi_i\rangle \langle\phi_i| , \tag{3.12}$$

with $p_i \geq 0$ and $\sum_i p_i = 1$ [75]. From this definition it is clear that $\mathrm{tr}(\rho) = 1$. This implies that any self-adjoint and positive semidefinite matrix of trace 1 can be interpreted as a density matrix. A notable consequence is that the set of density matrixes is a convex set. This means that the convex combination $\lambda\rho_1 + (1 - \lambda)\rho_2$ of two states ρ_1 and ρ_2 with $\lambda \in [0, 1]$ is again a state. The pure states are the extreme points of the convex set. A graphical representation of the full state space as a convex set is shown in Fig. 3.2. The set of separable mixed states is thus the *convex hull* of the pure separable states. In general, for some given coefficients $p_i \geq 0$ the convex combination $\sum_i p_i \rho_i$ of the density matrices ρ_i is again a density matrix. Now we have everything in order to define entanglement of mixed states.

Imagine two parties named Alice and Bob with Hilbert spaces $\mathcal{H}_\mathrm{A}$ $\mathcal{H}_\mathrm{B}$, respectively, who generate the states $\rho^\mathrm{A} \in \mathcal{B}(\mathcal{H}_\mathrm{A})$ and $\rho^\mathrm{B} \in \mathcal{B}(\mathcal{H}_\mathrm{B})$ independently from each other such that they are uncorrelated. We call $\rho \in \mathcal{B}(\mathcal{H}_\mathrm{A} \otimes \mathcal{H}_\mathrm{B})$ a *product state* if there are two density matrices ρ^A and ρ^B, such that

$$\rho = \rho^\mathrm{A} \otimes \rho^\mathrm{B}. \tag{3.13}$$

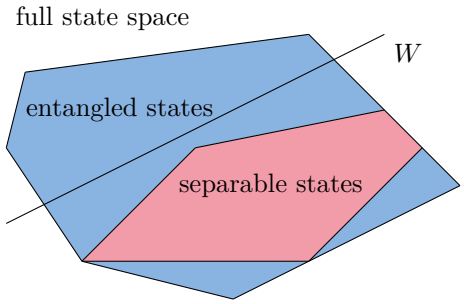

Figure 3.2: Graphical representation of the full state space as a convex set and the separable states as a convex subset (red). The extreme points of this subset are the pure states. All non-separable states are the entangled states (blue). The entanglement witness W defines a hyperplane given by $\mathrm{tr}(W\rho) = 0$. It divides the full state space into two sections, one with detected, i.e., entangled, states ($\mathrm{tr}(W\rho) < 0$) and one with non-detected states ($\mathrm{tr}(W\rho) \geq 0$).

The density matrix ρ is called *separable* if there exist product states $\rho_i^{\mathrm{A}} \otimes \rho_i^{\mathrm{B}} \in \mathcal{B}(\mathcal{H}_{\mathrm{A}} \otimes \mathcal{H}_{\mathrm{B}})$ such that

$$\rho = \sum_i p_i \rho_i^{\mathrm{A}} \otimes \rho_i^{\mathrm{B}}. \tag{3.14}$$

Otherwise, it is called *entangled*. Separable states are classically correlated. For the generation of a separable state only LOCC are necessary. Alice and Bob can share a random-number generator that produces the probabilities p_i, which they can communicate classically. Entangled states, however, cannot be generated classically in the way described above. Instead, their correlations are purely quantum mechanical [75].

A relevant example of a bipartite mixed state for real experiments is the Werner state ρ_{W}. Per definition, it is invariant under unitary transformations of the form $U \otimes U$ for all unitary operators U [81]:

$$(U \otimes U)\rho_{\mathrm{W}}(U^\dagger \otimes U^\dagger) = \rho_{\mathrm{W}}. \tag{3.15}$$

The Werner state is modelled by the Bell state $|\Psi_-\rangle = (|01\rangle - |10\rangle)/\sqrt{2}$ with some noise determined by $p \in [0, 1]$:

$$\rho_{\mathrm{W}} \equiv \rho_{\mathrm{W}}(p) = p\,|\Psi_-\rangle\langle\Psi_-| + \frac{1-p}{4} I. \tag{3.16}$$

A remarkable property is, that it is separable for $p \leq 1/3$ and entangled for $p > 1/3$, as we will discuss later.

3.2 Separability criteria

In quantum information theory, the question whether a given state is separable or not is in general a difficult question to answer and is thus referred to as the *separability problem*. Several separability criteria have been found but no general solution for the separability problem is known, yet [75]. An often used one is the *Peres–Horodecki*

criterion or *PPT criterion* [82, 83]. For composite system of two subsystems A and B with dimensions d_A and d_B, the general density matrix describing the state ρ of the system can be written as

$$\rho = \sum_{i,j}^{d_\mathrm{A}} \sum_{k,l}^{d_\mathrm{B}} \rho_{ij,kl} \left|i\right\rangle \left\langle j\right| \otimes \left|k\right\rangle \left\langle l\right|, \tag{3.17}$$

with the matrix elements $\rho_{ij,kl}$. The partial transposition of ρ with respect to subsystem A is given by

$$\rho^{\mathrm{T_A}} = \sum_{i,j}^{d_\mathrm{A}} \sum_{k,l}^{d_\mathrm{B}} \rho_{ji,kl} \left|i\right\rangle \left\langle j\right| \otimes \left|k\right\rangle \left\langle l\right|. \tag{3.18}$$

The definition for the partial transposition of ρ with respect to subsystem B is similar. Note, that it can be obtained by the transposition of the partial transposition with respect to A, i.e., $\rho^{\mathrm{T_B}} = (\rho^{\mathrm{T_A}})^{\mathrm{T}}$. A density matrix has a *positive partial transpose* (PPT), if its partial transposition with respect to A or B has no negative eigenvalues, i.e., it is positive semidefinite. One also says that the matrix is *PPT*. Else, if it is not PPT, it is NPT. A necessary condition for a bipartite density matrix ρ to be separable is that it has to be PPT. This is the PPT criterion. If ρ is the state of a 2×2 or a 2×3 system, then the PPT criterion is sufficient. As an example, the least eigenvalue of the partial transpose of the Werner state $\rho_\mathrm{W}(p)$ in Eq. (3.16) is $(1 - 3p)/4$. This eigenvalue is negative for $p > 1/3$, thus the Werner state is PPT, i.e., separable. For $p \leq 1/3$ the Werner state is entangled.

3.3 Entanglement measures

For a given density matrix of a quantum system, it may be that the underlying subsystems are not entangled. Instead, the amount of entanglement is continuous. A quantity that represents this amount of entanglement of a given state ρ is an entanglement measure $E(\rho)$. There are several properties that an entanglement measure should have [84]. The most important one is that for a separable state ρ_s, an entanglement measure should vanish: $E(\rho_\mathrm{s}) = 0$. There are several entanglement measures, which involve the density operator of the given system [74]. In this section, we give some examples of often used entanglement measures.

3.3.1 Entropy of entanglement

In order to use the von Neumann entropy, which is defined by Eq. (3.11), as an entanglement measure, we need to introduce the concept of the partial trace and reduced density matrices.

Let $\rho \in \mathcal{B}(\mathcal{H}_\mathrm{A} \otimes \mathcal{H}_\mathrm{B})$ be a density matrix that acts on the Hilbert space $\mathcal{H}_\mathrm{A} \otimes \mathcal{H}_\mathrm{B}$. The partial trace $\mathrm{tr_B}$ with respect to subspace $\mathcal{H}_\mathrm{B}$ is a unique operation, which reduces the density matrix ρ such that one obtains the linear operator $\rho_\mathrm{A} \in \mathcal{B}(\mathcal{H}_\mathrm{A})$, which acts on the subspace $\mathcal{H}_\mathrm{A}$:

$$\rho_\mathrm{A} \equiv \mathrm{tr_B}(\rho). \tag{3.19}$$

This operator is called the reduced density matrix with respect to the subsystem A. The partial trace with respect to the subsystem B is defined as

$$\mathrm{tr_B}(\rho) = \sum_j (I \otimes \langle j|)\rho(I \otimes |j\rangle). \tag{3.20}$$

For all operators $A \in \mathcal{B}(\mathcal{H}_\mathrm{A})$ the reduced density matrix ρ_A has the property that

$$\mathrm{tr}(\rho_\mathrm{A} A) = \mathrm{tr}(\rho(A \otimes I)), \tag{3.21}$$

that is the expectation value of the operator A in the state ρ_A of the subsystem A is equal to the one of the compound operator $A \otimes I$ in the state ρ on $\mathcal{H}_\mathrm{A} \otimes \mathcal{H}_\mathrm{B}$ of the compound system. Analogously, we find the reduced density matrix with respect to the subsystem B: $\rho_\mathrm{B} = \mathrm{tr_A}(\rho)$. Note that ρ_A and ρ_B do not need to be pure states even if the state of the joint system is pure.

For a bipartite system in a pure state $|\Psi\rangle$, the entropy of entanglement is given by the von Neumann entropy, which we defined in (3.11), of either one of the two reduced density matrices ρ_A and ρ_B of the system's density matrix $\rho = |\Psi\rangle\langle\Psi|$ [85]:

$$E(\rho) = S(\rho_\mathrm{A}) = S(\rho_\mathrm{B}). \tag{3.22}$$

This entanglement measure reaches from 0 for a separable state to $\ln N$ for a maximally entangled state of a system composed of two N-dimensional subsystems. There exist four bipartite quantum states that are maximally entangled: the Bell states. The notable property of the Bell states being maximally entangled can also be shown by calculating the positive partial transpose (PPT), which has been shown to be sufficient and necessary for quantum entanglement in bipartite systems, referred to as the PPT criterion [82, 83]. This criterion is an important example among many other separability criteria, especially for bipartite systems [75].

3.3.2 Concurrence

The concurrence is an entanglement measure for bipartite system with the density matrix that consists of two-level subsystems. For a pure state ρ, it is

$$C(\rho) = \sqrt{2\,[1 - \mathrm{tr}(\rho_\mathrm{A}^2)]}, \tag{3.23}$$

where $\rho_\mathrm{A} = \mathrm{tr_B}(\rho)$ is the reduced density matrix of subsystem A. For a mixed state ρ, the concurrence is defined as

$$C(\rho) = \max(0, \lambda_1 - \lambda_2 - \lambda_3 - \lambda_4), \tag{3.24}$$

where $\lambda_1, \ldots, \lambda_4$ are the eigenvalues of $R = \sqrt{\sqrt{\rho}\tilde{\rho}\sqrt{\rho}}$ [74] with

$$\tilde{\rho} = (\sigma_\mathrm{y} \otimes \sigma_\mathrm{y})\rho^*(\sigma_\mathrm{y} \otimes \sigma_\mathrm{y}), \tag{3.25}$$

in descending order. Alternatively, $\lambda_1, \ldots, \lambda_4$ are defined as the square roots of the eigenvalues of $\rho\tilde{\rho}$, in descending order. For $C = 0$, the state is separable, i.e., it shows no entanglement. The maximum value of the concurrence is $C = 1$ for which the subsystems are maximally entangled.

3.3.3 Negativity and logarithmic negativity

The negativity is an entanglement measure for systems that can be regarded as a quantitative version of the PPT criterion [86]. With respect to the i-th subsystem of the given system with the density matrix ρ it is defined as

$$\mathcal{N}_i(\rho) = \frac{||\rho^{T_i}||_1 - 1}{2}, \tag{3.26}$$

where ρ^{T_i} is the partial transpose of ρ with respect to the i-th subsystem and $||X||_1 = \mathrm{Tr}|X| = \mathrm{Tr}\sqrt{X^\dagger X}$ is the trace norm. An equivalent definition is:

$$\mathcal{N}_i(\rho) = \left|\sum_{\lambda_i<0} \lambda_j\right| = \sum_j \frac{|\lambda_j| - \lambda_j}{2}, \tag{3.27}$$

where the λ_j are the eigenvalues of ρ^{T_i}. A quite similar entanglement measure for bipartite systems is the logarithmic negativity. It is defined as

$$E_{\mathcal{N}_i}(\rho) = \log_2 ||\rho^{T_i}||_1. \tag{3.28}$$

This entanglement measure has its name from the logarithmic dependency on the negativity defined above:

$$E_{\mathcal{N}_i}(\rho) = \log_2(2\mathcal{N}_i + 1). \tag{3.29}$$

The advantage of the negativity and the logarithmic negativity is that they can be used for multipartite systems. However, these measures depend on the subsystem they are calculated for. Thus one obtains a value for each subsystem, which describes how strongly the corresponding subsystem is entangled with the rest of the system. Furthermore, the negativity and the logarithmic negativity are entanglement monotones, i.e., they do not increase under LOCC [86].

3.4 Entanglement witnesses

An entanglement witness $\mathcal{W}$ (or witness for short) is a measurable observable, which is used to detect whether a state is entangled or not. It is defined as follows:

$$\begin{cases} \mathrm{tr}(\mathcal{W}\rho_\mathrm{s}) \geq 0, & \text{for all separable states } \rho_\mathrm{s}, \\ \mathrm{tr}(\mathcal{W}\rho_\mathrm{e}) < 0, & \text{for at least one entangled state } \rho_\mathrm{e}. \end{cases} \tag{3.30}$$

A negative expectation value is a clear proof that a given state is entangled. A positive expectation value is a necessary, but not a sufficient criterion for a given state to be separable [75]. This means, that the state might be entangled but could not be detected by the witness. However, it can be proven that for any entangled state ρ_e there exists an entanglement witness that can detect it [83]. From the geometric point of view, a witness $\mathcal{W}$ defines a hyperplane given by $\mathrm{tr}(\mathcal{W}\rho) = 0$, dividing the state space into two parts, as it is shown in Fig. 3.2. The part with $\mathrm{tr}(\mathcal{W}\rho) \geq 0$ contains all separable states, the other one with $\mathrm{tr}(\mathcal{W}\rho) < 0$ is the set of all entangled states that are detected by $\mathcal{W}$. The problem with entanglement witnesses is the difficulty to construct one that detects all relevant entangled states of a given system. In the following, we give two examples of constructions of witnesses.

3.4.1 Witnesses for NPT states

A witness that detects an entangled state ρ_e that is NPT, i.e., its partial transposition has a negative eigenvalue $\lambda_- < 0$ a corresponding eigenstate $|\lambda_-\rangle$, is constructed by

$$\mathcal{W} = (|\lambda_-\rangle\langle\lambda_-|)^{\mathrm{T_A}}\,. \tag{3.31}$$

For two operators X and Y the relation $\mathrm{tr}(XY^{\mathrm{T_A}}) = \mathrm{tr}(X^{\mathrm{T_A}}Y)$ holds. Thus, $\mathrm{tr}(\mathcal{W}\rho_\mathrm{e}) = \mathrm{tr}[(|\lambda_-\rangle\langle\lambda_-|)^{\mathrm{T_A}}\rho_\mathrm{e}] = \mathrm{tr}(|\lambda_-\rangle\langle\lambda_-|\rho_\mathrm{e}^{\mathrm{T_A}}) = \lambda_- < 0$ for entangled states ρ_e and $\mathrm{tr}(\mathcal{W}\rho_\mathrm{s}) = \mathrm{tr}(|\lambda_-\rangle\langle\lambda_-|\rho_\mathrm{s}^{\mathrm{T_A}}) \geq 0$ for separable states ρ_s. Now, we consider the Werner state ρ_W in Eq. (3.16). Its partial transposition $\rho_\mathrm{W}^{\mathrm{T_A}} = \rho_\mathrm{W}^{\mathrm{T_B}}$ has the eigenvalues $(1-3p)/4$ and $(1+p)/4$ (with an algebraic multiplicity of 3). Therefore, ρ_W is entangled (i.e., NPT) if $p < 1/3$. The minimum eigenvalue $\lambda_- = (1-3p)/4$ has the corresponding eigenvector $|\Phi_+\rangle = (|00\rangle + |11\rangle)/\sqrt{2}$. A witness that detects entangled Werner states can thus be constructed by

$$\mathcal{W} = (|\Phi_+\rangle\langle\Phi_+|)^{\mathrm{T_A}} = \frac{1}{2}I - |\Psi_-\rangle\langle\Psi_-|\,, \tag{3.32}$$

with $|\Psi_-\rangle = (|01\rangle - |10\rangle)/\sqrt{2}$. Note that it does not depend on p but the expectation value with the Werner state that indicates whether the state is entangled or not. With the Pauli matrices

$$\sigma_\mathrm{x} = |0\rangle\langle 1| + |1\rangle\langle 0|\,, \tag{3.33a}$$
$$\sigma_\mathrm{y} = \mathrm{i}(|1\rangle\langle 0| - |0\rangle\langle 1|), \tag{3.33b}$$
$$\sigma_\mathrm{z} = |0\rangle\langle 0| - |1\rangle\langle 1|\,, \tag{3.33c}$$

Eq. (3.32) can be rewritten as

$$\mathcal{W} = \frac{1}{4}(I + \sigma_\mathrm{x}\otimes\sigma_\mathrm{x} + \sigma_\mathrm{y}\otimes\sigma_\mathrm{y} + \sigma_\mathrm{z}\otimes\sigma_\mathrm{z}). \tag{3.34}$$

This entanglement witness was the first reported to be experimentally realized [87].

3.4.2 Fidelity witnesses

Another example of an entanglement witness can be found if we consider that a given state that is close to an entangled state can be entangled, too. A witness that detects the genuine multipartite entangled pure state $|\psi\rangle$ and entangled states close to that is the *fidelity witness*

$$\mathcal{W}_\psi = \alpha I - |\psi\rangle\langle\psi|\,, \tag{3.35}$$

where

$$\alpha = \max_{|\phi\rangle\in\mathcal{B}} |\langle\phi|\psi\rangle|^2, \tag{3.36}$$

and $\mathcal{B}$ denotes the set of biseparable states. The value α is the maximum overlap of the entangled state $|\psi\rangle$ with any biseparable state $|\phi\rangle$. It can be shown that α is given by the square of the maximal Schmidt coefficient of $|\psi\rangle$ [88]. Let d be the smallest dimension of the Hilbert spaces of the subsystems that form the compound

Hilbert space in which we find the state $|\psi\rangle$. Then, the smallest value that α can take is $\alpha = 1/d$, which is the case if $|\psi\rangle$ is maximally entangled [89]. For example, in case of a bipartite system, $\alpha \geq 1/2$. A possible entanglement witness for the detection of the N qubit W state $|\mathrm{W}_N\rangle$ in Eq. (3.8) is given by

$$\mathcal{W}_{\mathrm{W}_N} = \frac{N-1}{N} I - |\mathrm{W}_N\rangle \langle \mathrm{W}_N| \,. \tag{3.37}$$

The calculation of the expectation value of witnesses given by Eq. (3.35) leads to the calculation of the quantity

$$F := \mathrm{tr}(\rho \, |\psi\rangle \langle\psi|) = \langle\psi|\rho|\psi\rangle \,. \tag{3.38}$$

This quantity is the fidelity F of the pure state $|\psi\rangle$ and the mixed state ρ [90], i.e., the overlap of these two states. Roughly speaking, it describes how similar one quantum state is to another. The fidelity is exactly the expectation value of the projection operator $|\psi\rangle \langle\psi|$ or, in other words, the probability of measuring the pure state $|\psi\rangle$ in the mixed state ρ. Therefore, it ranges from 0, if the states are orthogonal, to 1, if the state are equal. If the fidelity in Eq. (3.38) is larger than the critical value α in Eq. (3.36) the expectation value of the witness in Eq. (3.35) is negative and the state ρ must be entangled [75]. This makes the fidelity a useful tool for this thesis.

Chapter 4

Light-matter interaction and the Jaynes–Cummings model

We begin with the description of the system that is the fundamental building block for the generation of entangled states we are investigating in this thesis. It consists of an optical cavity with a two-level system, like an atom, a quantum dot (QD), or any other implementation of a quantum emitter. In quantum computing, such two-level systems are called qubits. The interaction between a cavity and a qubit is described by the Jaynes–Cummings model, which is well-known in quantum optics [91]. We give the analytic solution of the eigenenergies and -states of the cavity-qubit system and investigate the effect of pumping the qubits with an external excitation source.

4.1 Light-matter interaction in quantum optics

The branch of classical physics that studies the interaction of light and matter is optics. The term light is mostly associated with the visible part of the electromagnetic spectrum described as waves or rays for wavelengths small compared to the matter it interacts with. The interaction of light with matter includes diffraction, refraction and reflection. Optical instruments like lattices, lenses and mirrors make use of these phenomena. When dealing with matter on the atomic scale it is necessary to think of light as a collection of particles called photons with wave properties. The light-matter interaction of photons and quantum objects like atoms is the subject of quantum optics. The interaction of the electric and the magnetic components of an electromagnetic field is described by the Maxwell equations. It is sufficient to restrict calculations to the electronic or magnetic field in order to describe light.

We consider an atom, which we describe as a dipole, interacting with light within an optical cavity, which works as a resonator for the light. In this case, the atom-field interaction Hamiltonian is given by

$$H_{\text{int}} = -\boldsymbol{d} \cdot \boldsymbol{E}(\boldsymbol{r}, t), \tag{4.1}$$

where $\boldsymbol{d}$ is the dipole moment operator and $\boldsymbol{E}(\boldsymbol{r}, t)$ the electric field operator of a quantized electromagnetic field at the position $\boldsymbol{r}$ at the time t. A two-level atom

has the basis states $|\mathrm{g}\rangle$ and $|\mathrm{e}\rangle$, which are the ground and excited state, respectively. Thus, the dipole moment operator in second quantization is given by

$$\boldsymbol{d} = \boldsymbol{d}_{\mathrm{eg}}\sigma^{+} + \boldsymbol{d}_{\mathrm{eg}}^{*}\sigma^{-}, \tag{4.2}$$

where $\boldsymbol{d}_{\mathrm{eg}} = \langle \mathrm{e}|\boldsymbol{d}|\mathrm{g}\rangle = \boldsymbol{d}_{\mathrm{ge}}^{*}$ are the matrix elements of $\boldsymbol{d}$, and $\sigma^{+} = |\mathrm{e}\rangle\langle\mathrm{g}| = (\sigma^{-})^{\dagger}$ [92]. The electric field operator in the interaction picture is given by ($\hbar = 1$, $\varepsilon_0 = (4\pi)^{-1}$)

$$\boldsymbol{E}(\boldsymbol{r}, t) = \sum_{\boldsymbol{k}} \sum_{\lambda\in\{1,2\}} \left(\boldsymbol{E}_{\boldsymbol{k},\lambda} a_{\boldsymbol{k},\lambda} \mathrm{e}^{-\mathrm{i}\omega_{\boldsymbol{k}} t + \mathrm{i}\boldsymbol{k}\cdot\boldsymbol{r}} + \mathrm{h.c.}\right), \tag{4.3}$$

with $\boldsymbol{E}_{\boldsymbol{k},\lambda} = \mathrm{i}\sqrt{2\pi\omega_{\boldsymbol{k}}/V}\boldsymbol{e}_{\boldsymbol{k},\lambda}$, where $\omega_{\boldsymbol{k}} = c\boldsymbol{k}$ is the frequency of the mode of the wave with the wave vector $\boldsymbol{k}$, V is the volume of the cavity, $\boldsymbol{e}_{\boldsymbol{k},\lambda}$ is the unit polarization vector with the polarization λ, and $a_{\boldsymbol{k},\lambda}$ ($a_{\boldsymbol{k},\lambda}^{\dagger}$) is the photon lowering (raising) operator [92]. When the wavelength of the light is much smaller than the size of the atom, i.e., $\boldsymbol{k}\cdot\boldsymbol{r} \ll 1$, we can neglect the position-dependency and set $\boldsymbol{r} \equiv 0$. This is called the *electric dipole approximation*. By working in the Schrödinger picture, we can omit the time-dependency, too, and the atom-field Hamiltonian becomes

$$H_{\mathrm{int}} = -\boldsymbol{d}\cdot\boldsymbol{E}(0). \tag{4.4}$$

By defining the interaction strength $g_{\boldsymbol{k},\lambda} = -\boldsymbol{d}_{\mathrm{eg}}\cdot\boldsymbol{E}_{\boldsymbol{k},\lambda}$ and $\bar{g}_{\boldsymbol{k},\lambda} = -\boldsymbol{d}_{\mathrm{eg}}\cdot\boldsymbol{E}_{\boldsymbol{k},\lambda}^{*}$, we can write the interaction Hamiltonian as

$$H_{\mathrm{int}} = \sum_{\boldsymbol{k},\lambda}\left(g_{\boldsymbol{k},\lambda}a_{\boldsymbol{k},\lambda}\sigma^{+} + g_{\boldsymbol{k},\lambda}^{*}a_{\boldsymbol{k},\lambda}^{\dagger}\sigma^{-} + \bar{g}_{\boldsymbol{k},\lambda}a_{\boldsymbol{k},\lambda}^{\dagger}\sigma^{+} + \bar{g}_{\boldsymbol{k},\lambda}^{*}a_{\boldsymbol{k},\lambda}\sigma^{-}\right). \tag{4.5}$$

We consider a single-mode cavity with the frequency ω_{c}, such that the atom-field Hamiltonian simplifies to

$$H_{\mathrm{int}} = \left(ga\sigma^{+} + g^{*}a^{\dagger}\sigma^{-} + \bar{g}a^{\dagger}\sigma^{+} + \bar{g}^{*}a\sigma^{-}\right), \tag{4.6}$$

where g is the interaction strength of the atom with the single mode cavity and a ($a^{\dagger}$) the lowering (raising) operator of the photonic single mode. In the interaction picture we obtain

$$H_{\mathrm{int}}(t) = \left(ga\sigma^{+}\mathrm{e}^{\mathrm{i}(\omega_{\mathrm{a}}-\omega_{\mathrm{c}})t} + g^{*}a^{\dagger}\sigma^{-}\mathrm{e}^{-\mathrm{i}(\omega_{\mathrm{a}}-\omega_{\mathrm{c}})t} + \bar{g}a^{\dagger}\sigma^{+}\mathrm{e}^{\mathrm{i}(\omega_{\mathrm{a}}+\omega_{\mathrm{c}})t} + \bar{g}^{*}a\sigma^{-}\mathrm{e}^{-\mathrm{i}(\omega_{\mathrm{a}}+\omega_{\mathrm{c}})t}\right), \tag{4.7}$$

where ω_{a} is the frequency describing the energy difference between the two states of the atom, and ω_{c} is the frequency of the cavity mode. The interaction between the light field and the atom leads to four terms: The term proportional to $a^{\dagger}\sigma^{-}$ ($a\sigma^{+}$) lowers (raises) the qubit energy and creates (annihilates) a photon, and oscillates with the frequency $|\omega_{\mathrm{a}} - \omega_{\mathrm{c}}|$. The term proportional to $a\sigma^{-}$ ($a^{\dagger}\sigma^{+}$) lowers (raises) the atom energy and annihilates (creates) a photon, and oscillate with the frequency $\omega_{\mathrm{a}} + \omega_{\mathrm{c}}$. If the atom is close to resonance with the cavity, i.e., $\omega_{\mathrm{a}} \approx \omega_{\mathrm{c}}$, the frequencies of the oscillating terms of the light-matter interaction Hamiltonian will fulfill the relation $|\omega_{\mathrm{a}} - \omega_{\mathrm{c}}| \ll \omega_{\mathrm{c}} + \omega_{\mathrm{c}}$. This means, that while the resonant terms oscillating at $|\omega_{\mathrm{a}} - \omega_{\mathrm{c}}| \approx 0$ complete one cycle, the off-resonant terms oscillating at $\omega_{\mathrm{a}} + \omega_{\mathrm{c}} \approx 2\omega_{\mathrm{a}}$, complete significantly more cycles. Thus, the effect of the off-resonant terms can be neglected. This is called the rotating wave approximation (RWA) [93]. By applying this approximation, and assuming that g is real, the interaction Hamiltonian in the Schrödinger picture becomes

$$H_{\mathrm{int}} = g\left(a^{\dagger}\sigma^{-} + a\sigma^{+}\right). \tag{4.8}$$

4.2 Novel graphical eigensystem representation of the Jaynes–Cummings model

In order to describe a coupled-cavity array (CCA) we discuss the theoretical basics behind the building blocks of such CCAs, i.e., the single optical cavity with an atom inside. The quantum optical model that describes the interaction of a two-level atom with a single-mode cavity is the Jaynes–Cummings (JC) model [29]. It is a fundamental model in quantum optics and often discussed in the literature [91, 94, 95]. Despite that, the JC model is still an important framework for topics of quantum optical research [30, 31, 32]. Figure 4.1 shows the schematic setup of the JC model. In the following sections, we replace the two-level atom with the more theoretical

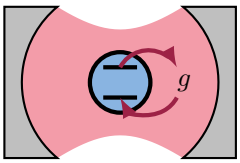

Figure 4.1: Schematic representation of the Jaynes–Cummings model, which describes an optical cavity interacting with a two-level atom.

concept of the qubit, i.e., a quantum bit represented by any two-level quantum system.

4.2.1 Jaynes–Cummings Hamiltonian

The Jaynes–Cummings Hamiltonian is given by

$$H_{\mathrm{JC}} = H_{\mathrm{c}} + H_{\mathrm{q}} + H_{\mathrm{c,q}}, \tag{4.9}$$

where H_{c} and H_{q} describe the photons in the optical cavity and the qubit, respectively, and $H_{\mathrm{c,q}}$ the interaction between them.

The cavity Hamiltonian is given by the Hamiltonian of a quantized electromagnetic field

$$H_{\mathrm{c}} = \omega_{\mathrm{c}} \left(a^{\dagger} a + \frac{1}{2} \right), \tag{4.10}$$

where ω_{c} is the cavity-photon frequency and a ($a^{\dagger}$) the photon annihilation (creation) operator with $\left[a^{\dagger}, a\right] = 1$. In an optical cavity with two mirrors at a distance of L, the wave function of a photon assumes the form of a standing wave with a wave length of $\lambda = 2L/n$, where $n \in \mathbb{N}$. Thus, the corresponding angular frequency is $\omega_{\mathrm{c}} = c\pi n/L$, where c is the speed of light. The cavity modes are therefore discrete and their spectral distance rises with increasing distance L between the mirrors. This allows to realize a single-mode cavity with a sufficiently small value of L. We neglect the constant term $\omega_{\mathrm{c}}/2$, which represents the zero-point energy of the photons.

The qubit Hamiltonian is given by

$$H_{\mathrm{q}} = \left(W + \frac{\omega_{\mathrm{q}}}{2} \right) \sigma^{+}\sigma^{-} + \left(W - \frac{\omega_{\mathrm{q}}}{2} \right) \sigma^{-}\sigma^{+}. \tag{4.11}$$

Here, ω_q is the excitation energy between the two levels of the qubit, and σ^- (σ^+) is the corresponding raising (lowering) operator with $(\sigma^-)^\dagger = \sigma^+$ ($(\sigma^+)^\dagger = \sigma^-$). With the Pauli matrices σ^x, σ^y, and σ^z, we define $\sigma^\pm = \frac{1}{2}(\sigma^\mathrm{x} \pm \mathrm{i}\sigma^\mathrm{y})$, with $[\sigma^+, \sigma^-] = \sigma^\mathrm{z}$ and $[\sigma^\mathrm{z}, \sigma^\pm] = \pm 2\sigma^\pm$. W is the mean energy of the two levels, which can be arbitrarily chosen. Two common choices are $W = \omega_\mathrm{q}/2$, such that $H_\mathrm{q} = \omega_\mathrm{q}\sigma^+\sigma^-$ [32], or $W = 0$, such that $H_\mathrm{q} = \omega_\mathrm{q}\sigma^\mathrm{z}/2$ [30]. We set $W = \omega_\mathrm{q}/2$, i.e., we set the ground state energy of the qubit equal to 0.

In the rotating-wave approximation, the cavity-qubit interaction Hamiltonian is given by Eq. (4.8).

The orthonormal basis of the qubit is given by the ground state $|\mathrm{g}\rangle$ and the excited state $|\mathrm{e}\rangle$, while the photon state is $|n\rangle$, where $n = 0, 1, 2, \ldots$ denotes the number of photons in the cavity. The basis states of the system are the product states of the qubit and the photon states, i.e., $|\mathrm{g}\rangle \otimes |n\rangle \equiv |\mathrm{g}, n\rangle$ and $|\mathrm{e}, n\rangle$.

4.2.2 Dynamics of Jaynes–Cummings Hamiltonian

When the qubit is in the ground state and the cavity in the vacuum state, the joint system is in the zero-excitation state $|\mathrm{g}, 0\rangle$ [96]. In a system with n excitations, the interaction Hamiltonian $H_\mathrm{c,q}$ only acts on the subspace $\{|\mathrm{e}, n-1\rangle, |\mathrm{g}, n\rangle\}$ with $n \geq 1$. The eigenenergies of the JC Hamiltonian in Eq. (4.9) are

$$E_{n,\pm} = \left(n\omega_\mathrm{c} + \frac{1}{2}\Delta\right) \pm \frac{1}{2}\Omega_n(\Delta), \tag{4.12}$$

where

$$\Omega_n(\Delta) = \sqrt{\Omega_n^2 + \Delta^2} \tag{4.13}$$

is the generalized Rabi frequency, $\Omega_n = 2\sqrt{n}g$ is the (common) Rabi frequency (with $\Omega_n = \Omega_n(0)$), and $\Delta = \omega_\mathrm{q} - \omega_\mathrm{c}$ is the qubit-cavity detuning. The generalized Rabi frequency is defined as the difference between the eigenenergies $E_{n,-}$ and $E_{n,+}$, i.e., $\Omega_n(\Delta) := |E_{n,+} - E_{n,-}|$. This non-linear scaling of the eigenenergies is called the Jaynes–Cummings ladder, which scales as $\sqrt{n}$. The cavity-qubit coupling causes avoided crossings (anticrossings) at $\Delta = 0$, as shown in in Fig. 4.2.

The eigenstates corresponding to the eigenenergies in Eq. (4.12) are

$$|n, \pm\rangle = N_{n,\mp}|\mathrm{g}, n\rangle \pm N_{n,\pm}|\mathrm{e}, n-1\rangle, \tag{4.14}$$

where

$$N_{n,\pm} = \frac{1}{\sqrt{2}}\left(1 \pm \frac{\Delta}{\sqrt{\Delta^2 + \Omega_n^2}}\right)^{\frac{1}{2}}. \tag{4.15}$$

The basis states $|\mathrm{e}, n-1\rangle$ and $|\mathrm{g}, n\rangle$ are called bare states. The eigenstates $|n, \pm\rangle$ are called dressed states, because they are a superposition of the uncoupled bare states. We define the squared overlaps $P_{\mathrm{g},n;\pm}$ and $P_{\mathrm{e},n-1;\pm}$ as the square of the absolute value of the scalar product of the bare with the dressed states, i.e., $P_{\mathrm{g},n;\pm} := |\langle \mathrm{g}, n|n, \pm\rangle|^2$ and $P_{\mathrm{e},n-1;\pm} := |\langle \mathrm{e}, n-1|n, \pm\rangle|^2$. In other words, they represent the respective

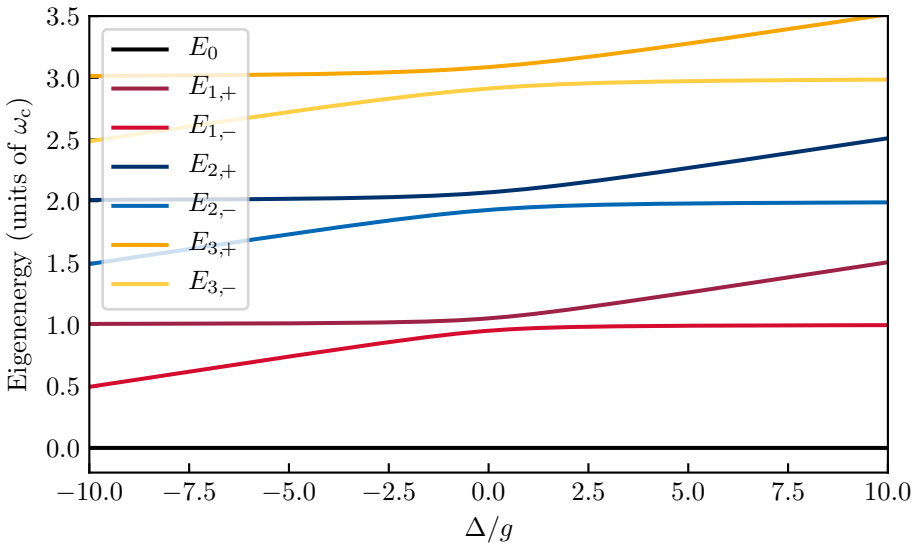

Figure 4.2: Eigenspectrum of a single cavity-qubit system exhibiting the Jaynes–Cummings ladder (for $\omega_c = 20g$). At $\Delta = 0$, avoided crossings emerge between the eigenenergies $E_{n,-}$ and $E_{n,+}$ of the JC Hamiltonian in the RWA. The energy difference there scale as $\sqrt{n}$. The zero-excitation state with the eigenenergy E_0 (black) is not coupled to any other state.

contribution of the bare to the dressed states. For the JC model, the squared overlaps are

$$P_{\mathrm{g},n;\pm} = N_{n,\mp}^2, \tag{4.16a}$$
$$P_{\mathrm{e},n-1;\pm} = N_{n,\pm}^2. \tag{4.16b}$$

Note that $P_{\mathrm{g},n;\pm} = P_{\mathrm{e},n-1;\mp}$. The squared overlap $P_{\mathrm{g},0}$ of the zero-excitation state with itself is 1. Figure 4.3 depicts the squared overlaps in dependence of the detuning Δ. A joint diagram for the representation of the eigensystem is shown in Fig. 4.4. For several values of Δ the squared overlaps of the bare with the dressed states are visualized as colored disks. Each disk represents the eigenstate that corresponds to the eigenenergy the disk is located at. The colored segments of each disk represent the respective bare states. The size of one segment is proportional to the squared overlap of the bare state it represents with the eigenstate represented by the disk. That means for example, that a single-colored disk represents a squared overlap of 1. In Fig. 4.4, this is the case for the zero-excitation state $|\mathrm{g}, 0\rangle$ since it is the only contribution to the eigenstate corresponding to the eigenenergy 0 for all Δ. For $\Delta = 0$, the squared overlaps of the other bare states with the eigenstates are equal to 0.5, such that every bare state contribution is represented by a half-disk. From this result, we build a bridge to the time-dependent dynamics of the JC model. First, we express the bare states with the dressed states by rearranging Eq. (4.14):

$$|\mathrm{g}, n\rangle = N_{n,-} |n, +\rangle + N_{n,+} |n, -\rangle , \tag{4.17a}$$
$$|\mathrm{e}, n-1\rangle = N_{n,+} |n, +\rangle - N_{n,-} |n, -\rangle . \tag{4.17b}$$

The general initial state of a JC model with n being the number of excitations in

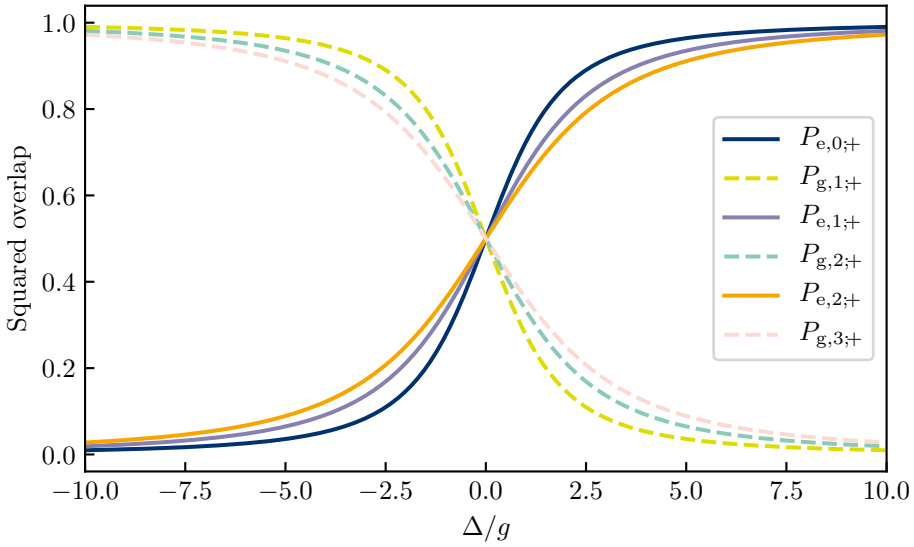

(a) $P_{g,n;+}$, $P_{e,n-1;+}$

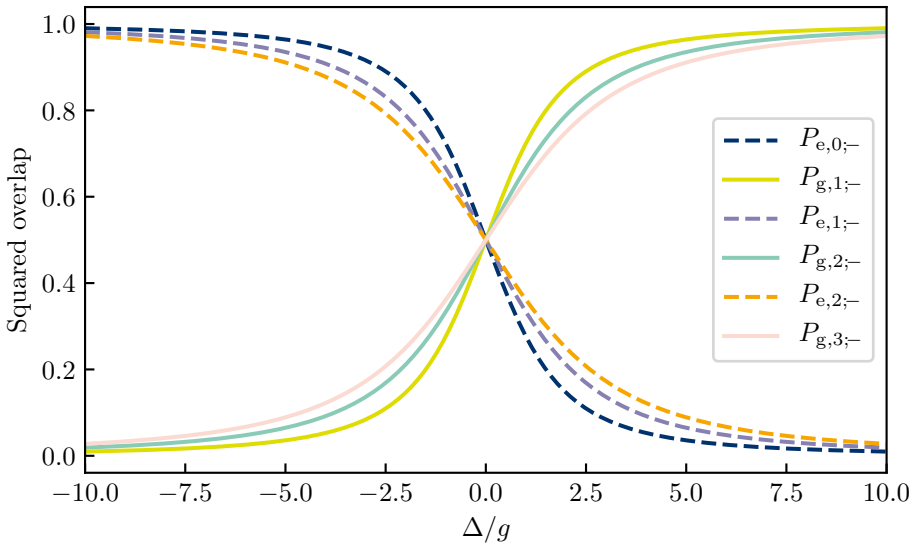

(b) $P_{g,n;-}$, $P_{e,n-1;-}$

Figure 4.3: Squared overlaps in dependence of the detuning Δ. In (a), the dashed (solid) lines represent $P_{e,n-1;-}$ ($P_{g,n;-}$) for $n = 1, 2, 3$ excitations. They are equal to the dashed (solid) lines in (b) that represent $P_{g,n;+}$ ($P_{e,n-1;+}$).

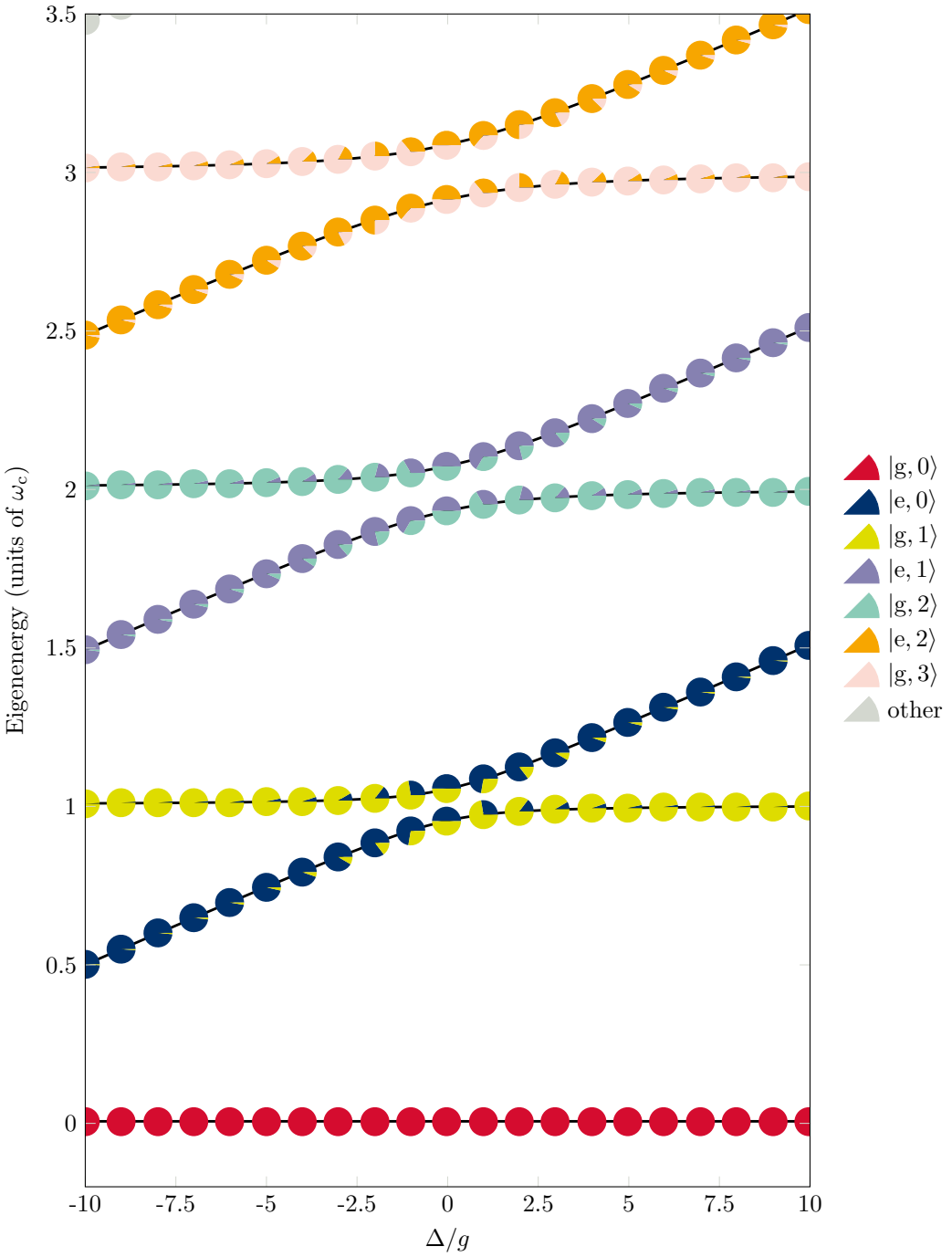

Figure 4.4: Eigensystem of the JC Hamiltonian as a function of the qubit-cavity detuning Δ. The black lines represent the eigenenergies. The colored disks represent the eigenstates to the eigenenergies they are located at. The size of each colored segment of a disk is proportional to the squared overlap of the bare state it represents with the eigenstate represented by the disk. Avoided crossings (anticrossings) appear at $\Delta = 0$ (qubit-cavity resonance).

the system reads

$$\begin{aligned}|\psi(0)\rangle &= \sum_{n=0}^{\infty} \left[c_{\mathrm{g},n}(0)\,|\mathrm{g},n\rangle + c_{\mathrm{e},n}(0)\,|\mathrm{e},n\rangle\right] \\ &= c_{\mathrm{g},0}(0)\,|\mathrm{g},0\rangle + \sum_{n=1}^{\infty} \left[c_{\mathrm{g},n}(0)\,|\mathrm{g},n\rangle + c_{\mathrm{e},n-1}(0)\,|\mathrm{e},n-1\rangle\right].\end{aligned} \tag{4.18}$$

Here, $c_{\mathrm{e},n}(0)$ and $c_{\mathrm{g},n}(0)$ are the initial probability amplitudes. In the Schrödinger picture, the time-dependence of the state $|\psi(t)\rangle$ is given by

$$|\psi(t)\rangle = \mathrm{e}^{-\mathrm{i}Ht}\,|\psi(0)\rangle\,. \tag{4.19}$$

As a consequence, the time-dependent state $|\psi(t)\rangle$ of the JC model with the general initial state given by Eq. (4.18) can be written as

$$|\psi(t)\rangle = c_{\mathrm{g},0}\,|\mathrm{g},0\rangle + \sum_{n=1}^{\infty} \left[c_{\mathrm{g},n}(t)\,|\mathrm{g},n\rangle + c_{\mathrm{e},n-1}(t)\,|\mathrm{e},n-1\rangle\right], \tag{4.20}$$

where $c_{\mathrm{g},0}(t) \equiv c_{\mathrm{g},0} = c_{\mathrm{g},0}(0)$. The probability amplitudes $c_{\mathrm{g},n}(t)$ and $c_{\mathrm{e},n-1}(t)$ are found by substituting the bare with the dressed states, using the eigenvalue equation for the dressed states with the eigenenergies $E_{n,\pm}$, which are given by Eq. (4.12), and substituting back the dressed with the bare states. The result is

$$\begin{aligned}c_{\mathrm{g},n}(t) = \Bigg\{ &\left[\cos\left(\frac{\Omega_n(\Delta)}{2}t\right) + \frac{\mathrm{i}\Delta}{\Omega_n(\Delta)}\sin\left(\frac{\Omega_n(\Delta)}{2}t\right)\right] c_{\mathrm{g},n} \\ &- \frac{\mathrm{i}\Omega_n}{\Omega_n(\Delta)}\sin\left(\frac{\Omega_n(\Delta)}{2}t\right) c_{\mathrm{e},n-1}\Bigg\} \mathrm{e}^{-\mathrm{i}\left(n\omega_\mathrm{c}+\frac{\Delta}{2}\right)t},\end{aligned} \tag{4.21a}$$

$$\begin{aligned}c_{\mathrm{e},n-1}(t) = \Bigg\{ &\left[\cos\left(\frac{\Omega_n(\Delta)}{2}t\right) - \frac{\mathrm{i}\Delta}{\Omega_n(\Delta)}\sin\left(\frac{\Omega_n(\Delta)}{2}t\right)\right] c_{\mathrm{e},n-1} \\ &- \frac{\mathrm{i}\Omega_n}{\Omega_n(\Delta)}\sin\left(\frac{\Omega_n(\Delta)}{2}t\right) c_{\mathrm{g},n}\Bigg\} \mathrm{e}^{-\mathrm{i}\left(n\omega_\mathrm{c}+\frac{\Delta}{2}\right)t},\end{aligned} \tag{4.21b}$$

with $c_{\mathrm{g},n}(0) = c_{\mathrm{g},n}$ and $c_{\mathrm{e},n-1}(0) = c_{\mathrm{e},n-1}$. From this, we obtain the probabilities of measuring the system being in one of the bare states by taking the square of the absolute value of the probability amplitudes $c_{\mathrm{g},n}(t)$ and $c_{\mathrm{e},n-1}(t)$, respectively:

$$P_{\mathrm{g},n}(t) = |c_{\mathrm{g},n}|^2 + \frac{\Omega_n^2}{\Omega_n^2(\Delta)}\left(|c_{\mathrm{e},n-1}|^2 - |c_{\mathrm{g},n}|^2\right)\sin^2\left(\frac{\Omega_n(\Delta)}{2}t\right), \tag{4.22a}$$

$$P_{\mathrm{e},n-1}(t) = |c_{\mathrm{e},n-1}|^2 - \frac{\Omega_n^2}{\Omega_n^2(\Delta)}\left(|c_{\mathrm{e},n-1}|^2 - |c_{\mathrm{g},n}|^2\right)\sin^2\left(\frac{\Omega_n(\Delta)}{2}t\right). \tag{4.22b}$$

For the zero-excitation state, the probability is $P_{g,0}(t) \equiv |c_{\mathrm{g},0}|^2$. The other probabilities are Rabi oscillations with a frequency determined by the generalized Rabi frequency $\Omega_n(\Delta)$. Note that $P_{\mathrm{e},n-1}(t)$ and $P_{\mathrm{g},n}(t)$ are also equivalent to the fidelity. By setting $n = 1$ one gets the vacuum Rabi oscillation, which is shown in Fig. 4.5 for different detunings Δ.

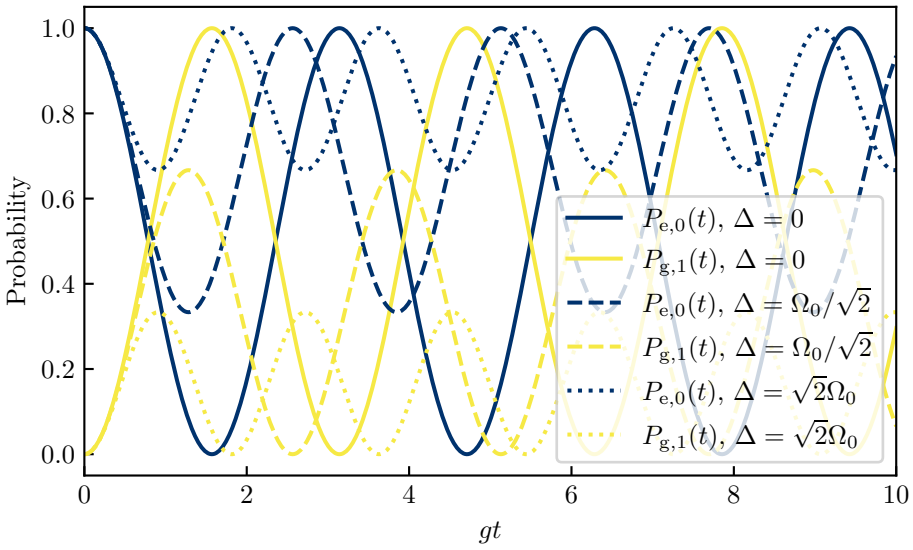

Figure 4.5: Vacuum Rabi oscillations of the probabilities of the system to be in a specific state. Here, we plotted the probabilities $P_{e,0}(t)$ (blue lines) and $P_{g,1}(t)$ (lime green lines) with the initial state $|\psi(0)\rangle = |e, 0\rangle$ for the qubit-cavity detunings $\Delta = 0$ (solid lines), $\Omega_0/\sqrt{2}$ (dashed lines), and $\sqrt{2}\Omega_0$ (dotted lines).

The visibility V_n of an oscillation is defined as the peak-to-peak amplitude. For the expression in Eq. (4.22) it is given by

$$\begin{aligned} V_n &= \left| P_{g,n}(m\pi) - P_{g,n}\left(\frac{2}{\Omega_n(\Delta)}\left[\frac{\pi}{2} + m\pi\right]\right)\right|, \\ &= \left| P_{e,n-1}(m\pi) - P_{e,n-1}\left(\frac{2}{\Omega_n(\Delta)}\left[\frac{\pi}{2} + m\pi\right]\right)\right|, \end{aligned} \tag{4.23}$$

with $m \in \mathbb{Z}$. Here, the visibility is equal for $P_{g,n}(t)$ and $P_{e,n-1}(t)$:

$$V_n = \frac{\Omega_n^2}{\Omega_n^2(\Delta)}\left||c_{e,n-1}|^2 - |c_{g,n}|^2\right|. \tag{4.24}$$

The connection between the visibility given in Eq. (4.24), and the squared overlaps given in Eq. (4.16) is given by

$$\begin{aligned} V_n &= 4P_{g,n;+}P_{e,n-1;+}\left||c_{e,n-1}|^2 - |c_{g,n}|^2\right|, \\ &= 4P_{g,n;-}P_{e,n-1;-}\left||c_{e,n-1}|^2 - |c_{g,n}|^2\right| \end{aligned} \tag{4.25}$$

Considering that $P_{g,n;\pm} + P_{e,n-1;\pm} = 1$, we can see that the visibility reaches its maximum for $P_{e,n-1;\pm} = P_{g,n;\pm} = 0.5$, i.e., when the squared overlaps of the basis states $|g, n\rangle$ and $|e, n-1\rangle$ with the eigenstates $|n, \pm\rangle$ equals 0.5. This implies for the graphical representation in Fig. 4.4 that the highest visibility is obtained, when the basis states $|e, n-1\rangle$ and $|g, n\rangle$ share the same contribution to the filling of the disc on the upper branch $E_{n,+}$ and the lower branch $E_{n,-}$. In Fig. 4.4 this is the case for $\Delta = 0$. Finally, in order to maximize the visibility, the initial state of the JC model must be $|g, n\rangle$ or $|e, n-1\rangle$.

Up to this point, we have seen that Rabi oscillations with a high visibility can be found for two states with one or more excitations in the system. However, it is

possible to generate Rabi oscillations for the zero-excitation state and an excited cavity-qubit state by introducing a coherent pump, which generates excitations in the system.

4.2.3 Influence of qubit pumping on the Jaynes–Cummings Hamiltonian

We now investigate the influence of coherently pumping the qubit with and without cavity-qubit interaction. We extend the JC Hamiltonian in Eq. (4.9) with the driving Hamiltonian H_d:

$$H = H_\mathrm{JC} + H_\mathrm{d}. \tag{4.26}$$

It is given by

$$H_\mathrm{d} = 2\varepsilon_\mathrm{q}\cos(\omega_\mathrm{d}t)\left(\sigma^+ + \sigma^-\right), \tag{4.27}$$

where ε_q is the strength and ω_d is the frequency of the pump.

The time-dependence of H_d can be eliminated by going into the rotating frame of the qubit drive. In order to do this, we apply a unitary transformation operator:

$$U = \exp\left[\mathrm{i}\omega_\mathrm{d}t\left(\sigma^+\sigma^- + a^\dagger a\right)\right]. \tag{4.28}$$

From the unitary transformation $H \mapsto U(H - \mathrm{i}\partial_t)U^\dagger$ (see Appendix A) we obtain

$$H = \Delta_\mathrm{qd}\sigma^+\sigma^- + \Delta_\mathrm{cd}a^\dagger a + H_\mathrm{c,q} + \varepsilon_\mathrm{q}\left[\sigma^+\left(\mathrm{e}^{2\mathrm{i}\omega_\mathrm{d}t}+1\right) + \sigma^-\left(\mathrm{e}^{-2\mathrm{i}\omega_\mathrm{d}t}+1\right)\right], \tag{4.29}$$

where $\Delta_\mathrm{qd} = \omega_\mathrm{q} - \omega_\mathrm{d}$ ($\Delta_\mathrm{cd} = \omega_\mathrm{c} - \omega_\mathrm{d}$) is the detuning between the qubit (cavity) and the pump. We neglect fast rotating terms of the form $\mathrm{e}^{2\mathrm{i}\omega_\mathrm{d}t}\sigma^+$ and get the time-independent Hamiltonian

$$H = \Delta_\mathrm{qd}\sigma^+\sigma^- + \Delta_\mathrm{cd}a^\dagger a + g\left(a^\dagger\sigma^- + a\sigma^+\right) + \epsilon_\mathrm{d}\left(\sigma^+ + \sigma^-\right). \tag{4.30}$$

In the JC model, anticrossings occurs only between the eigenstates $|E_{n,+}\rangle$ and $|E_{n,-}\rangle$ for each $n \in \mathbb{N}_0$ at $\Delta = 0$, in other words, when the qubit and the cavity are in resonance ($\omega_\mathrm{q} = \omega_\mathrm{d}$). The coherent qubit pump generates anticrossings between all eigenenergies, including the eigenenergy of the zero-excitation state. Besides the anticrossings at $\Delta = 0$, the most dominant are at $\Delta = -\Delta_\mathrm{qd}$, where the qubit and the pump are in resonance ($\omega_\mathrm{q} = \omega_\mathrm{d}$). Furthermore, the eigenstates carry contributions of all basis states, as shown in Fig. 4.6. This implies that it is possible to drive the cavity-qubit system from the zero-excitation state into any other state with n excitation. However, the corresponding Rabi frequencies are reduced on the order in Δ/g [32] which significantly reduces the attainable amplitudes.

In order to get a better insight into the effect of the qubit drive, we neglect the cavity and focus on the qubit. Similarly to the cavity-qubit interaction, the coherent pump splits the eigenenergies at $\Delta_\mathrm{qd} = 0$, where the qubit and the pump are in resonance. This causes Rabi oscillation with the frequency $2\epsilon_\mathrm{q}$, which is derived equivalently to the previous discussion for Ω_n. Let us now consider a time-dependent pump strength: $\varepsilon_\mathrm{q} \to \varepsilon_\mathrm{q}(t)$. Such a time dependence occurs for example when the qubits are pulsed.

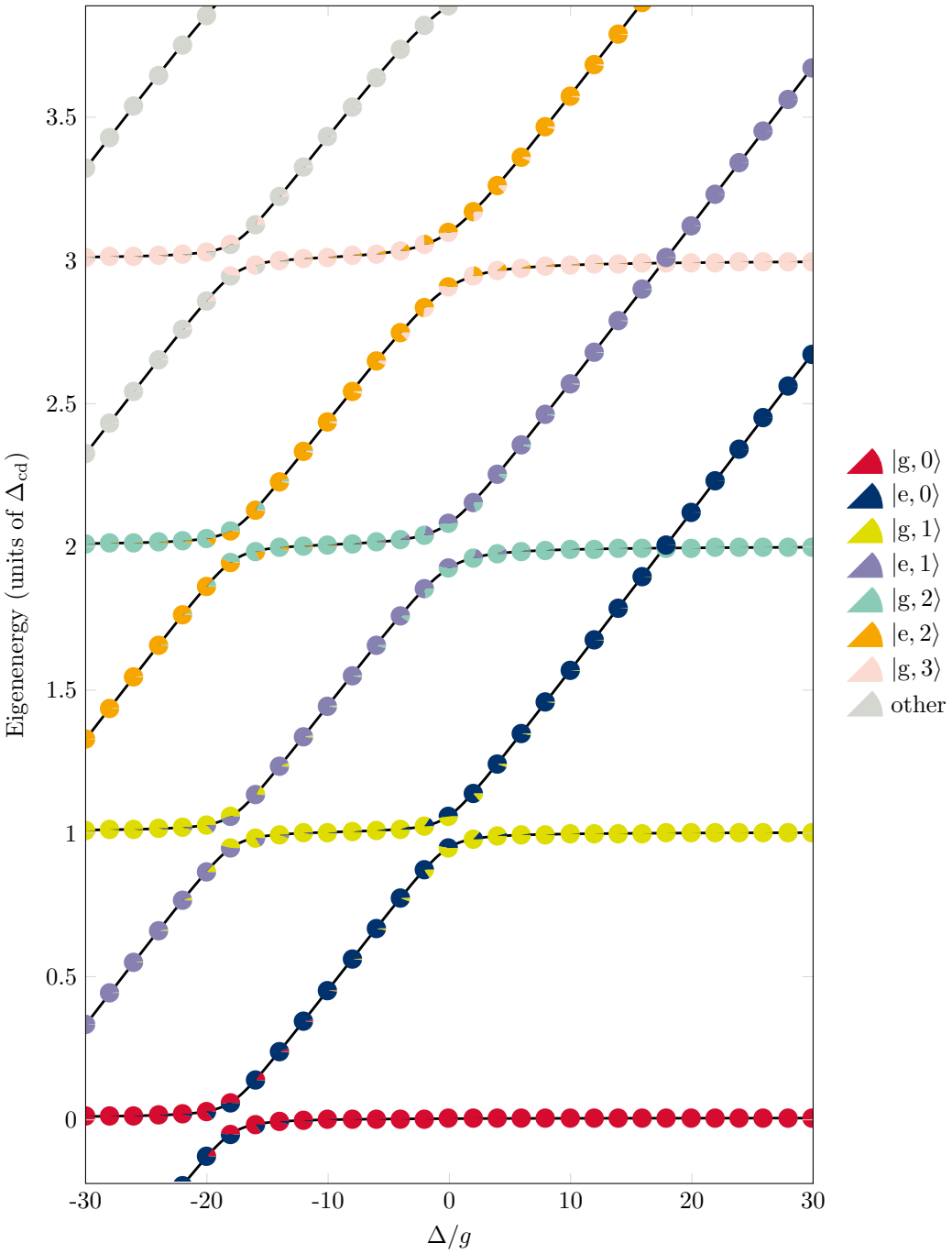

Figure 4.6: Eigensystem of the JC Hamiltonian including a coherent qubit pump as a function of the qubit-cavity detuning Δ. The gray lines represent the eigenenergies. The colored disks represent the eigenstates to the eigenenergies they are located at. The size of each colored segment of a disk is proportional to the squared overlap of the bare state it represents with the eigenstate represented by the disk. Compared to Fig. 4.4, the additional coherent qubit pump generates anticrossings between all eigenenergies. The most dominant are at $\Delta = 0$ (qubit-cavity resonance) and $\Delta = -\Delta_{cd}$ (qubit-pump resonance).

The interaction of a single qubit which interacts with a light pulse can be described by the JC Hamiltonian in RWA with a time-dependent pump strength:

$$H(t) = \Delta_{\mathrm{qd}}\sigma^{+}\sigma^{-} + \varepsilon_{\mathrm{q}}(t)\left(\sigma^{+} + \sigma^{-}\right). \tag{4.31}$$

In the interaction picture, the qubit-drive Hamiltonian is given by

$$H_{\mathrm{d,I}}(t) = \varepsilon_{\mathrm{q}}(t)\left(\sigma^{+}\mathrm{e}^{\mathrm{i}\Delta_{\mathrm{qd}}t} + \sigma^{-}\mathrm{e}^{-\mathrm{i}\Delta_{\mathrm{qd}}t}\right). \tag{4.32}$$

The general form of a qubit state in the interaction picture is

$$|\psi_{\mathrm{I}}(t)\rangle = c_{\mathrm{g}}(t)\,|\mathrm{g}\rangle + c_{\mathrm{e}}(t)\,|\mathrm{e}\rangle\,. \tag{4.33}$$

From the equation $\mathrm{i}\frac{\mathrm{d}}{\mathrm{d}t}|\psi_{\mathrm{I}}(t)\rangle = H_{\mathrm{d,I}}(t)\,|\psi_{\mathrm{I}}(t)\rangle$, which describes the time-evolution of a state in the interaction picture, one finds two coupled differential equations for the coefficients $c_{\mathrm{g}}(t)$ and $c_{\mathrm{e}}(t)$:

$$\begin{aligned} \mathrm{i}\dot{c}_{\mathrm{g}}(t) &= \varepsilon_{\mathrm{q}}(t)\mathrm{e}^{-\mathrm{i}\Delta_{\mathrm{qd}}t}c_{\mathrm{e}}(t), \\ \mathrm{i}\dot{c}_{\mathrm{e}}(t) &= \varepsilon_{\mathrm{q}}(t)\mathrm{e}^{\mathrm{i}\Delta_{\mathrm{qd}}t}c_{\mathrm{g}}(t). \end{aligned} \tag{4.34}$$

If the qubit and pump are in resonance ($\Delta_{\mathrm{qd}} = 0$), this differential equation system can be solved analytically by substituting the time variable t with the pulse area up to time t given by

$$\theta(t) = \int_{t_0}^{t} \mathrm{d}t'\Omega(t'), \tag{4.35}$$

where $\Omega(t) = 2\varepsilon_{\mathrm{q}}(t)$ is the Rabi frequency and t_0 the initial time of the pulse [97, 98]. Note that the pulse area $\Theta = \lim_{t\to\infty}\theta(t)$ is twice the area under the curve of the function $\varepsilon_{\mathrm{q}}(t)$. The general solution of the differential equation system is given by

$$\begin{aligned} c_{\mathrm{g}}(t) &= \cos\left(\frac{\theta(t)}{2}\right)c_{\mathrm{g}}(t_0) - \mathrm{i}\sin\left(\frac{\theta(t)}{2}\right)c_{\mathrm{e}}(t_0), \\ c_{\mathrm{e}}(t) &= \cos\left(\frac{\theta(t)}{2}\right)c_{\mathrm{e}}(t_0) - \mathrm{i}\sin\left(\frac{\theta(t)}{2}\right)c_{\mathrm{g}}(t_0), \end{aligned} \tag{4.36}$$

for $\Delta_{\mathrm{qd}} = 0$, where $c_{\mathrm{g}}(t_0)$ and $c_{\mathrm{e}}(t_0)$ are the initial conditions [95, 97]. Suppose a qubit that is initially in the ground state, which is the case if $c_{\mathrm{g}}(t_0) = 1$ and $c_{\mathrm{e}}(t_0) = 0$, for example, then $c_{\mathrm{g}}(t) = \cos(\theta(t)/2)$ and $c_{\mathrm{e}}(t) = -\mathrm{i}\sin(\theta(t)/2)$. Further, we want the qubit to be in its excited state after pumping it with a pulse, meaning we seek $\lim_{t\to\infty} c_{\mathrm{g}}(t) = 0$ and $\lim_{t\to\infty}|c_{\mathrm{e}}(t)|^2 = 1$. This is obtained if $\Theta = \pi$, thus if the area under the curve of the function $\varepsilon_{\mathrm{q}}(t)$ is $\pi/2$. The final state of the qubit after a pulse does not depend on its shape, but on its pulse area Θ. Let the period of a given Rabi cycle of a coherently pumped qubit be $T = 2\pi/\Omega$, with $\Omega = 2\varepsilon_{\mathrm{q}}$, where ε_{q} is the strength of the qubit pump. The time it takes for the probability to measure the qubit in the excited state to change from 0 to 1 is then $\Delta t = T/2$. We consider a rectangular pulse, whose strength is ε_{q} during the time interval Δt and 0 else. In order to generate the excited qubit state, the time interval Δt, in other words the width of the rectangular pulse, has to be $\Delta t = T/2$. The area under the curve of the rectangular function of the pulse is then actually $\varepsilon_{\mathrm{q}}\Delta t = \pi/2$, i.e., its pulse area is $\Theta = \pi$. We see, that the effect of a given pulse is specified by pulse area Θ. Figure 4.7 shows the effect of pulses with three different pulse areas. A $\pi/2$

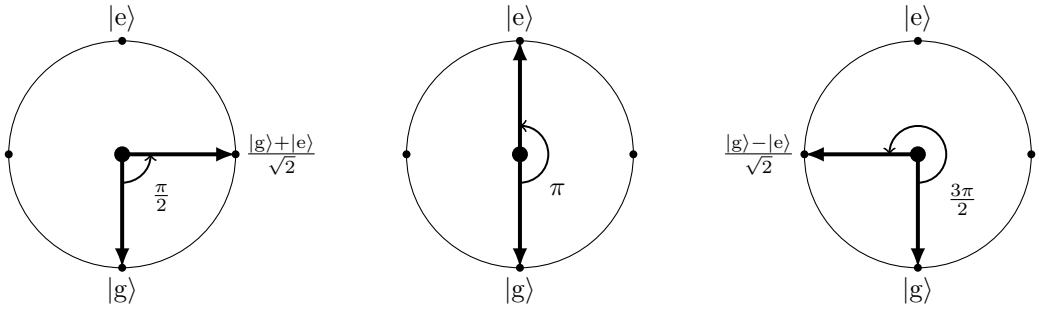

(a) $\pi/2$ pulse (b) π pulse (c) $3\pi/2$ pulse

Figure 4.7: Pumping the Bloch vector of a qubit from the ground state $|\mathrm{g}\rangle$ with pulses of different pulse ares. The system is pumped (a) with a $\pi/2$ pulse into the superposition state $(|\mathrm{g}\rangle + |\mathrm{e}\rangle)/\sqrt{2}$, (b) with a π pulse into the excited state $|\mathrm{e}\rangle$, and (c) with a $3\pi/2$ pulse into the superposition state $(|\mathrm{g}\rangle - |\mathrm{e}\rangle)/\sqrt{2}$.

pulse rotates the Bloch vector of the qubit by an angle of $\pi/2$, therefore the system will be in the superposition state $(|\mathrm{g}\rangle + |\mathrm{e}\rangle)/\sqrt{2}$. A π pulse drives the system from the ground state to the excited state [94]. A $3\pi/2$ pulse generated the superposition state $(|\mathrm{g}\rangle - |\mathrm{e}\rangle)/\sqrt{2}$.

In this section we have considered the external excitation of the qubits, which is an appropriate description, e.g., for optical excitation of micropillar laser arrays [41]. However, the pumping of cavity photons instead is unitarily equivalent up to a scaling factor, as we show in Appendix B.

4.3 Dissipation processes

In experimental setups, any quantum system is interacting with its environment. These systems are referred to as open quantum systems. One approach to describe such open quantum systems theoretically is to work with the Lindblad master equation. In the following, we provide a general derivation of the system-environment coupling leading to the commonly used Lindblad form in Born–Markov approximation.

The Hamiltonian of a total system, where a given system $\mathcal{S}$ is coupled to an environment $\mathcal{E}$, is assumed to be

$$H_{\mathrm{tot}} = H_{\mathcal{S}} + H_{\mathcal{E}} + H_{\mathrm{int}}, \tag{4.37}$$

where $H_{\mathcal{S}}$ and $H_{\mathcal{E}}$ are the free Hamiltonians of the system $\mathcal{S}$ and the environment $\mathcal{E}$, respectively, and H_{int} describes the interaction between the system and the environment. The time evolution of the total density operator ρ_{tot} is given by the von Neumann equation ($\hbar = 1$):

$$\mathrm{i}\frac{\mathrm{d}}{\mathrm{d}t}\rho_{\mathrm{tot}} = [H_{\mathrm{tot}}, \rho_{\mathrm{tot}}]\,, \tag{4.38}$$

where $[A, B] = AB - BA$ defines the commutator of two operators A and B. The total density operator in the interaction picture is given by

$$\rho_{\text{tot}}^{(\text{I})}(t) = \mathrm{e}^{\mathrm{i}H_0 t}\rho_{\text{tot}}(t)\mathrm{e}^{-\mathrm{i}H_0 t}, \tag{4.39}$$

where $H_0 = H_{\mathcal{S}} + H_{\mathcal{E}}$ is the free Hamiltonian of the total system. The time-derivative of the total density operator in the interaction picture is given by

$$\mathrm{i}\frac{\mathrm{d}}{\mathrm{d}t}\rho_{\text{tot}}^{(\text{I})}(t) = \left[H_{\text{int}}(t), \rho_{\text{tot}}^{(\text{I})}(t)\right]. \tag{4.40}$$

The time evolution of the total density operator in the interaction picture therefore only depends on the interaction Hamiltonian $H_{\text{int}}(t)$ in the interaction picture. An important assumption is that there are no correlations between the system and the environment at the initial time $t = 0$, i.e.,

$$\rho_{\text{tot}}^{(\text{I})}(0) = \rho_{\text{tot}}(0) = \rho_{\mathcal{S}}(0) \otimes \rho_{\mathcal{E}}(0). \tag{4.41}$$

Here, $\rho_{\mathcal{S}}$ and $\rho_{\mathcal{E}}$ are the reduced density operators of the system $\mathcal{S}$ and the environment $\mathcal{E}$, respectively. Usually, one is not interested in the time evolution of the total system but on the system $\mathcal{S}$ which is described by the reduced density operator $\rho_{\mathcal{S}}(t)$. It can be derived by taking the partial trace of the total density operator $\rho_{\text{tot}}(t)$ over the degrees of the environment $\mathcal{E}$:

$$\rho_{\mathcal{S}}(t) = \mathrm{tr}_{\mathcal{E}}\left[\rho_{\text{tot}}(t)\right]. \tag{4.42}$$

In order to derive a master equation whose solution yields the reduced density matrix only of the system one has to make three approximations [99, 100, 101].

1. **Born approximation**: The coupling between the system and the environment is assumed to be weak and the environment is assumed to be reasonably large compared to the system. As a result, the total density operator should only consist of terms of order H_{int}. In the Born approximation terms higher than second order in H_{int} are neglected due to the weak coupling. Thus, the total density operator remains a product state and the time evolution of the density operator of the environment can be neglected:

$$\rho_{\text{tot}}(t) = \rho_{\mathcal{S}}(t) \otimes \rho_{\mathcal{E}} + \mathcal{O}(H_{\text{int}}) \approx \rho_{\mathcal{S}}(t) \otimes \rho_{\mathcal{E}} \quad \forall t \geq 0. \tag{4.43}$$

2. **Markov approximation**: The time-scale $\tau_{\mathcal{E}}$ of the environment is short compared to time-scale $\tau_{\mathcal{S}}$ of the system: $\tau_{\mathcal{E}} \ll \tau_{\mathcal{S}}$. Any memory effects of the environment are therefore negligible. This makes the master equation local in time and independent of earlier times.

3. **Rotating wave approximation (RWA)**: Frequency differences occurring in the given problem are small compared to the time-scale of the system: $|\omega' - \omega| \ll \tau_{\mathcal{S}}^{-1}$. As a consequence, all terms proportional to the fast rotating wave $\exp[\mathrm{i}(\omega' - \omega)t]$ for $\omega' \neq \omega$ can be neglected.

The general form of the Lindblad master equation for an N-dimensional system is given by [100, 101]

$$\frac{\mathrm{d}}{\mathrm{d}t}\rho_{\mathcal{S}} = \mathrm{i}\left[H'_{\mathcal{S}}, \rho_{\mathcal{S}}\right] + \frac{1}{2}\sum_{n=1}^{N^2-1}\gamma_n\left(2L_n\rho_{\mathcal{S}}L_n^\dagger - \rho_{\mathcal{S}}L_n^\dagger L_n - L_n^\dagger L_n\rho_{\mathcal{S}}\right). \tag{4.44}$$

Here, $H'_{\mathcal{S}}$ is the renormalization due to the coupling of the system and the environment which is often called Lamb shift [101, 100]. The operators L_n form an orthonormal basis on the system's Hilbert space. The eigenvalues γ_n are called decay rates. By introducing the collapse operators $C_n = \sqrt{\gamma_n} L_n$ and neglecting the Lamb shift, the Lindblad master equation takes the form

$$\frac{\mathrm{d}}{\mathrm{d}t}\rho_{\mathcal{S}} = -\mathrm{i}\left[H_{\mathcal{S}}, \rho_{\mathcal{S}}\right] + \frac{1}{2}\sum_n \left[2C_n\rho_{\mathcal{S}}C_n^\dagger - \left\{C_n^\dagger C_n, \rho_{\mathcal{S}}\right\}\right], \tag{4.45}$$

where $\{A, B\} = AB + BA$ defines the anti-commutator of two operators A and B.

We consider three kinds of dissipation processes, cavity decay, qubit dissipation, and pure dephasing. Cavity decay is the loss of photons from the cavity. The cause of this can be for example the imperfect reflectivity of the mirrors the cavity it is made of. Qubit dissipation is the relaxation of an excited qubit falling into its ground state by emitting a photon into free space modes. This relaxation process is the result of spontaneous emission into modes other than the resonant cavity mode. Pure dephasing is the main mechanism of decay of quantum correlations without changing the population of the system and originates from the coupling between the quantum system and its environment [102].

We consider these dissipative processes in terms of the Lindblad master equation,

$$\frac{\mathrm{d}}{\mathrm{d}t}\rho = \mathcal{L}\rho \equiv -\mathrm{i}[H, \rho] + \sum_n \mathcal{D}[C_n]\rho, \tag{4.46}$$

with the (non-unitary) Liouvillian superoperator $\mathcal{L}$ and the Lindblad dissipators

$$\mathcal{D}[C_n]\rho \equiv \frac{1}{2}\left(C_n\rho C_n^\dagger - C_n^\dagger C_n\rho + \text{h.c.}\right), \tag{4.47}$$

where $C_n = \sqrt{\gamma_n} A_n$ are the collapse operators with an operator A_n that couples the system to an environment at rate γ_n.

For our model of a CCA we consider three different dissipation processes, which are firstly the dissipation of the qubit energy, secondly the loss of cavity-photons, and thirdly the pure dephasing of the qubits. The respective collapse operators are given by

$$C_{\gamma,i} = \sqrt{\gamma}\sigma_i^-, \quad C_{\kappa,i} = \sqrt{\kappa}a_i, \quad C_{\gamma_\phi,i} = \sqrt{\gamma_\phi}\sigma_i^z, \tag{4.48}$$

where γ, κ, and γ_ϕ are the corresponding dissipation rates.

Chapter 5

Coupled-cavity arrays and entanglement generation

In the previous chapter we examined the energy spectrum of the Jaynnes-Cummings model, which consists of an optical resonator with a two-level atom inside, and introduced a novel graphical representation of the eigenstates and eigenenergies in a single diagram. We extended this model by an optical coherent drive and examined how this helps to drive the given system from the zero-excitation state into an excited state with an optical pulse. In this chapter we introduce a system of N cavity-qubit systems, where the cavities are coupled to each other. The photon-hopping within such a coupled-cavity array (CCA) can experimentally be realized via photonic waveguides [103]. We focus on CCAs, because systems like homogenous quantum dot micropillar cavities are a promising platform for realizing optical reservoir computing [104]. We begin by giving an overview of the formalism on how to drive specific entangled target states before presenting numerical results and analytic insights.

5.1 Model of a coupled-cavity array

We consider a symmetric system consisting of N coupled cavities, each of them containing one qubit, as shown in Fig. 5.1 for $N = 2$. We extend the JC Hamiltonian

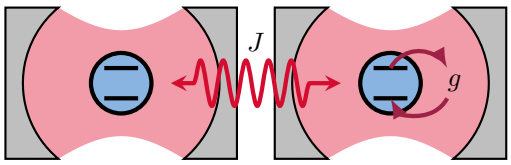

Figure 5.1: Two coupled cavities with the interaction strength J. Each cavity contains a qubit it interacts with. The interaction between the cavities and the qubits is described by the Jaynes–Cummings model with the light-matter interaction strength g.

in Eq. (4.9) with a cavity-cavity coupling term. The physical cause of this extra coupling is the overlap of the photonic field modes in the adjacent cavities [105]. When the spatial distance between the two cavities is short enough so that the field

modes overlap (see Fig. 5.2), photon-hopping from one to the other cavity can occur [50]. The Hamiltonian of a coupled-cavity array is given by

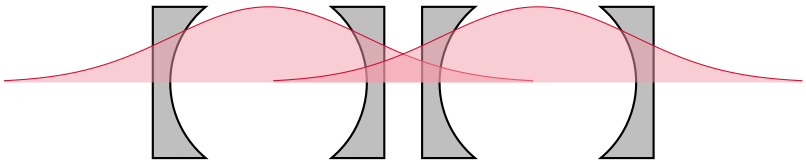

Figure 5.2: Two spatially separated cavities, which are coupled due to the overlap of their field modes.

$$H = H_{\mathrm{q}} + H_{\mathrm{c}} + H_{\mathrm{c,q}} + H_{\mathrm{c,c}}. \tag{5.1}$$

The first term of Eq. (5.1) is the qubit Hamiltonian

$$H_{\mathrm{q}} = \sum_{i=1}^{N} \omega_{\mathrm{q}} \sigma_i^+ \sigma_i^-. \tag{5.2}$$

The Pauli matrices σ_i^x, σ_i^y, and σ_i^z only act on the i-th qubit. Thus, $[\sigma_i^a, \sigma_j^b] = 2\mathrm{i}\delta_{ij}\epsilon_{abc}\sigma_i^c$, where $a, b, c \in \{x, y, z\}$ and $i, j \in \{1, 2\}$. The same applies to the raising operators $\sigma_i^+ = (\sigma_i^x + \mathrm{i}\sigma_i^y)/2$ and the lowering operators $\sigma_i^- = (\sigma_i^x - \mathrm{i}\sigma_i^y)/2$, i.e., $[\sigma_i^+, \sigma_j^-] = \delta_{ij}\sigma_i^z$ and $[\sigma_i^z, \sigma_j^\pm] = \pm 2\delta_{ij}\sigma_i^\pm$. The second term is the cavity Hamiltonian

$$H_{\mathrm{c}} = \sum_{i=1}^{N} \omega_{\mathrm{c}} a_i^\dagger a_i. \tag{5.3}$$

The creation operator $a_i^\dagger$ and the annihilation operator $\hat{a}_i$ only act on the i-th cavity-photon. They fulfill the relation $[a_i^\dagger, a_j] = \delta_{ij}$. The third term is the cavity-qubit coupling Hamiltonian in the RWA:

$$H_{\mathrm{c,q}} = \sum_{i=1}^{N} g \left(a_i^\dagger \sigma_i^- + a_i \sigma_i^+ \right). \tag{5.4}$$

The last term of Eq. (5.1) is the Hamiltonian that describes the photon-hopping between the cavities:

$$H_{\mathrm{c,c}} = -J \sum_{\langle i,j \rangle} \left(a_i^\dagger a_j + a_i a_j^\dagger \right), \tag{5.5}$$

where J is the strength of the cavity-cavity coupling, given by the overlap of the field modes. The sum runs over all cavity-cavity pairs $\langle i, j \rangle$ with $i \neq j$. For the qubit subsystem we use basis states $|q_1\rangle \otimes |q_2\rangle \otimes \cdots \equiv |q_1 q_2 \ldots\rangle$, where $q_i \in \{\mathrm{g}, \mathrm{e}\}$ denotes the state of the i-th qubit. Analogously, we define the cavity-photon basis states $|n_1\rangle \otimes |n_2\rangle \otimes \cdots \equiv |n_1 n_2 \ldots\rangle$, where $n_i = 0, 1, 2, \ldots$ denotes the number of photons in the i-th cavity. For the whole cavity-qubit system the basis states are $|q_1 q_2 \ldots\rangle \otimes |n_1 n_2 \ldots\rangle \equiv |q_1 q_2 \ldots, n_1 n_2 \ldots\rangle$.

5.2 Two coupled cavity-qubit systems

For a system with two cavity-qubit subsystems, i.e., $N = 2$, the qubit subspace is spanned by the orthonormal basis $\{|ee\rangle, |eg\rangle, |ge\rangle, |gg\rangle\}$. An alternative orthonormal basis that we will use is $\{|ee\rangle, |\mathrm{T}\rangle, |\mathrm{S}\rangle, |gg\rangle\}$, where $|\mathrm{T}\rangle = (|eg\rangle + |ge\rangle)/\sqrt{2}$ $|\mathrm{S}\rangle = (|eg\rangle - |ge\rangle)/\sqrt{2}$ are the antisymmetric singlet and the symmetric triplet state, respectively. They are two of the four Bell states, which are maximally entangled. A cavity-photon subsystem with maximally one photon per cavity has the basis $\{|11\rangle, |10\rangle, |01\rangle, |00\rangle\}$. Similar to the qubit basis, we choose for the cavity photons $\{|11\rangle, |\mathrm{T_p}\rangle, |\mathrm{S_p}\rangle, |00\rangle\}$, where $|\mathrm{T_p}\rangle = (|10\rangle + |01\rangle)/\sqrt{2}$ $|\mathrm{S_p}\rangle = (|10\rangle - |01\rangle)/\sqrt{2}$. Due to the infinitely large matrix representation of the full coupled-cavity array, it is necessary to restrict the number of photons per cavity. Additionally we divide the Hilbert space of the full system into subspaces, where each subspace is characterized by the number of total excitations in the system. For a bipartite system ($N = 2$), a subspace with m excitations has a basis with $4m$ ($m = 1, 2, 3, \dots$) basis states (see Appendix C). Because the Hamiltonian H in Eq. (5.1) does not include any term that changes the number of excitations, the subspaces are decoupled. The one dimensional subspace with zero excitations has only one basis state, namely the zero-excitation state $|gg, 00\rangle$ with the eigenenergy $E_{gg,00} = 0$. For the subspace with one excitation we work with the four dimensional basis $\{|\mathrm{T}, 00\rangle, |gg, \mathrm{T_p}\rangle, |\mathrm{S}, 00\rangle, |gg, \mathrm{S_p}\rangle\}$.

For an easier usage of this basis we rewrite the Hamiltonian H by introducing operators, which act on symmetric and antisymmetric states, respectively. The annihilation operator for the symmetric (antisymmetric) mode ω_c^- (ω_c^+) with $\omega_\mathrm{c}^\pm = \omega_\mathrm{c} \pm J$ is defined as $A = (a_1 + a_2)/\sqrt{2}$ $[a = (a_1 - a_2)/\sqrt{2}]$. In a similar way the annihilation operator for the symmetric (antisymmetric) qubit states is defined as $\Sigma = (\sigma_1^- + \sigma_2^-)/\sqrt{2}$ $[\sigma = (\sigma_1^- - \sigma_2^-)/\sqrt{2}]$. Thus, the qubit Hamiltonian and the cavity-qubit coupling Hamiltonian can be written as

$$H_\mathrm{q} = \omega_\mathrm{q} \left(\Sigma^\dagger \Sigma + \sigma^\dagger \sigma\right), \tag{5.6}$$

and

$$H_\mathrm{c,q} = g \left(A^\dagger \Sigma + a^\dagger \sigma + A \Sigma^\dagger + a \sigma^\dagger\right), \tag{5.7}$$

respectively. The sum of the cavity Hamiltonian and the cavity-cavity coupling Hamiltonian can be written as

$$H_\mathrm{c} + H_\mathrm{c,c} = \omega_\mathrm{c}^- A^\dagger A + \omega_\mathrm{c}^+ a^\dagger a. \tag{5.8}$$

The matrix representation of the Hamiltonian for the subsystem with one excitation is given by

$$H^{(1)} = \begin{bmatrix} \omega_\mathrm{q} & g & 0 & 0 \\ g & \omega_\mathrm{c}^- & 0 & 0 \\ 0 & 0 & \omega_\mathrm{q} & g \\ 0 & 0 & g & \omega_\mathrm{c}^+ \end{bmatrix}, \tag{5.9}$$

As we can see, this block matrix is dived into two 2×2 submatrices, one for the symmetric states ($|\mathrm{T}, 00\rangle$ and $|gg, \mathrm{T_p}\rangle$) and one for the antisymmetric states ($|\mathrm{S}, 00\rangle$ and $|gg, \mathrm{S_p}\rangle$). The symmetry refers to the exchange of the single cavity-qubit systems. The division into two submatrices means that the parity is conserved in our system.

Both 2×2 submatrices of the block matrix $H^{(1)}$ can be treated as singe JC Hamiltonians. Thus, the we find for the four eigenenergies of $H^{(1)}$:

$$E_{T,\pm} = \left[\omega_{\mathrm{c}}^{-} + \frac{1}{2}(\Delta + J)\right] \pm \frac{1}{2}\Omega_{\mathrm{T}}(\Delta), \tag{5.10a}$$

$$E_{S,\pm} = \left[\omega_{\mathrm{c}}^{+} + \frac{1}{2}(\Delta - J)\right] \pm \frac{1}{2}\Omega_{\mathrm{S}}(\Delta), \tag{5.10b}$$

where $\Omega_{\mathrm{T}}(\Delta) = \sqrt{\Omega_1^2 + (\Delta + J)^2}$ [$\Omega_{\mathrm{S}}(\Delta) = \sqrt{\Omega_1^2 + (\Delta - J)^2}$] is the generalized Rabi frequency of the symmetric (antisymmetric) states and $\Omega_1 = 2g$ [cf. Eq. (4.13)]. The four corresponding eigenstates are given by

$$|E_{\mathrm{T},\pm}\rangle = N_{\mathrm{T},\mp} |\mathrm{gg}, \mathrm{T_p}\rangle \pm N_{\mathrm{T},\pm} |\mathrm{T}, 00\rangle , \tag{5.11a}$$

$$|E_{\mathrm{S},\pm}\rangle = N_{\mathrm{S},\mp} |\mathrm{gg}, \mathrm{S_p}\rangle \pm N_{\mathrm{S},\pm} |\mathrm{S}, 00\rangle , \tag{5.11b}$$

where

$$N_{T,\pm} = \frac{1}{\sqrt{2}} \left(1 \pm \frac{\Delta + J}{\sqrt{(\Delta + J)^2 + \Omega_1^2}}\right)^{\frac{1}{2}}, \tag{5.12a}$$

$$N_{S,\pm} = \frac{1}{\sqrt{2}} \left(1 \pm \frac{\Delta - J}{\sqrt{(\Delta - J)^2 + \Omega_1^2}}\right)^{\frac{1}{2}}. \tag{5.12b}$$

The conservation of the parity can also bee seen for the block matrix that represents the Hamiltonian of the subspace with two excitations in the CCA. First, we introduce the so-called NOON states, which are defined as

$$|\Psi_{N,\pm}\rangle = \frac{1}{\sqrt{2}} \left(|N, 0\rangle \pm |0, N\rangle\right). \tag{5.13}$$

That definition represents an entangled bosonic state with N particles. We will use these states to combine the states $|\mathrm{gg}, 20\rangle$ and $|\mathrm{gg}, 02\rangle$ to the symmetric state $|\Psi_{2,+}\rangle$ and the antisymmetric state $|\Psi_{2,-}\rangle$. With these, our the basis for the two excitation subspace is $\{|\mathrm{ee}, 00\rangle , |\mathrm{gg}, 11\rangle , |\mathrm{T}, \mathrm{T_p}\rangle , |\mathrm{S}, \mathrm{S_p}\rangle , |\mathrm{gg}, \Psi_{2,+}\rangle , |\mathrm{T}, \mathrm{S_p}\rangle , |\mathrm{S}, \mathrm{T_p}\rangle , |\mathrm{gg}, \Psi_{2,-}\rangle\}$. The first five basis states are symmetric, the last three are antisymmetric. With this basis the matrix representation of the Hamiltonian for the two-excitation subspace is given by

$$H^{(2)} = \begin{bmatrix} 2\omega_{\mathrm{q}} & 0 & g & -g & 0 & 0 & 0 & 0 \\ 0 & 2\omega_{\mathrm{c}} & g & -g & -2J & 0 & 0 & 0 \\ g & g & \omega_{\mathrm{c}}^{-} + \omega_{\mathrm{q}} & 0 & g & 0 & 0 & 0 \\ -g & -g & 0 & \omega_{\mathrm{c}}^{+} + \omega_{\mathrm{q}} & g & 0 & 0 & 0 \\ 0 & -2J & g & g & 2\omega_{\mathrm{c}} & 0 & 0 & 0 \\ 0 & 0 & 0 & 0 & 0 & \omega_{\mathrm{c}}^{+} + \omega_{\mathrm{q}} & 0 & g \\ 0 & 0 & 0 & 0 & 0 & 0 & \omega_{\mathrm{c}}^{-} + \omega_{\mathrm{q}} & g \\ 0 & 0 & 0 & 0 & 0 & g & g & 2\omega_{\mathrm{c}} \end{bmatrix} \tag{5.14}$$

A joint representation of the eigenenergies and eigenstates of the full Hamiltonian for zero, one, and two excitations without driving the qubits is shown in Fig. 5.3.

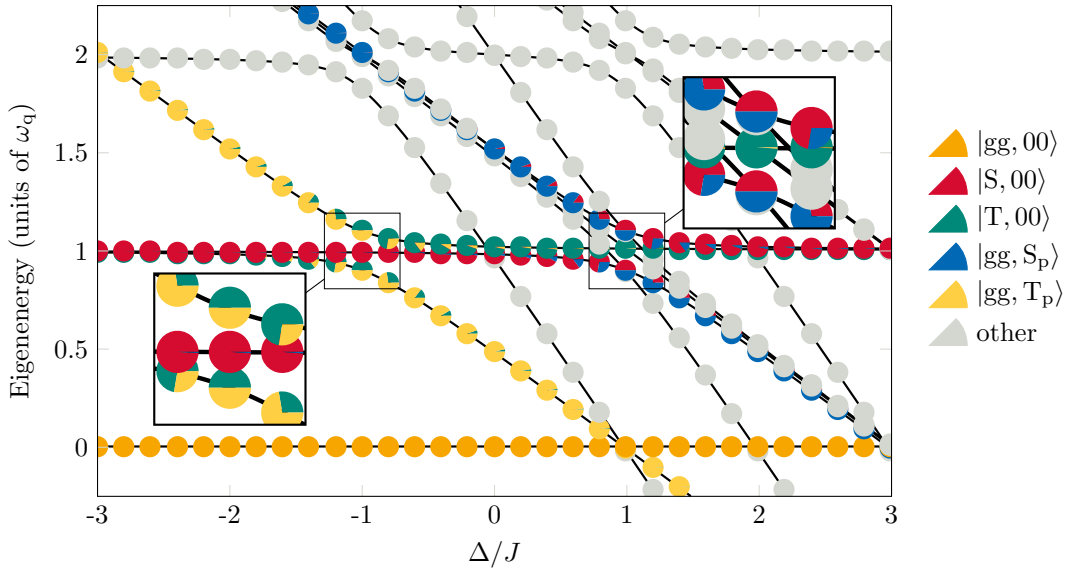

Figure 5.3: Eigenspectrum representing the eigenenergies and eigenstates of the two cavity-qubit model in dependence of the cavity-qubit detuning Δ. The insets are magnifications of the anticrossing regions around $\Delta = \pm J$, at which the splitting is given by $\Omega_T(-J) = \Omega_S(J) = 2g$.

5.3 Coherently driven system

We extent the Hamiltonian H in Eq. (5.1) by adding a coherent qubit drive Hamiltonian H_d, which has the form

$$H_d = \sum_{i=1}^{N} 2\varepsilon_q \cos(\omega_d t + \phi_i) \left(\sigma_i^+ + \sigma_i^-\right), \tag{5.15}$$

where ω_d and ε_q are the frequency and the strength of the pump, respectively, and ϕ_i the phase of the i-th qubit drive [106]. In order to eliminate the time-dependence we change into the rotating frame of the qubit drive by applying a unitary transformation with the unitary operator

$$U = \prod_{i=1}^{N} \exp\left[i\omega_d t \left(\sigma_i^+\sigma_i^- + a_i^\dagger a_i\right)\right]. \tag{5.16}$$

From the unitary transformation $H \mapsto U(H - i\partial_t)U^\dagger$ (see Appendix A) of the Hamiltonian H we obtain

$$\begin{aligned} H' = &\sum_{i=1}^{N} \Delta_{qd}\sigma_i^+\sigma_i^- + \sum_{i=1}^{N} \Delta_{cd} a_i^\dagger a_i + H_{c,q} + H_{c,c} \\ &+ \sum_{i=1}^{N} \varepsilon_d \left[\sigma_i^+ e^{-i\phi_i}\left(e^{2i(\omega_d t+\phi_i)} + 1\right) + \sigma_i^- e^{i\phi_i}\left(e^{-2i(\omega_d t+\phi_i)} + 1\right)\right], \end{aligned} \tag{5.17}$$

where $\Delta_{qd} \equiv \omega_q - \omega_d$ ($\Delta_{cd} \equiv \omega_c - \omega_d$) is the detuning between the qubit (cavity) and the pump. The cavity-qubit coupling Hamiltonian $H_{c,q}$ and the cavity-cavity coupling Hamiltonian $H_{c,c}$ remain unchanged. In the rotating wave approximation,

i.e., in the case of $|\omega_\mathrm{q} - \omega_\mathrm{d}| \ll \omega_\mathrm{q} + \omega_\mathrm{d}$, we can neglect fast rotating terms and obtain a time-independent Hamiltonian:

$$H' = \sum_{i=1}^{N} \Delta_\mathrm{qd} \sigma_i^+ \sigma^- + \sum_{i=1}^{N} \Delta_\mathrm{cd} a_i^\dagger a_i + H_\mathrm{c,q} + H_\mathrm{c,c} + \sum_{i=1}^{N} \varepsilon_\mathrm{q} \left(\sigma_i^+ \mathrm{e}^{-\mathrm{i}\phi_i} + \sigma_i^- \mathrm{e}^{\mathrm{i}\phi_i} \right). \quad (5.18)$$

The pump generates direct coupling only between two neighboring block matrices. Moreover, the parity is still conserved by the coherent pump.

The conservation of parity and the direct pumping between the m-th and the $(m+1)$-th block matrix can also be seen in matrix representation of the Hamiltonian $\hat{H}$ in Eq. (5.18) for zero, one, and two excitations:

$$H' = \left[\begin{array}{c|cccc|cccccccc}
0 & \sqrt{2}\varepsilon_\mathrm{q} & 0 & 0 & 0 & 0 & 0 & 0 & 0 & 0 & 0 & 0 & 0 \\
\hline
\sqrt{2}\varepsilon_\mathrm{q} & \Delta_\mathrm{qd} & g & 0 & 0 & \sqrt{2}\varepsilon_\mathrm{q} & 0 & 0 & 0 & 0 & 0 & 0 & 0 \\
0 & g & \Delta_\mathrm{cd}^- & 0 & 0 & 0 & 0 & \sqrt{2}\varepsilon_\mathrm{q} & 0 & 0 & 0 & 0 & 0 \\
0 & 0 & 0 & \Delta_\mathrm{qd} & g & 0 & 0 & 0 & 0 & 0 & 0 & 0 & 0 \\
0 & 0 & 0 & g & \Delta_\mathrm{cd}^+ & 0 & 0 & 0 & 0 & 0 & \sqrt{2}\varepsilon_\mathrm{q} & 0 & 0 \\
\hline
0 & \sqrt{2}\varepsilon_\mathrm{q} & 0 & 0 & 0 & 2\Delta_\mathrm{qd} & 0 & g & -g & 0 & 0 & 0 & 0 \\
0 & 0 & 0 & 0 & 0 & 0 & 2\Delta_\mathrm{cd} & g & -g & -2J & 0 & 0 & 0 \\
0 & 0 & \sqrt{2}\varepsilon_\mathrm{q} & 0 & 0 & g & g & \Delta_\mathrm{cd}^- + \Delta_\mathrm{qd} & 0 & g & 0 & 0 & 0 \\
0 & 0 & 0 & 0 & 0 & -g & -g & 0 & \Delta_\mathrm{cd}^+ + \Delta_\mathrm{qd} & g & 0 & 0 & 0 \\
0 & 0 & 0 & 0 & 0 & 0 & -2J & g & g & 2\Delta_\mathrm{cd} & 0 & 0 & 0 \\
0 & 0 & 0 & 0 & \sqrt{2}\varepsilon_\mathrm{q} & 0 & 0 & 0 & 0 & 0 & \Delta_\mathrm{cd}^+ + \Delta_\mathrm{qd} & 0 & g \\
0 & 0 & 0 & 0 & 0 & 0 & 0 & 0 & 0 & 0 & 0 & \Delta_\mathrm{cd}^- + \Delta_\mathrm{qd} & g \\
0 & 0 & 0 & 0 & 0 & 0 & 0 & 0 & 0 & 0 & g & g & 2\Delta_\mathrm{cd}
\end{array}\right], \quad (5.19)$$

where $\Delta_\mathrm{cd}^\pm = \Delta_\mathrm{cd} \pm (N-1)J$.

Considering that our initial state is the zero-excitation state, and that our main goal is to achieve an entangled state of two qubits, we first create Rabi oscillation of the zero-excitation state and our target state with as large amplitudes as possible, i.e., oscillations between 0 and 1. According the effects of coherent pumping mentioned above, a possible target state for our purposes is $|\mathrm{T}, 00\rangle$.

5.4 Analytic approach for providing insight

In this section we answer the question which parameters have to be chosen in order to generate Rabi oscillations with a maximum amplitude of specific states. The initial state is the zero-excitation state $|\mathrm{g}\rangle^{\otimes N} \otimes |0\rangle^{\otimes N}$. A relevant multipartite entangled qubit state is the Dicke state [78], which is defined as

$$|\mathrm{D}_{N,k}\rangle = \binom{N}{k}^{-\frac{1}{2}} \sum_{j=1}^{\binom{N}{k}} P_j(|\mathrm{e}\rangle^{\otimes k} \otimes |\mathrm{g}\rangle^{\otimes (N-k)}), \quad (5.20)$$

where P_j is the permutation operator of the j-th possible permutations. A special case of the Dicke states is the Dicke state with $k = 1$, which is called W state. For N qubits, the W state is given by

$$|\mathrm{W}_N\rangle = \frac{1}{\sqrt{N}} \left(|\mathrm{egg} \ldots \mathrm{g}\rangle + |\mathrm{geg} \ldots \mathrm{g}\rangle + \cdots + |\mathrm{ggg} \ldots \mathrm{e}\rangle \right). \quad (5.21)$$

We will chose this state as the target state. Note that $|\mathrm{W}_2\rangle \equiv |\mathrm{T}\rangle$. The Dicke and the W state are defined equivalently for the cavity modes. The restriction on a system with maximally one excitation allows to consider just the reduced Hamiltonian of a three dimensional Hilbert space with the symmetric basis states $|\mathrm{g}\ldots,0\ldots\rangle$, $|\mathrm{W}_N,0\ldots\rangle$, and $|\mathrm{g}\ldots,\mathrm{W}_{N,\mathrm{p}}\rangle$:

$$H'_{0,1} = \begin{bmatrix} 0 & \sqrt{N}\varepsilon_\mathrm{q} & 0 \\ \sqrt{N}\varepsilon_\mathrm{q} & \Delta_\mathrm{qd} & g \\ 0 & g & \Delta^-_\mathrm{cd} \end{bmatrix}. \tag{5.22}$$

We will discuss two different ansätze both leading to an effective Hamiltonian of the relevant two-level system with the zero-excitation state an our target state as its basis states.

The first ansatz is the elimination of the dynamics of the third state from the three-level system. The general time-dependent state of the Hamiltonian above is given by

$$|\Psi(t)\rangle = c_\alpha(t)\,|\alpha\rangle + c_\beta(t)\,|\beta\rangle + c_\gamma(t)\,|\gamma\rangle\,, \tag{5.23}$$

where $|\alpha\rangle \equiv |\mathrm{g}\ldots,0\ldots\rangle$, $|\beta\rangle \equiv |\mathrm{W}_N,0\ldots\rangle$, and $|\gamma\rangle \equiv |\mathrm{g}\ldots,\mathrm{W}_{N,\mathrm{p}}\rangle$. The Schrödinger equation $\mathrm{i}\,|\dot\Psi(t)\rangle = H'_{0,1}\,|\Psi(t)\rangle$ leads to a system of ODE for the probability amplitudes $c_\alpha(t)$, $c_\beta(t)$, and $c_\gamma(t)$.

$$\mathrm{i}\dot c_\alpha(t) = \sqrt{N}\varepsilon_\mathrm{q} c_\beta(t), \tag{5.24a}$$
$$\mathrm{i}\dot c_\beta(t) = \sqrt{N}\varepsilon_\mathrm{q} c_\alpha(t) + \Delta_\mathrm{qd} c_\beta(t) + g c_\gamma(t), \tag{5.24b}$$
$$\mathrm{i}\dot c_\gamma(t) = g c_\beta(t) + \Delta^-_\mathrm{cd} c_\gamma(t). \tag{5.24c}$$

In the regime $|\Delta^-_\mathrm{cd}| \gg |\Delta_\mathrm{qd}|, \varepsilon_\mathrm{q}, g$ the energy level of $|\gamma\rangle$ is much higher than the two of $|\alpha\rangle$ and $|\beta\rangle$. Thus, these two states are decoupled from the third state and we can set $\dot c_\gamma = 0$ with the result that

$$c_\gamma(t) = -\frac{g}{\Delta^-_\mathrm{cd}} c_\beta(t). \tag{5.25}$$

Eliminating $c_\gamma(t)$ leads to the effective Hamiltonian

$$H_\mathrm{eff} = \begin{bmatrix} 0 & \frac{1}{2}\Omega_\mathrm{eff} \\ \frac{1}{2}\Omega_\mathrm{eff} & \Delta_\mathrm{eff} \end{bmatrix}, \tag{5.26}$$

with the effective Rabi frequency

$$\Omega_\mathrm{eff} = 2\sqrt{N}\varepsilon_\mathrm{q} \tag{5.27}$$

and the effective detuning

$$\Delta_\mathrm{eff} = \Delta_\mathrm{qd} - \frac{g^2}{\Delta^-_\mathrm{cd}} \tag{5.28}$$

of the two levels of the effective two-level system. From the case of resonance, i.e., for $0 = \Delta_\mathrm{eff}$, we obtain the theoretical driving frequency for entanglement generation with a fidelity close to 1:

$$\omega_\mathrm{d}^\pm = \frac{1}{2}\left(2\omega_\mathrm{q} - \Delta_+ \pm \sqrt{\Delta_+^2 + 4g^2}\right), \tag{5.29}$$

where $\Delta_+ = \Delta + (N-1)J$. This formula is a fundamental result of this thesis and will be used to verify the systematic approach to adjust the parameters of the system for optimal results. The asymptotes of thr formula, which ine obtains for $g \to 0$, are $\omega_\mathrm{d}^+ = \omega_\mathrm{q}$ and $\omega_\mathrm{d}^- = \omega_\mathrm{q} - \Delta_+$. As we can see in Fig. 5.4, a raising cavity number N causes the theoretically predicted driving frequency $\omega_\mathrm{d}^\pm$ to shift by $(N-1)J$ to the left along the Δ axis. Of course, it is also possible to derive a formula for other

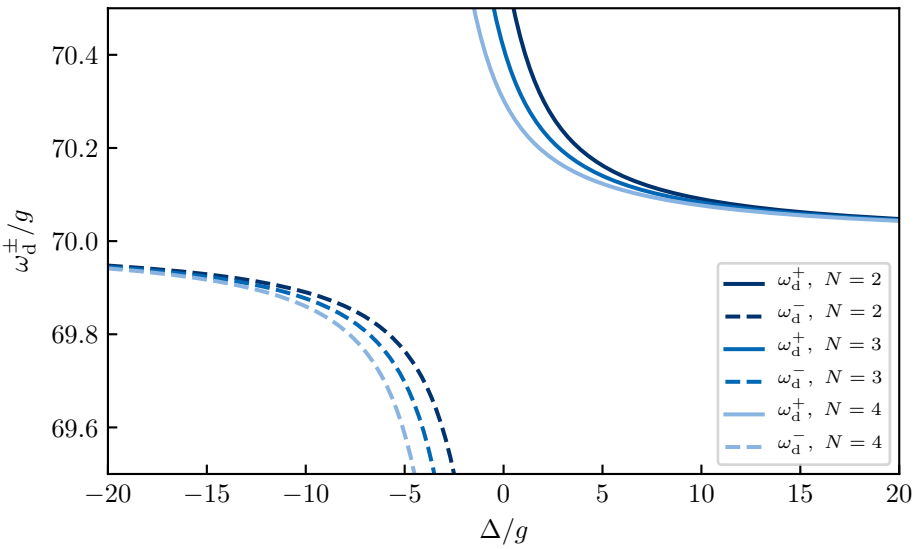

Figure 5.4: Theoretically predicted driving frequencies $\omega_\mathrm{d}^\pm$ in dependence of the qubit-cavity detuning Δ, which is given by Eq. (5.29), for different numbers of cavities N. The remaining parameters in the formula are $J = g$, $\omega_\mathrm{q} = 70g$.

parameters, e.g., the cavity-cavity coupling:

$$J_0 = \frac{\Delta_\mathrm{qd} - \Delta - \frac{g^2}{\Delta_\mathrm{qd}}}{N-1} \tag{5.30}$$

We will investigate this formula in the next chapter.

Let $|\mathrm{g}\ldots,0\ldots\rangle$ be the initial state of the two-level system described by the effective Hamiltonian H_eff in Eq. (5.26). The time evolution of the squared overlap of the current state of the system with the target state $|\mathrm{W}_N,0\ldots\rangle$ exhibits Rabi oscillation and is comparable with the result in Eq. (4.22b). The maximum squared overlap F_max is the peak-to-peak amplitude:

$$F_\mathrm{max} = \frac{\Omega_\mathrm{eff}^2}{\Omega_\mathrm{eff}^2 + \Delta_\mathrm{eff}^2}, \tag{5.31}$$

We will come back to this important result later in this theses in order to compare the theoretical approaches with our numerical scheme for entanglement generation.

We show now that the assumption $|\Delta_\mathrm{cd}^-| \gg |\Delta_\mathrm{qd}|, \varepsilon_\mathrm{q}, g$ is valid by deriving the exact solution of the Schrödinger equation. Beginning by writing the Hamiltonian as

$$\frac{H'_{0,1}}{\Delta_\mathrm{cd}^-} = \begin{bmatrix} 0 & \lambda\epsilon & 0 \\ \lambda\epsilon & \lambda_\mathrm{q}\epsilon & \lambda_\mathrm{c,q}\epsilon \\ 0 & \lambda_\mathrm{c,q}\epsilon & 1 \end{bmatrix}, \tag{5.32}$$

with $0 < \epsilon \ll 1$, where $\lambda\epsilon = \sqrt{N}\epsilon_\mathrm{d}/\Delta_\mathrm{cd}^-$, $\lambda_\mathrm{g}\epsilon = g/\Delta_\mathrm{cd}^-$, $\lambda_\mathrm{q}\epsilon = \Delta_\mathrm{qd}/\Delta_\mathrm{cd}^-$, $\lambda, \lambda_\mathrm{c,q}, \lambda_\mathrm{q} = \mathcal{O}(1)$. The exact solution of the Schrödinger equation is given by the unitary time-evolution operator $U(t) = \exp(-\mathrm{i}H'_{0,1}t)$ applied to the initial state $|\psi(0)\rangle = \sum_k c_k(0)\,|u_k\rangle$:

$$|\Psi(t)\rangle = \sum_{k=1}^{3} c_k(0)\mathrm{e}^{-\mathrm{i}\Delta_\mathrm{cd}^- x_k t}\,|u_k\rangle\,, \tag{5.33}$$

where the initial coefficients $c_k(0)$ are determined by the boundary conditions, the vectors $|u_k\rangle$ are the basis vectors, and x_k are the eigenvalues of $H'_{0,1}/\Delta_\mathrm{cd}^-$, which are the solutions of the equation

$$x^3 - (1+\lambda_\mathrm{q}\epsilon)x^2 + (\lambda_\mathrm{q} - \lambda^2\epsilon - \lambda_\mathrm{c,q}^2\epsilon)\epsilon x + \lambda^2\epsilon^2 = 0, \tag{5.34}$$

These eigenvalues are given by

$$x_1 = \frac{1}{2}\left(\lambda_\mathrm{q} - \sqrt{\lambda_\mathrm{q}^2 + 4\lambda^2}\right)\epsilon + \mathcal{O}(\epsilon^2) \tag{5.35a}$$

$$x_2 = \frac{1}{2}\left(\lambda_\mathrm{q} + \sqrt{\lambda_\mathrm{q}^2 + 4\lambda^2}\right)\epsilon + \mathcal{O}(\epsilon^2) \tag{5.35b}$$

$$x_3 = 1 + \mathcal{O}(\epsilon^2). \tag{5.35c}$$

Regarding the eigenstates $|u_k\rangle$ as linear combinations of the basis states allows to write the time-dependent probability amplitudes of $|\Psi(t)\rangle$ as

$$c_\alpha(t) = \sum_{k=1}^{3} A_k \mathrm{e}^{-\mathrm{i}\Delta_\mathrm{cd}^- x_k t}, \tag{5.36a}$$

$$c_\beta(t) = \sum_{k=1}^{3} B_k \mathrm{e}^{-\mathrm{i}\Delta_\mathrm{cd}^- x_k t}, \tag{5.36b}$$

$$c_\gamma(t) = \sum_{k=1}^{3} C_k \mathrm{e}^{-\mathrm{i}\Delta_\mathrm{cd}^- x_k t}. \tag{5.36c}$$

The coefficients A_k, B_k, and C_k are determined by the boundary conditions. With $c_\alpha(0) = \alpha_0$, $c_\beta(0) = \beta_0$, and $c_\gamma(0) = 0$, these coefficients emerge to be

$$A_1 = -\frac{2\beta_0\lambda - \alpha_0\left(\lambda_\mathrm{q} + \sqrt{\lambda_\mathrm{q}^2 + 4\lambda^2}\right)}{2\sqrt{\lambda_\mathrm{q}^2 + 4\lambda^2}} - \frac{\lambda\lambda_\mathrm{c,q}^2(2\alpha_0\lambda + \beta_0\lambda_\mathrm{q})}{\left(\lambda_\mathrm{q}^2 + 4\lambda^2\right)^{3/2}}\epsilon + \mathcal{O}(\epsilon^2), \tag{5.37a}$$

$$A_2 = \frac{2\beta_0\lambda - \alpha_0\left(\lambda_\mathrm{q} - \sqrt{\lambda_\mathrm{q}^2 + 4\lambda^2}\right)}{2\sqrt{\lambda_\mathrm{q}^2 + 4\lambda^2}} + \frac{\lambda\lambda_\mathrm{c,q}^2(2\alpha_0\lambda + \beta_0\lambda_\mathrm{q})}{\left(\lambda_\mathrm{q}^2 + 4\lambda^2\right)^{3/2}}\epsilon + \mathcal{O}(\epsilon^2), \tag{5.37b}$$

$$A_3 = \mathcal{O}(\epsilon^2), \tag{5.37c}$$

$$B_1 = -\frac{2\alpha_0\lambda + \beta_0\left(\lambda_\mathrm{q} - \sqrt{\lambda_\mathrm{q}^2 + 4\lambda^2}\right)}{2\sqrt{4\lambda^2 + \lambda_\mathrm{q}^2}} + \frac{\lambda\lambda_\mathrm{c,q}^2(2\beta_0\lambda - \alpha_0\lambda_\mathrm{q})}{\left(\lambda_\mathrm{q}^2 + 4\lambda^2\right)^{3/2}}\epsilon + \mathcal{O}(\epsilon^2), \tag{5.38a}$$

$$B_2 = \frac{2\alpha_0\lambda + \beta_0\left(\lambda_\mathrm{q} + \sqrt{\lambda_\mathrm{q}^2 + 4\lambda^2}\right)}{2\sqrt{\lambda_\mathrm{q}^2 + 4\lambda^2}} - \frac{\lambda\lambda_\mathrm{c,q}^2(2\beta_0\lambda - \alpha_0\lambda_\mathrm{q})}{\left(\lambda_\mathrm{q}^2 + 4\lambda^2\right)^{3/2}}\epsilon + \mathcal{O}(\epsilon^2), \tag{5.38b}$$

$$B_3 = \mathcal{O}(\epsilon^2), \tag{5.38c}$$

$$C_1 = \lambda_{\mathrm{c,q}} \frac{2\alpha_0\lambda + \beta_0\left(\lambda_\mathrm{q} - \sqrt{\lambda_\mathrm{q}^2 + 4\lambda^2}\right)}{2\sqrt{\lambda_\mathrm{q}^2 + 4\lambda^2}}\epsilon + \mathcal{O}(\epsilon^2), \tag{5.39a}$$

$$C_2 = -\lambda_{\mathrm{c,q}} \frac{2\alpha_0\lambda + \beta_0\left(\lambda_\mathrm{q} + \sqrt{\lambda_\mathrm{q}^2 + 4\lambda^2}\right)}{2\sqrt{\lambda_\mathrm{q}^2 + 4\lambda^2}}\epsilon + \mathcal{O}(\epsilon^2), \tag{5.39b}$$

$$C_3 = \beta_0\lambda_{\mathrm{c,q}}\epsilon + \mathcal{O}(\epsilon^2). \tag{5.39c}$$

In the regime $|\Delta_\mathrm{cd}^-| \gg |\Delta_\mathrm{qd}|, \varepsilon_\mathrm{q}, g$, the angular frequencies of the exact solution in Eq. (5.36) can be approximated as

$$\Delta_\mathrm{cd}^- x_1 \approx \frac{1}{2}\left(\Delta_\mathrm{qd} - \sqrt{\Delta_\mathrm{qd}^2 + 8\varepsilon_\mathrm{q}}\right) \ll \Delta_\mathrm{cd}^-, \tag{5.40a}$$

$$\Delta_\mathrm{cd}^- x_2 \approx \frac{1}{2}\left(\Delta_\mathrm{qd} + \sqrt{\Delta_\mathrm{qd}^2 + 8\varepsilon_\mathrm{q}}\right) \ll \Delta_\mathrm{cd}^-, \tag{5.40b}$$

$$\Delta_\mathrm{cd}^- x_3 \approx \Delta_\mathrm{cd}^-, \tag{5.40c}$$

in the order $\mathcal{O}(\epsilon)$. This allows to write $c_\gamma(t)$ as the sum of the relevant part

$$c_\gamma^\mathrm{rel}(t) = \sum_{k=1}^{2} C_k \mathrm{e}^{-\mathrm{i}\Delta_\mathrm{cd}^- x_k t} \tag{5.41}$$

and the rapidly oscillating part $C_3 \exp(-\mathrm{i}\Delta_\mathrm{cd}^- x_3 t)$:

$$c_\gamma(t) = c_\gamma^\mathrm{rel}(t) + C_3 \mathrm{e}^{-\mathrm{i}\Delta_\mathrm{cd}^- x_3 t}. \tag{5.42}$$

Inserting Eq. (5.24) into the time derivative of the above equation reveals a relation of $c_\gamma^\mathrm{rel}(t)$ with $c_\beta(t)$ and $c_\gamma(t)$:

$$\mathrm{i}\frac{\dot{c}_\gamma^\mathrm{rel}(t)}{\Delta_\mathrm{cd}^-} + (x_3 - 1)\left[c_\gamma(t) - c_\gamma^\mathrm{rel}(t)\right] = \frac{g}{\Delta_\mathrm{cd}^-} c_\beta + c_\gamma^\mathrm{rel}(t). \tag{5.43}$$

Since $x_1, x_2 = \mathcal{O}(\epsilon)$ and $C_1, C_2 = \mathcal{O}(\epsilon)$, it can be seen from Eq. (5.41) that $\mathrm{i}\dot{c}_\gamma^\mathrm{rel}(t)/\Delta_\mathrm{cd}^- = \mathcal{O}(\epsilon^2)$. Further, $x_3 - 1 = \mathcal{O}(\epsilon^2)$, $c_\gamma, c_\gamma^\mathrm{rel} = \mathcal{O}(\epsilon)$, and $c_\alpha, c_\beta = \mathcal{O}(1)$. Hence, we can write the relation in Eq. (5.43) as

$$c_\gamma^\mathrm{rel}(t) = -\frac{g}{\Delta_\mathrm{cd}^-} c_\beta(t) + \mathcal{O}(\epsilon^2). \tag{5.44}$$

This expression matches Eq. (5.25), implying the assumption $|\Delta_\mathrm{cd}^-| \gg |\Delta_\mathrm{qd}|, \varepsilon_\mathrm{q}, g$ to be correct to the order $\mathcal{O}(\epsilon)$ [107].

The second ansatz is the decoupling of the relevant two-level system from the three-level system via Schrieffer-Wolff transformation (SWT). In general, the SWT is motivated by treating the coupling part of the relevant part of the given Hamiltonian as a sufficiently small perturbation. It is a second order perturbation theory from which a Hamiltonian is obtained, which is diagonal to first order in the perturbation. Let the Hamiltonian of an arbitrary system be

$$H = H_0 + V, \tag{5.45}$$

where H_0 and V are the diagonal and the off-diagonal part, respectively. The SWT is a unitary transformation of the form

$$H \mapsto H' = \mathrm{e}^{S} H \mathrm{e}^{S^\dagger}, \tag{5.46}$$

where S is an anti-Hermitian operator, i.e., $S^\dagger = -S$, which is called generator. Using the relation (see Appendix D)

$$\mathrm{e}^{X} Y \mathrm{e}^{-X} = Y + [X, Y] + \frac{1}{2!}[X, [X, Y]] + \ldots, \tag{5.47}$$

the transformation becomes

$$H' = H_0 + V + [S, H_0] + [S, V] + \frac{1}{2}[S, [S, H_0]] + \frac{1}{2}[S, [S, V]] + \ldots \tag{5.48}$$

In order to make the transformed Hamiltonian diagonal to the first order in V, the condition

$$V + [S, H_0] = 0 \tag{5.49}$$

has to be satisfied. Thus, the SWT of the Hamiltonian H becomes

$$H' = H_0 + \frac{1}{2}[S, V] + \mathcal{O}(V^3). \tag{5.50}$$

This transformation can be easily performed. However, an expression for the generator S has to be found first. Now, we write the Hamiltonian $H'_{0,1}$ in terms of an effective two-level system weakly coupled to a perturbing third level, i.e., $H = H_0 + V$, where

$$H_0 = \begin{bmatrix} 0 & \sqrt{N}\varepsilon_\mathrm{q} & 0 \\ \sqrt{N}\varepsilon_\mathrm{q} & \Delta_\mathrm{qd} & 0 \\ 0 & 0 & \Delta^-_\mathrm{cd} \end{bmatrix}, \tag{5.51}$$

and

$$V = \begin{bmatrix} 0 & 0 & 0 \\ 0 & 0 & g \\ 0 & g & 0 \end{bmatrix} \tag{5.52}$$

are the uncoupled (H_0) and the coupling Hamiltonian (V) connecting the subspace of the zero-excitation state and the target state to the perturbing third level. We apply the SWT to this effective Hamiltonian, using

$$S = \begin{bmatrix} 0 & 0 & S_{13} \\ 0 & 0 & S_{23} \\ -S_{13} & -S_{23} & 0 \end{bmatrix}, \tag{5.53}$$

with

$$S_{13} = \frac{\sqrt{N}\varepsilon_\mathrm{q} g}{N\varepsilon_\mathrm{q}^2 - \Delta^-_\mathrm{cd}(\Delta^-_\mathrm{cd} - \Delta_\mathrm{qd})}, \tag{5.54a}$$

$$S_{23} = \frac{\Delta^-_\mathrm{cd} g}{N\varepsilon_\mathrm{q}^2 - \Delta^-_\mathrm{cd}(\Delta^-_\mathrm{cd} - \Delta_\mathrm{qd})}, \tag{5.54b}$$

obtained by solving $[H_0, S] = V$. This leads to an expansion of the transformed Hamiltonian such that the first two levels become decoupled from the third one up

to first order in V, i.e., $H' = H_0 + \frac{1}{2}[S, V] + \mathcal{O}(V^3)$. This results in an effective two-level system with the Hamiltonian

$$\tilde{H} = \begin{bmatrix} 0 & \frac{1}{2}\tilde{\Omega}_{\text{eff}} \\ \frac{1}{2}\tilde{\Omega}_{\text{eff}} & \tilde{\Delta}_{\text{eff}} \end{bmatrix}, \tag{5.55}$$

in which the detuning and coupling strength are renormalized by the presence of the third level according to

$$\tilde{\Omega}_{\text{eff}} = 2\sqrt{N}\varepsilon_{\text{q}} + \frac{\sqrt{N}\varepsilon_{\text{q}} g^2}{N\varepsilon_{\text{q}}^2 - \Delta_{\text{cd}}^-(\Delta_{\text{cd}}^- - \Delta_{\text{qd}})}, \tag{5.56a}$$

$$\tilde{\Delta}_{\text{eff}} = \Delta_{\text{qd}} + \frac{\Delta_{\text{cd}}^- g^2}{N\varepsilon_{\text{q}}^2 - \Delta_{\text{cd}}^-(\Delta_{\text{cd}}^- - \Delta_{\text{qd}})}. \tag{5.56b}$$

From the resonance case $\tilde{\Delta}_{\text{eff}} = 0$ we find a formula, which connects the driving frequency ω_{d} with the other parameters:

$$\tilde{\omega}_{\text{d}}^{\pm} = \frac{1}{2\Delta}\left[g^2 + N\varepsilon_{\text{q}}^2 - \Delta(\Delta - 2\omega_{\text{q}}) \pm \sqrt{(g^2 - \Delta^2 + N\varepsilon_{\text{q}}^2)^2 + 4g^2\Delta^2}\right]. \tag{5.57}$$

Figure 5.5 shows the plot of this formula in comparison with that in Eq. (5.4). A

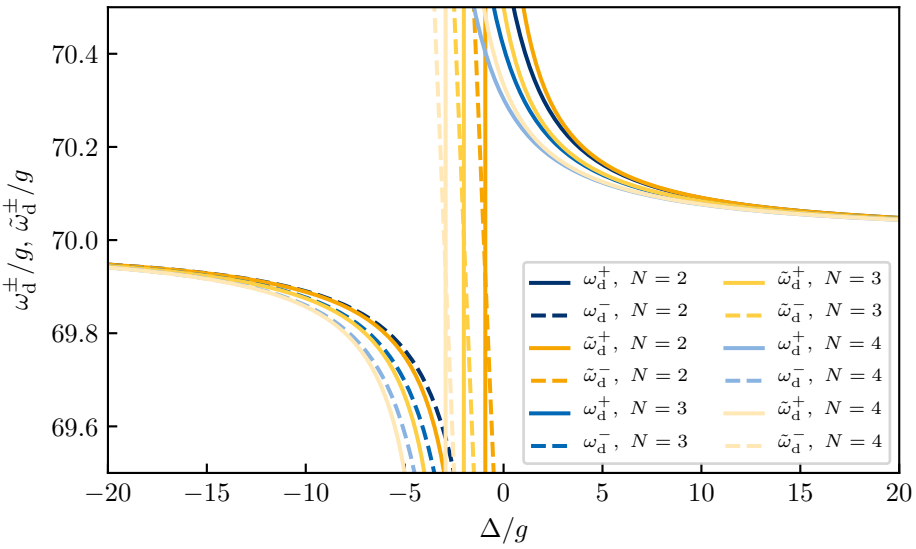

Figure 5.5: Theoretically predicted driving frequencies $\tilde{\omega}_{\text{d}}^{\pm}$ given by Eq. (5.57) (yellow) and ω_{d} given by Eq. (5.29) (blue) in dependence of the qubit-cavity detuning Δ for different numbers of cavities N. The remaining parameters in the formulas are $J = g$, $\omega_{\text{q}} = 70g$, and $\varepsilon_{\text{q}} = 0.01$.

similar derivation to the one above for the driving frequency can also be performed for other parameters, e.g., the cavity-cavity coupling strength:

$$\tilde{J} = \frac{\Delta_{\text{qd}}^2 - 2\Delta\Delta_{\text{qd}} - g^2 \pm \sqrt{(\Delta_{\text{qd}}^2 + g^2)^2 + 4\Delta_{\text{qd}}^2 N\varepsilon_{\text{q}}^2}}{2\Delta_{\text{qd}}(N-1)} \tag{5.58}$$

A detailed discussion of this formula can be found in the next chapter.

The effective Hamiltonian $\tilde{H}$ in Eq. (5.55) describes the N-partite system as a two-level system. Let $|\mathrm{g}\ldots,0\ldots\rangle$ be the initial state of the system. Then, the calculation of the time evolution of that two-level system yields Rabi oscillation of the squared overlap of the state of the system with the target state $|\mathrm{W}_N,0\ldots\rangle$ that is comparable with that in Eq. (4.22b). The maximum squared overlap $\tilde{F}_{\max}$ is the peak-to-peak amplitude:

$$\tilde{F}_{\max} = \frac{\varepsilon_{\mathrm{q}}^2}{\left(\frac{\Delta_{\mathrm{qd}}}{2}\right)^2 + \varepsilon_{\mathrm{q}}^2}, \tag{5.59}$$

Later in this theses we will compare this theoretical result with with Eq. (5.31) and our numerical scheme for entanglement generation.

5.5 Generating Rabi oscillation

Controlled generation of entanglement requires a detailed understanding of the spectrum of the interacting system and its dependence on the parameters. Figure 5.6 shows the eigenenergies and the components of the eigenstates in dependence of the detuning Δ. We infer from Fig. 5.6 that we can expect Rabi oscillations with

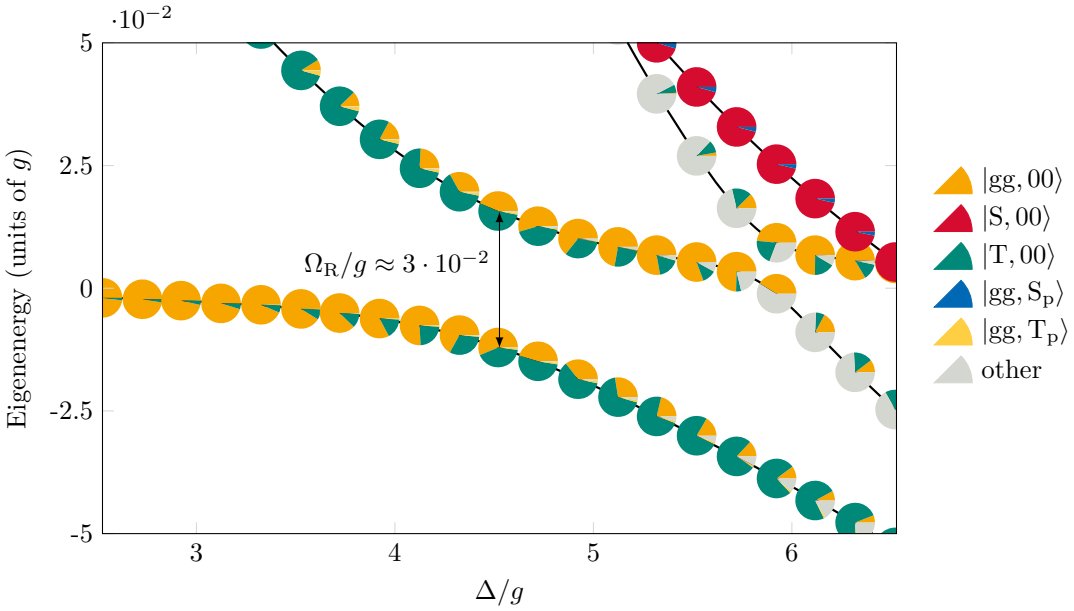

Figure 5.6: Eigenspectrum for a system with two cavity-qubit systems as a function of their detuning Δ. The parameters used here are $J = g$, $\omega_{\mathrm{q}} = 70g$, $\varepsilon_{\mathrm{q}} = 0.01g$. At $\Delta = 4.527g$ (i.e., $\omega_{\mathrm{c}} = 65.473g$) and $\omega_{\mathrm{d}} = 70.174g$ we expect Rabi oscillation of frequency $\Omega = 0.03g$ with a maximum amplitude.

relatively large amplitudes for $\Delta = 4.527g$. That is because the contributions to the eigenstate of the system from the ground state and the symmetric state $|\mathrm{T},00\rangle$ are both near 50 % (orange and green parts of the pie chart) while contributions from other states are relatively small.

Figure 5.7 shows the fidelities obtained from the Hamiltonian H' in Eq. (5.18) with the detuning $\Delta = 4.527g$ and the driving frequency $\omega_\mathrm{d} = 70.174g$. The ground state reaches a fidelity value almost 1 while the entangled state $|\mathrm{T}, 00\rangle$ has a fidelity value of about 0.95. The anti-symmetric states $|\mathrm{S}, 00\rangle$ and $|\mathrm{gg}, \mathrm{S_p}\rangle$ are not affected by the pump. This also pertains to anti-symmetric states with more than one excitation. The shown Rabi oscillations have a frequency Ω_R, i.e., the splitting of the corresponding energy levels, of about $0.03g$, which is equivalent to a period of about $200g^{-1}$. In order to use entangled states for quantum information protocols and quantum computers, their fidelity needs to be above a specific value for a certain time. Thus, an oscillating fidelity value generated by a coherent pump is not desirable. By using a pulse instead of a coherent pump it is possible to achieve a value of the fidelity that is constant when there are no dissipation processes.

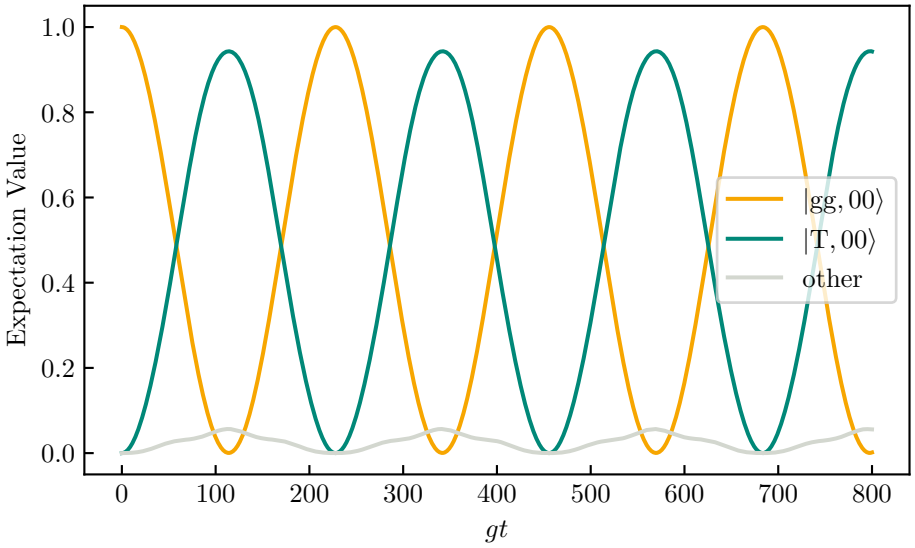

Figure 5.7: Rabi oscillation of the ground state $|\mathrm{gg}, 00\rangle$ and the symmetric state $|\mathrm{T}, 00\rangle$. The fidelity of $|\mathrm{T}, 00\rangle$ reaches values about 0.95. There are also smaller oscillations of $|\mathrm{gg}, \mathrm{T_p}\rangle$ and other symmetric states with more than one excitation. The fidelity of the anti-symmetric states stays zero.

5.6 Generating bipartite entanglement via optical pulses

Up to this point we have a set of system parameters, which allows to generate Rabi oscillation of the zero-excitation state and the qubit triplet state with a high amplitude by coherently driving the system, as it is shown in Fig. 5.7. We discussed earlier the different behavior of a single cavity-qubit system when it is driven coherently or with an optical pulse. The latter offers the possibility to drive the fidelity of a target state with the value 0 to a value close to 1. This mechanism can be adopted for the multipartite system with N cavities, except that the Rabi frequency $\Omega(t)$, which determines the pulse area Θ, is now equal to $2\sqrt{N}\varepsilon_\mathrm{q}$ (cf. Sec. 5.4). In case

of a rectangular pulse, its duration should be half the period $T = 2\pi/\Omega$ of a Rabi cycle with the frequency Ω and the pulse strength of the pulse should be ε_q, i.e., the strength of the coherent drive that generates Rabi oscillation. Thus, the area under the rectangular pulse function is $\varepsilon_\mathrm{q} T/2 = \pi/(2\sqrt{N})$, where we used $\Omega = 2\sqrt{N}\varepsilon_q$. With the analogue time-dependent Rabi frequency $\Omega(t) = 2\sqrt{N}\varepsilon_q(t)$ we find for the pulse area, which is defined as $\Theta = \int_{-\infty}^{\infty} \Omega(t)\mathrm{d}t$: $\Theta = \pi$. This means, that we drive the N cavity-qubit system with a π pulse as we discussed before for the case of a single cavity-qubit system. Note that the pulse area Θ is $2\sqrt{N}$ times the actual area under the function $\varepsilon_\mathrm{q}(t)$. For a more realistic setup we use a Gaussian function as the pulse shape. We define the Gaussian pulse by

$$\varepsilon_\mathrm{q}(t) = \frac{A}{\sigma\sqrt{2\pi}} \mathrm{e}^{-\frac{1}{2}\left(\frac{t-\mu}{\sigma}\right)^2}, \tag{5.60}$$

where A is the area under the function $\varepsilon_\mathrm{q}(t)$, i.e., $A = 2\sqrt{N}\Theta$, σ is the standard deviation, and μ the mean value. The mean value μ just determines the time at which the pulse reaches its peak with the value of $A/(\sigma\sqrt{2\pi})$, so that it can be chosen freely. The standard deviation σ determines the pulse duration τ, which is defined as the full width at half maximum (FWHM) of the pulse shape:

$$\tau = 2\sqrt{2\ln 2}\sigma. \tag{5.61}$$

We consider now the bipartite system with the eigenspectrum shown in Fig. 5.6, where $\varepsilon_\mathrm{q} = 0.01g$ and $\Omega = 0.03g \approx 2\sqrt{2}\varepsilon_\mathrm{q}$. For the rectangular pulse its measures, i.e., its width and height, are clear. However, for the Gaussian pulse we now that A depends on the pulse area Θ, which is given, but we have no rule for the FWHM, yet. In Fig. 5.8 we plot the fidelity of the target state after the interaction of the bipartite system without dissipation with a Gaussian pulse with a fixed pulse area of π versus the FWHM (τ) of this very pulse. From the plot we find that the highest fidelity is reached for $\tau = T/2$, as it is the case for the rectangular pulse. Thus, we drive our CCA with a Gaussian pulse with a FWHM of $T/2$. The result we obtain for the bipartite system with dissipation effects is depicted in Fig. 5.9. The highest fidelity, which the entangled target state reaches, is about 0.95. The deviation from the optimum value of 1 is caused by the admixture of residual states. In our bipartite system, it is mainly the state $|\mathrm{gg}, \mathrm{T_p}\rangle$, whose contribution (yellow) to the eigenstate can be recognized in Fig. 5.6.

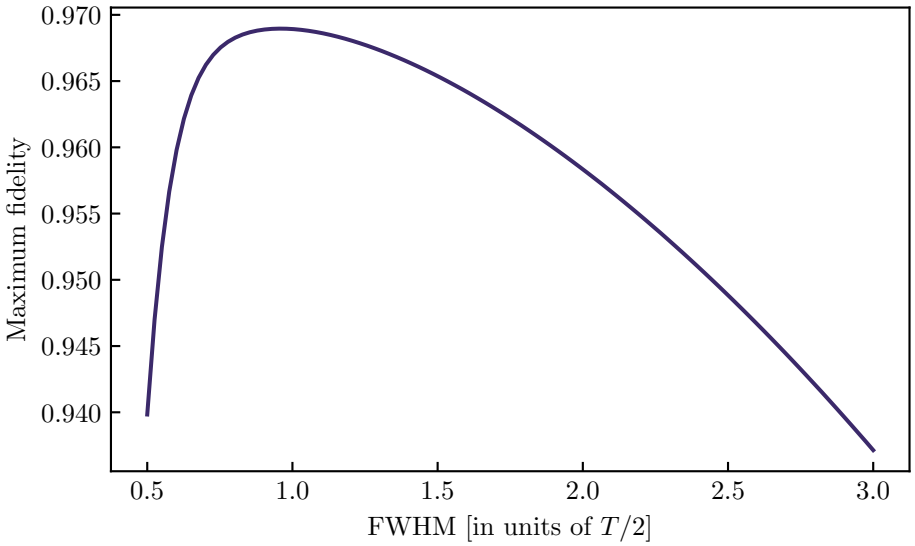

Figure 5.8: Fidelity of the qubit triplet state $|\mathrm{T}, 00\rangle$ versus the FWHM of the Gaussian pulse. Initially, the system is in the zero-excitation state $|\mathrm{gg}, 00\rangle$. With the Gaussian pulse with the FWHM $\tau = T/2$, the fidelity of the qubit triplet state reaches the highest fidelity as it is the case for a rectangular pulse. Dissipation effects are not included here.

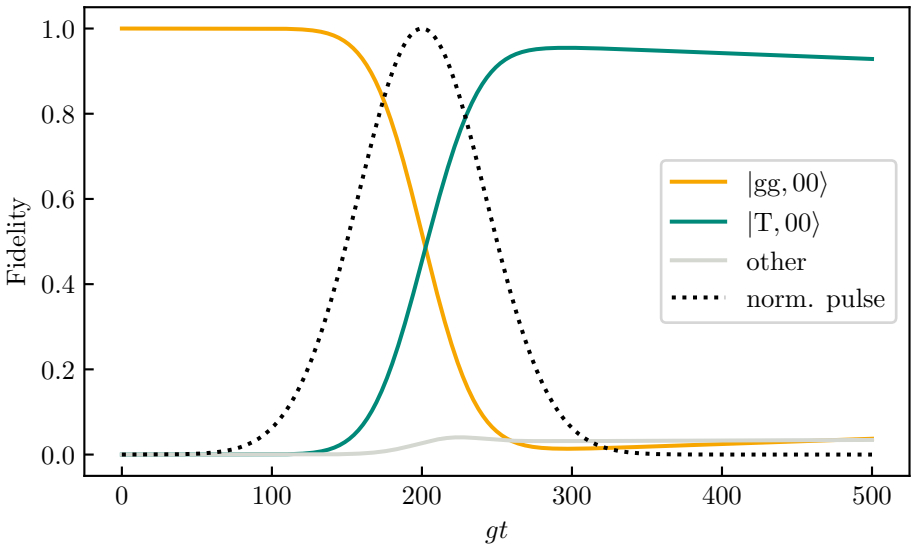

Figure 5.9: Fidelities of the zero-excitation state $|\mathrm{gg}, 00\rangle$, the qubit triplet state $|\mathrm{T}, 00\rangle$, the sum of the fidelities of all other states, and the normalized Gaussian pulse. Initially, the system is in the zero-excitation state. After driving the system with the Gaussian pulse, the fidelity of the qubit triplet state reaches a value of about 0.95. Here, the parameters are $J = g$, $\omega_\mathrm{q} = 70g$, $\omega_\mathrm{c} = 65.473g$, $\varepsilon_\mathrm{q} = 0.01g$, and $\omega_\mathrm{d} = 70.174g$. The included dissipation effects have the rates $\kappa = 10^{-3}g$, $\gamma = 10^{-4}g$, $\gamma_\varphi = 10^{-5}g$.

Chapter 6

Targeted generation of multipartite entanglement

In general, entanglement generation in a system of coupled-cavity-qubit systems is possible. In the previous chapter we drove the system from its zero-excitation state directly into the targeted entangled state by using an optical pulse. We have seen that the question, whether this can be performed with a given system can be answered by having a look at the systems' energy eigenspectrum. To make this easier, we introduced a new graphical representation of the eigenstates. This revealed that a given target state can be achieve if the initial state and the target state equally contribute to the same eigenstate of the system. In this chapter we introduce a systematic approach to generate entangled target states within a CCA using coherent optical excitation. For this we make use of the knowledge we acquired in the previous chapter. This means, that we calculate eigenspectra, evaluate a newly defined figure of merit, which represents the maximum overlap quality of the basis states, and tailor an optical pulse with the Rabi frequency that we gain from the eigenspectrum. It is an efficient scheme that can be applied to systems with two or more cavities. We begin to present results for generating a bipartite entangled Bell state and finish with tri- and quadripartite entangled Dicke states.

6.1 Generalization by schematically finding system parameters

We observed that it is possible to drive a system of coupled cavity-qubit systems from its zero-excitation state into an entangled target state by means of an optical pulse. This pulse was tailored by making use of the eigenspectrum of the system for a specific set of parameters. The systematic approach for finding these specific parameters can be broken down into the following steps: First, we calculate the eigenstates $|\psi_i\rangle$ of the system for a given set of parameters. Next, we calculate the squared overlaps of these eigenstates with the initial state $|\alpha\rangle$ and the target state $|\beta\rangle$, respectively, i.e., we obtain the fidelities $F_{\alpha,i} = |\langle\psi_i|\alpha\rangle|^2$ and $F_{\beta,i} = |\langle\psi_i|\beta\rangle|^2$. Our goal is to find an eigenstate with equal contribution of the initial state and the target state only, therefore, the optimum value of their squared overlap with this

eigenstate is 0.5. The absolute deviation of the fidelities $F_{\alpha,i}$ and $F_{\beta,i}$ from the value 0.5 is used to introduce the overlap quality Q_i of the eigenstate $|\psi_i\rangle$ as

$$Q_i \equiv 1 - |0.5 - F_{\alpha,i}| - |0.5 - F_{\beta,i}|, \tag{6.1}$$

which is a value between 0 and 1 with 1 being the optimal case. For the present example, $Q_i = 1$ means that the eigenstate is of the form

$$|\psi_i\rangle = (|\alpha\rangle + \mathrm{e}^{\mathrm{i}\varphi}\,|\beta\rangle)/\sqrt{2}, \tag{6.2}$$

where φ is an undetermined phase. We compute the Q_i for each $|\psi_i\rangle$ and select the one, which gives the highest value:

$$Q_{\max} \equiv \max_i(Q_i). \tag{6.3}$$

This is the figure of merit of our numerical scheme. In our bipartite system, the initial state is the zero-excitation state and the target state is the entangled qubit triplet state, i.e., $|\alpha\rangle = |\mathrm{gg}, 00\rangle$ and $|\beta\rangle = |\mathrm{T}, 00\rangle$. In Fig. 6.1 we determine $Q_{\max}$ in dependence of the cavity-qubit detuning Δ and the driving frequency ω_d while the other parameters are kept fixed. The resulting parameter map reveals for which of the two varied parameters the maximum overlap quality $Q_{\max}$ becomes optimal. The white areas belong to $Q_{\max} = 0.5$ and indicate parameters, for which one eigenstate of the system is composed of either 50 % of the zero-excitation state, the target state, or the mixture of both, while the other 50 % of the eigenstate consist of contributions of other basis states with one or more excitations. Optimal parameters for driving the target state can be found in the green regions, where $Q_{\max}$ is close or equal to 1. In addition to the numerical results, the analytic expressions $\omega_\mathrm{d}^\pm$ in Eq. (5.29) and $\tilde{\omega}_\mathrm{d}^\pm$ in Eq. (5.57), which give the ideal driving frequency to a given cavity-qubit detuning, are shown as the blue line in the left panel and as the yellow line in the right panel in Figure 6.1, respectively. Fig. 6.1 reveals two areas, which are correctly predicted by the analytic expression $\omega_\mathrm{d}^\pm$. As we can see in Fig. 6.1, both approximations, $\omega_\mathrm{d}^\pm$

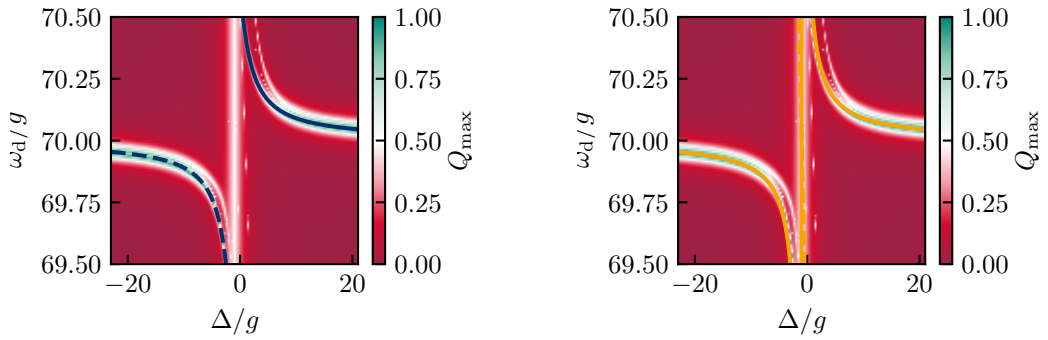

(a) Comparison with $\omega_\mathrm{d}^\pm$.

(b) Comparison with $\tilde{\omega}_\mathrm{d}^\pm$.

Figure 6.1: Maximum overlap quality $Q_{\max}$ for generating the target state $|\mathrm{T}, 00\rangle$ as a function of cavity-qubit detuning Δ and the driving frequency ω_d. The blue and the yellow lines represent the analytic result ω_d^+ (solid) and ω_d^- (dashed) in Eq. (5.29) and $\tilde{\omega}_\mathrm{d}^+$ (solid) and $\tilde{\omega}_\mathrm{d}^-$ (dashed) in Eq. (5.57), respectively, for $N = 2$.

and $\tilde{\omega}_\mathrm{d}^\pm$, indicate the positions of the green areas with optimal parameters with a high accuracy.

Similar conclusions can be drawn for the variation of other parameters. From the first ansatz in the previous chapter and the condition that the effective detuning in Eq. (5.28) equals zero, we find the expression for the cavity-cavity coupling J_0 that is given by Eq. (5.30). The same can be done for the second ansatz, which utilizes the SWT, and the effective detuning in Eq. (5.56b). The resulting expression for $\tilde{J}^{\pm}$ is given by Eq. (5.58). In both approximations, the cavity-cavity coupling strength is linear to the qubit-cavity detuning Δ. The left panel of Fig. 6.2 reveals that J_0 (blue line) and $\tilde{J}^{+}$ (solid yellow line) are almost identical. However, the approximation J_0, which we obtained from the first ansatz with the optimized time-dependence, lies a bit better within the green area that indicates optimal parameters. The approximation $\tilde{J}^{-}$ (dashed yellow line) lies within a white area, which is not interesting for our entanglement generation scheme. From the expression in Eq. (5.29) we expect that the driving frequency is independent of the driving strength. However, the right panel in Fig. 6.2 reveals that this independence is only valid for large driving strengths around the optimum driving frequency of $\omega_{\mathrm{d}} = 70.174g$. From the expression in Eq. (5.57) we find a function of the driving frequency in dependence of the driving strength. As shown in the right panel in Fig. 6.2, the function $\tilde{\omega}_{\mathrm{d}}^{+}$ (solid line) is almost constant, whereby the constant value equals the theoretically found optimal driving frequency. The driving frequency $\tilde{\omega}_{\mathrm{d}}^{-}$ (dashed line) only indicates an white area with parameters that are not suitable for our purposes.

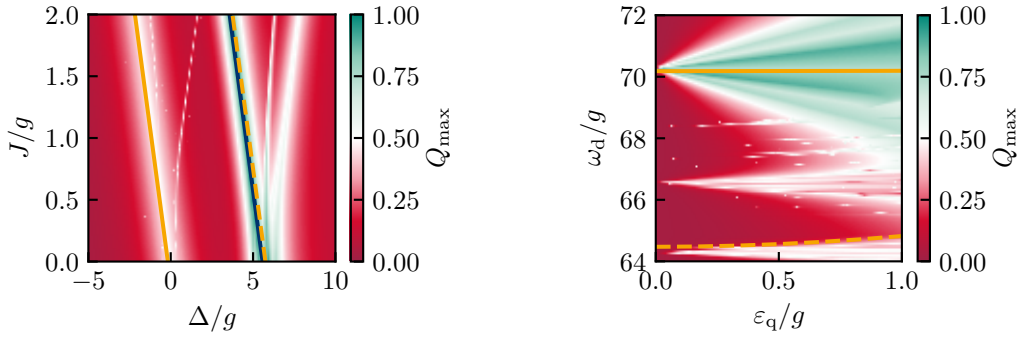

(a) Comparison with J_0 and $\tilde{J}^{\pm}$.

(b) Comparison with $\tilde{\omega}^{\pm}$.

Figure 6.2: Maximum overlap quality Q_{max} for generating the target state $|\mathrm{T}, 00\rangle$ as a function of two variables. These are (a) the cavity-qubit detuning Δ and the cavity-cavity coupling strength J, and (b) the qubit driving strength ε_{q} and the qubit driving frequency ω_{d}. In (a), the blue and the yellow lines represent the analytic result for J_0 in Eq. (5.30), and $\tilde{J}^{+}$ (solid) and $\tilde{J}^{-}$ (dashed) in Eq. (5.58), respectively. In (b), the yellow lines represent the analytic result for $\tilde{\omega}_{\mathrm{d}}^{+}$ (solid) and $\tilde{\omega}_{\mathrm{d}}^{-}$ (dashed) in Eq. (5.57), respectively. The expression for $\omega_{\mathrm{d}}^{\pm}$ in Eq. (5.29) is not included since it does simply not depend ε_{q}.

The suitable parameters for the generation of entanglement with a high fidelity are found in quite narrow domains. Many of these are hard to resolve properly. This implies a small fault tolerance of the system parameters in experimental setups. However, the usage of our systematic approach is an efficient way in order to find the best parameter settings.

6.2 Influence of dissipation

In addition to the coherent dynamics we have addressed so far, irreversible dissipation due to cavity decay, qubit dissipation, or pure dephasing arises from the nonunitary Liouvillian superoperator in Eq. (4.46). The dephasing that is associated with dissipative processes is a limitation for entanglement in quantum systems. We evaluate the impact of pure dephasing, radiative, and cavity losses on the attainable target-state fidelity. In Fig. 6.3 the maximum fidelity of the target state $|\mathrm{T}, 00\rangle$ is shown as a function of the dissipation rate for three different dissipation mechanisms.

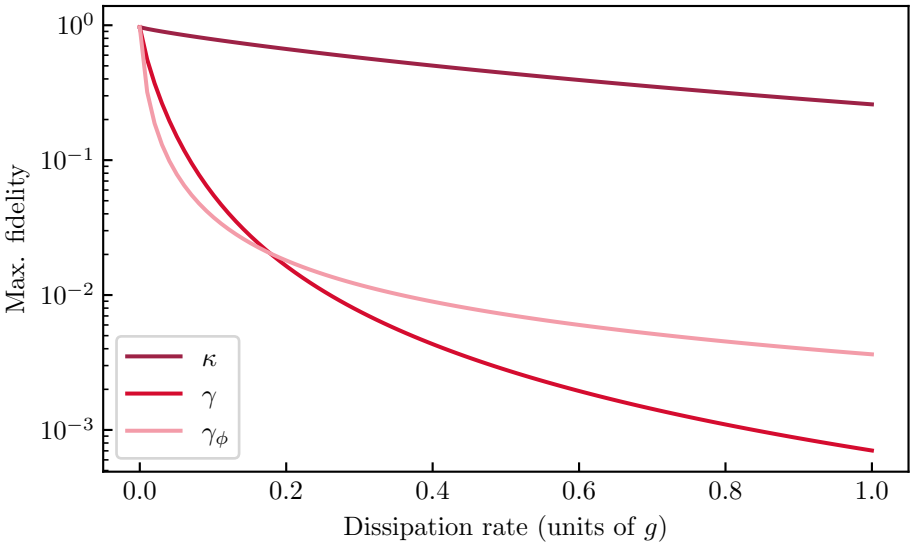

Figure 6.3: Maximum fidelity with the state $|\mathrm{T}, 00\rangle$ reached after excitation with Gaussian pulse as a function of different dissipation rates κ, γ, and γ_ϕ. Qubit dissipation (γ) and pure dephasing (γ_ϕ) act directly on the qubit state and thus have a stronger deteriorating effect than cavity decay (κ).

It can be seen that the physical dissipation mechanism described by the collapse operator C_n significantly impacts the possible fidelity. In particular, cavity losses, which can be the predominant loss mechanism in coupled micropillar cavities, have a much weaker impact on the target fidelity than qubit dephasing or radiative losses that directly act on the emitter degrees of freedom. In Fig. 6.4 we augment the parameter map of Fig. 6.1 by directly showing the maximum fidelity for the target state $|\mathrm{T}, 00\rangle$ for the cases without (left) and with small cavity dissipation rate (right). It can be seen that for values of experimentally realizable dissipation rates, the size of the areas of suitable parameters for entanglement generation are only slightly reduced.

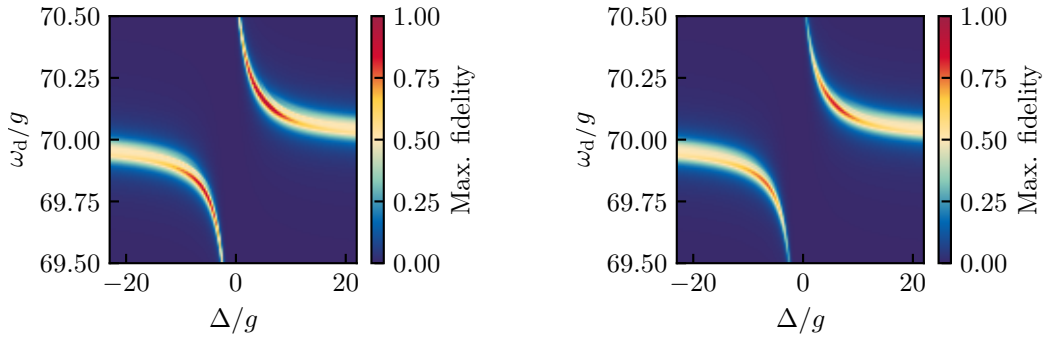

(a) $\kappa = 0$ (b) $\kappa = 10^{-1}g$

Figure 6.4: Maximum fidelities for the target state $|\mathrm{T}, 00\rangle$ without (a) and with (b) cavity dissipation ($\kappa = 10^{-1}g$) as a function of the cavity-qubit detuning Δ and the driving frequency ω_d. The red areas indicate parameters for which the fidelity is close to the maximum value of 1. The presence of dissipation slightly decreases the size of the red areas and thus the parameter space for entanglement generation.

6.3 Targeted generation of tri- and quadripartite entanglement

So far, we restricted our study of entanglement generation to bipartite entanglement in a system with two coupled cavities. We now explore the potential of the systematic approach, which we have introduced, for the generation of MPE in systems with more than two cavities. In general, our scheme allows to find parameters for driving direct transitions between states that form an orthogonal basis. In this thesis, we drive transitions between the zero-excitation state and entangled states that together belong to the same orthogonal basis. One has to keep in mind that not any arbitrary entangled state can be considered in our systematic approach. Such relevant multipartite entangled qubit states are for instance the Dicke states in Eq. (5.20) and their lowest excited states, the W states given by Eq. (5.21). In the following, we target the qubit W state with $N = 3$ and $N = 4$ qubits with the cavities in the vacuum state. Therefore, the joint target state will be $|\mathrm{W}_3, 000\rangle$ and $|\mathrm{W}_4, 0000\rangle$. With the previously discussed systematic approach we generate the parameter maps in Fig. 6.5 to reveal the parameter space in which the target states $|\mathrm{W}_3, 000\rangle$ (left panel) and $|\mathrm{W}_4, 0000\rangle$ (right panel) can be driven directly from the corresponding zero-excitation states $|\mathrm{ggg}, 000\rangle$ and $|\mathrm{gggg}, 0000\rangle$.
As before in Fig. 6.1, the blue lines represent the analytic result from Eq. (5.29). With the fixed parameters $J = g$, $\omega_\mathrm{q} = 70g$, and $\varepsilon_\mathrm{q} = 0.01g$, we obtain the eigenspectrum of the tripartite system, which is shown in Fig. 6.6, and the quadripartite system. From these eigenspectra we find the Rabi frequencies $\Omega \approx 0.03g$ for $N = 3$ and $\Omega \approx 0.04g$ for $N = 4$. This is in a good agreement with the analytical prediction in Eq. (5.27).

From the left panel in Fig. 6.5 we extract the detuning $\Delta = 3.04g$ and the qubit driving frequency $\omega_\mathrm{d} = 70.19g$ as an example of good parameters for generating the tripartite qubit W state. By using a Gaussian pulse with a duration of $\pi/2$ (half the

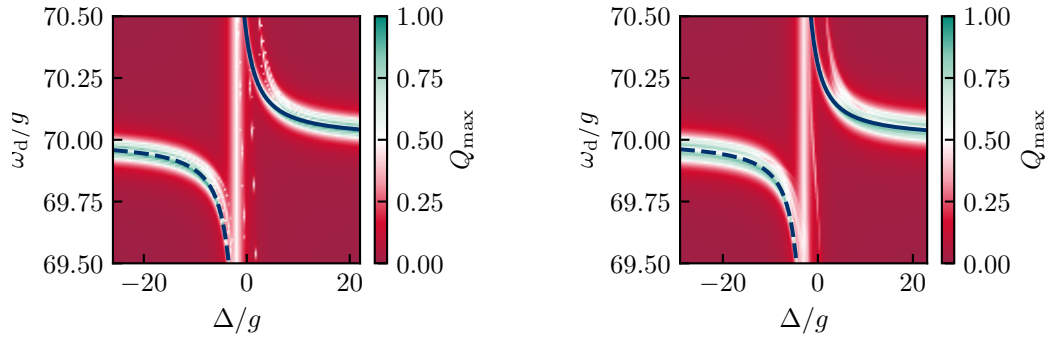

(a) $N = 3$ (b) $N = 4$

Figure 6.5: Parameter maps as a function of the cavity-qubit detuning Δ and the driving frequency ω_d for generating the multipartite target states. (a) For the tripartite target state $|W_3, 000\rangle$ ($N = 3$) we determine $\Delta = 3.04g$ (i.e., $\omega_c = 66.96g$) and $\omega_d = 70.19g$ to be optimal parameters. (b) For the multipartite target state $|W_4, 0000\rangle$ with four parts ($N = 4$), we determine $\Delta = 2.61g$ (i.e., $\omega_c = 67.39g$) and $\omega_d = 70.17g$ to be optimal parameters. In both cases, the blue lines represent the analytic result from Eq. (5.29).

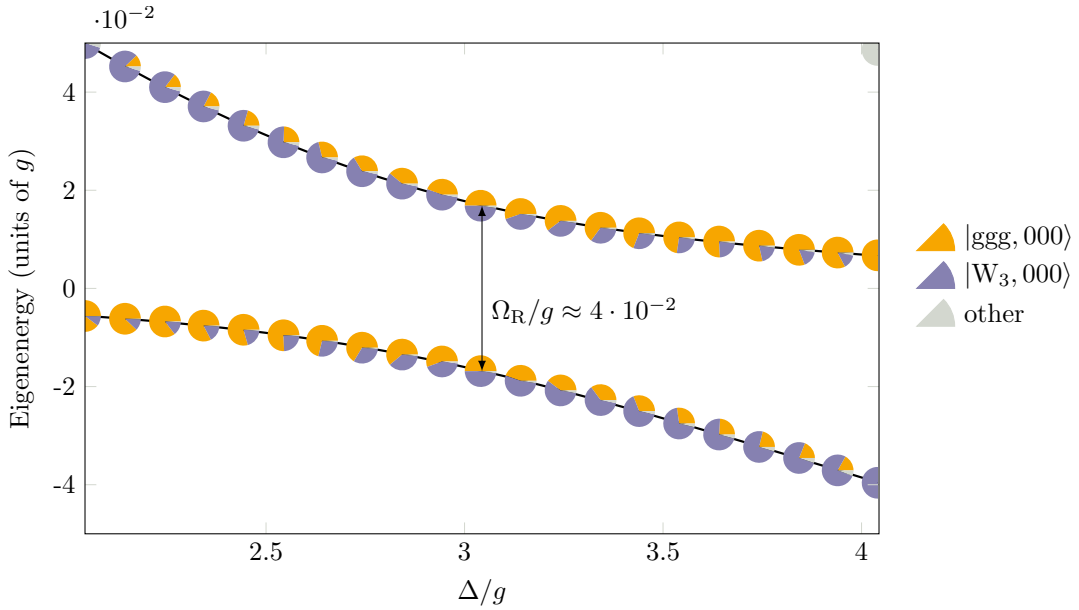

Figure 6.6: Eigenspectrum of the Hamiltonian with colored charts representing the eigenstates and their squared overlap with the vacuum state $|ggg, 000\rangle$, and the target state $|W_3, 000\rangle$. At $\Delta = 3.04g$ contributions of the vacuum state (orange) and the target state (blue) are maximal at almost 50 %, respectively. Gray contributions represent the sum of fidelities of other states. The energy gap between the two eigenenergies at the chosen detuning determines the Rabi frequency $\Omega_R \approx 0.03g$.

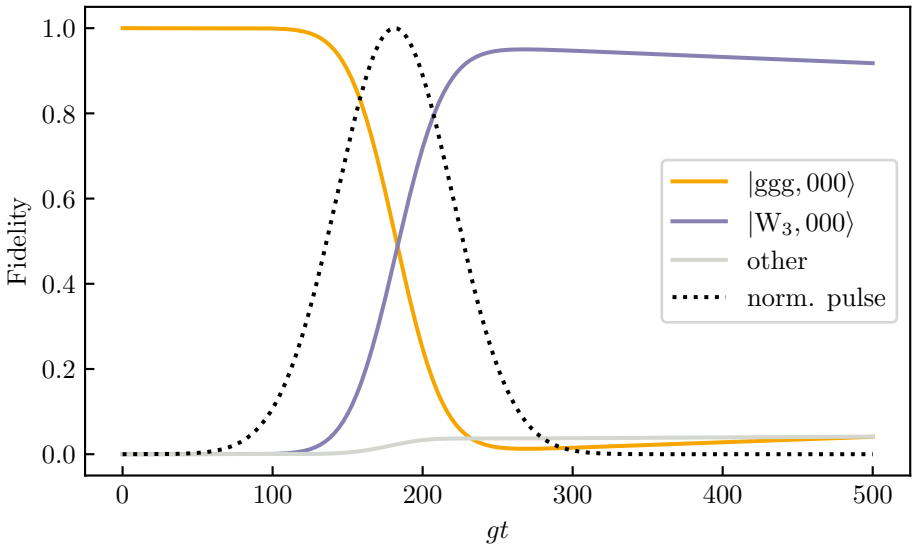

Figure 6.7: Time-dependence of the squared overlaps of the basis states of the tripartite system. Each qubit is driven by a Gaussian π pulse (dotted black line, normalized) with a FWHM of $\pi/\Omega = 104.7g^{-1}$. The fidelity of the target state $|\mathrm{W}_3, 000\rangle$ reaches a value of approximately 95 %. The included dissipation effects have the rates $\kappa = 10^{-3}g$, $\gamma = 10^{-4}g$, $\gamma_\phi = 10^{-5}g$.

period of one Rabi cycle) and a pulse area that we tailor with the corresponding Rabi frequency, we obtain the time dependency of the fidelity of the zero-excitation state, the target state and the sum of the other states. Figure 6.7 reveals for $N = 3$ cavities that the fidelity of the targeted W state reaches a value of about 95 %. From the right panel in Fig. 6.5 we extract the detuning $\Delta = 2.61g$ and the qubit driving frequency $\omega_\mathrm{d} = 70.17g$ as an example of good parameters for generating the quadripartite qubit W state. The time-evolution of the squared overlaps of the quadripartite states is shown in Fig. 6.8. It reveals that the fidelity of the targeted W state reaches a value of about 95 % for $N = 4$. The results demonstrate the feasibility of the developed systematic approach.

In Fig. 6.9 we evaluate our two analytical approaches of the maximum fidelity for the bipartite system as a function of qubit-cavity detuning Δ in the region of optimal parameters for driving the system into the target state $|\mathrm{T}, 00\rangle$. The approximation F_max in Eq. (5.31) (violet line), which we obtained from modelling the time-dynamics of the system, and the approximation $\tilde{F}_\mathrm{max}$ in Eq. (5.59) (green line), which we obtained from the SWT, behave the same way as the numerical results (crosses). Additionally, Fig. 6.9 shows the maximum overlap quality Q_max defined in Eq. (6.3) (black). The analytical approaches that we made are less accurate for detunings larger than the optimum value of $\Delta = 4.527g$ as seen in Fig. 5.6. That is because of the influence of non-target states that increases for larger detunings. For detunings below the optimum value, the graph that represents F_max lies much closer to the numerical results than the one representing $\tilde{F}_\mathrm{max}$.

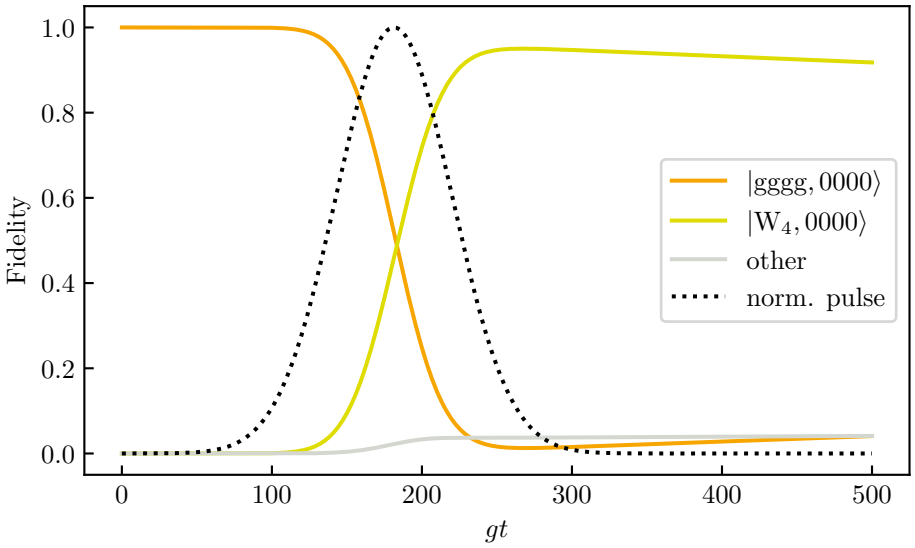

Figure 6.8: Time-dependence of the squared overlaps of the basis states of the multipartite system with four parts. Each qubit is driven by a Gaussian π pulse (dotted black line, normalized) with a FWHM of $\pi/\Omega = 78.5g^{-1}$. The fidelity of the target state $|\mathrm{W}_4, 0000\rangle$ reaches a value of approximately 95 %. The included dissipation effects have the rates $\kappa = 10^{-3}g$, $\gamma = 10^{-4}g$, $\gamma_\phi = 10^{-5}g$.

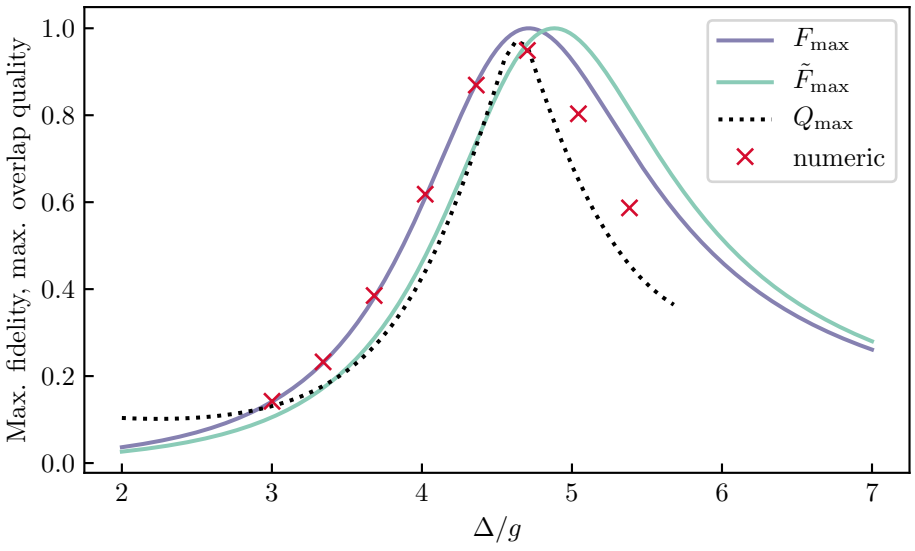

Figure 6.9: Maximum fidelity for the target state $|\mathrm{T}, 00\rangle$, as a function of qubit-cavity detuning. The approximations of the maximum fidelity $F_{\max}$ given by Eq. (5.31) (green line), and $\mathrm{F}_{\max}$ given by Eq. (5.59) show the same behavior as the numerical results (crosses). The maximum overlap quality $Q_{\max}$ from Eq. (6.3) follows is also shown (dotted) and behaves similar to the approximations maximum fidelity and the numerical values.

6.4 Symmetry steering via local excitation

Here we analyze the possibility of applying local phase factors to access entangled multipartite states that could not be generated from a homogeneous excitation scheme for the whole CCA. A simple example is the generation of the singlet qubit state $|\mathrm{S}\rangle$. This is not directly possible with the previously used excitation scheme because the antisymmetric states (like $|\mathrm{S}, 00\rangle$) are not interacting with the homogeneous coherent pump. However, the generation of an antisymmetric target state from the symmetric zero-excitation state $|\mathrm{gg}, 00\rangle$ can be realized by modifying the single qubit drives with a local phase factor, i.e., by creating a phase difference between the excitations of the qubits. In case of the state $|\mathrm{S}, 00\rangle$, the phase difference has to be π and the matrix of the bipartite Hamiltonian in Eq. (5.1) for zero and one excitation becomes

$$H^{(0,1)} = \left[\begin{array}{c|cccc} 0 & 0 & 0 & \sqrt{2}\varepsilon_\mathrm{q} & 0 \\ \hline 0 & \Delta_\mathrm{qd} & g & 0 & 0 \\ 0 & g & \Delta_\mathrm{cd}^- & 0 & 0 \\ \sqrt{2}\varepsilon_\mathrm{q} & 0 & 0 & \Delta_\mathrm{qd} & g \\ 0 & 0 & 0 & g & \Delta_\mathrm{cd}^+ \end{array}\right]. \tag{6.4}$$

In contrast to the corresponding submatrix of the Hamiltonian H' in Eq. (5.19), the zero-excitation state $|\mathrm{gg}, 00\rangle$ is coupled to the antisymmetric states including the target state $|\mathrm{S}, 00\rangle$. Based on this insight, we can apply our systematic entanglement generation scheme to a more general class of entangled multipartite states of the form

$$|\mathrm{W}_N^\mathrm{ph}\rangle = \frac{1}{\sqrt{N}} \left(\mathrm{e}^{\mathrm{i}\phi_1} |\mathrm{eg}\ldots\mathrm{g}\rangle + \cdots + \mathrm{e}^{\mathrm{i}\phi_N} |\mathrm{g}\ldots\mathrm{ge}\rangle\right). \tag{6.5}$$

Arbitrary phases ϕ_i that are not 0 or π lead to additional couplings between the basis states. This makes the theoretical prediction of suitable parameters for the

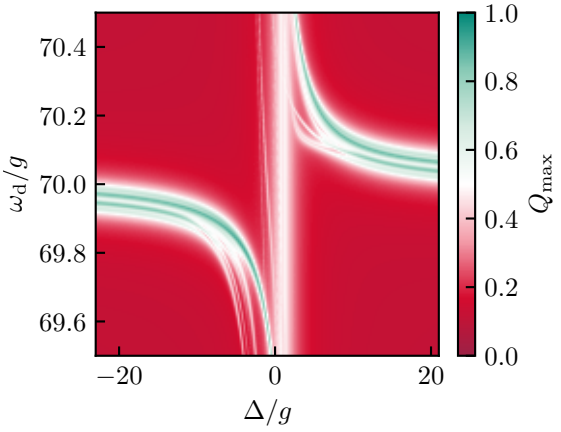

Figure 6.10: Parameter map as a function of the cavity-qubit detuning Δ and the driving frequency ω_d for generating the phased W state $|\mathrm{W}_3^\mathrm{ph}, 000\rangle$ given by Eq. (6.6). We determine as optimal parameters $\Delta = -4.71g$ and $\omega_\mathrm{d} = 69.83g$.

generation of targeted phased entangled states more sophisticated. The fact that this is possible at all is a unique feature of the CCA platform with individually

addressable sites. By allowing for different phases of the individual external qubit excitations, phased entangled states can actually be generated, opening the door for accessing larger parts of the Hilbert space and to go beyond the more conventional entangled states. We demonstrate this by generating a phased W state for three coupled cavities ($\phi_1 = \phi_2 = 0$, $\phi_3 = \pi$):

$$|\mathrm{W}_3^{\mathrm{ph}}, 000\rangle = \frac{1}{\sqrt{3}} \left(|\mathrm{egg}\rangle + |\mathrm{geg}\rangle - |\mathrm{gge}\rangle\right) \otimes |000\rangle \,, \tag{6.6}$$

The order of the three phases is reflected in phases of the individual qubit drives, where only the relative phase determines the excited state. Figure. 6.10 shows the maximum overlap quality $Q_{\max}$ in dependence of the parameters Δ and ω_{d}. Choosing optimal parameters for the targeted generation yields a value of about 83 % for the fidelity of the targeted phased entangled state.

In this chapter we have restricted the discussion of our systematic entanglement generation scheme to multipartite entangled qubit states with at most one excitation. In principle also multi-excitation states can be targeted. However, the corresponding Rabi frequencies are reduced on the order in Δ/g [32] which significantly reduces the attainable fidelity values due to the competition with the discussed dephasing mechanisms.

Chapter 7

Conclusion

The insights and methods, both analytic and numeric, developed in this thesis provide an important building block for future quantum technologies. We have shown, that entangled multipartite target states can be driven directly from the zero-excitation state by means of detuned optical excitation pulses. As building blocks, we have considered coupled-cavity arrays, whose Hamiltonian is based on the Jaynes–Cummings model extended by photon exchange between distant cavities and a coherent optical qubit drive. Introducing a novel graphical representation of the eigenenergies and eigenstates of a given Hamiltonian allows us to use it for further investigations of a single cavity-qubit system that is externally excited by a coherent pump or a laser pulse. Based on these insights, we are able to make predictions about the behavior of multiple symmetric coupled cavities and demonstrate the generation of bipartite entanglement. The graphical representation of the system's eigenenergy structure lays the foundation for a numerical scheme that we have developed, and which enables us to predict suitable driving parameters for different classes of entangled target states. We also implemented that numerical scheme on multipartite systems. For systems with a few cavity-qubit subsystems, we have shown that entangled states, such as W and Bell states, can be generated with fidelities above 90 %. The additional tunability of the phases of the individual qubit pumps allow us to enlarge the set of entangled target states by phased W states.

The generalized numerical scheme for the generation of different entangled multipartite target states in coupled-cavity arrays will be of direct relevance for using the solid-state cavity quantum electrodynamics platform in future quantum photonic applications, such as quantum reservoir computing. Even in the context of quantum information transfer, i.e., via optical fibres, entangled multipartite states offer advantages in robustness over bipartite Bell states.

This thesis constitutes a first step towards more complex network topologies based on coupled-cavity arrays with individually tailored inter-cavity couplings. The developed scheme lays open how to generate entanglement in a controllable way, which is a key resource for quantum reservoir computing. Conventional, gate-based quantum computers rely on fault tolerant qubit and gate operations. The underlying idea behind quantum reservoir computing is to connect quantum systems and classical machine learning to enable a mid-term quantum technology that is able to play out its advantages over classical systems even on noisy intermediate-scale quantum (NISQ)

hardware. Multipartite entanglement in coupled-cavity arrays is a key resource for the advantage of quantum reservoir computers over classical reservoir computers. Therefore, the coherent driving of entangled states could be an important component of the future development of quantum reservoir computers.

Appendix A

Unitary transformation

A unitary transformation is performed with a unitary operator U, which has to fulfill the condition $UU^\dagger = U^\dagger U = 1$. We begin with the von Neumann equation,

$$\dot{\rho} = -\frac{\mathrm{i}}{\hbar}\left[H, \rho\right], \tag{A.1}$$

insert $U^\dagger U = 1$ and premultiply with U and postmultiply with $U^\dagger$:

$$\begin{aligned} U\dot{\rho}U^\dagger &= -\frac{\mathrm{i}}{\hbar} UHU^\dagger U\rho U^\dagger + \frac{\mathrm{i}}{\hbar} U\rho U^\dagger UHU^\dagger \\ &= -\frac{\mathrm{i}}{\hbar}\left[UHU^\dagger, U\rho U^\dagger\right]. \end{aligned} \tag{A.2}$$

By the product rule,

$$\frac{\mathrm{d}}{\mathrm{d}t}\left(U\rho U^\dagger\right) = \dot{U}\rho U^\dagger + U\dot{\rho}U^\dagger + U\rho\dot{U}^\dagger. \tag{A.3}$$

Note, that $\frac{\mathrm{d}}{\mathrm{d}t}\left(U^\dagger\right) = \left(\dot{U}\right)^\dagger \equiv \dot{U}^\dagger$. After rearranging and inserting $U^\dagger U = 1$, we get

$$\begin{aligned} U\dot{\rho}U^\dagger &= \frac{\mathrm{d}}{\mathrm{d}t}\left(U\rho U^\dagger\right) - \dot{U}U^\dagger U\rho U^\dagger - U\rho U^\dagger U\dot{U}^\dagger \\ &= \frac{\mathrm{d}}{\mathrm{d}t}\left(U\rho U^\dagger\right) - \left[\dot{U}U^\dagger, U\rho U^\dagger\right]. \end{aligned} \tag{A.4}$$

Here, we have used the fact that $\frac{\mathrm{d}}{\mathrm{d}t}\left(UU^\dagger\right) = \dot{U}U^\dagger + U\dot{U}^\dagger = 0$. By combining (A.2) and (A.4), we finally get

$$\frac{\mathrm{d}}{\mathrm{d}t}\left(U\rho U^\dagger\right) = -\frac{\mathrm{i}}{\hbar}\left[UHU^\dagger + \mathrm{i}\hbar\dot{U}U^\dagger, U\rho U^\dagger\right]. \tag{A.5}$$

Since the von Neumann equation should be valid for the transformed density operator $\rho' := U\rho U^\dagger$ and the transformed Hamiltonian H', we find

$$\frac{\mathrm{d}}{\mathrm{d}t}\left(\rho'\right) = -\frac{\mathrm{i}}{\hbar}\left[H', \rho'\right], \tag{A.6}$$

with $H' = UHU^\dagger + \mathrm{i}\hbar\dot{U}U^\dagger$. For a unitary operator of the form $U = \exp\left(\mathrm{i}Xt/\hbar\right)$, we can also write

$$H' = U\left(H - \mathrm{i}\hbar\partial_t\right)U^\dagger. \tag{A.7}$$

Appendix B

Driving qubits versus driving cavities

We begin with a unitary transformation of the Hamiltonian performed by applying the displacement operator

$$D(\mu_i) = \exp\left(\mu_i a_i^\dagger - \mu_i^* a_i\right), \tag{B.1}$$

where $\mu_i = \mu \exp(-\mathrm{i}\phi_i)$ with $\mu = \varepsilon_\mathrm{q}/g$. The effect is that the bosonic annihilation and creation operators are shifted by μ_i and μ_i^*, respectively:

$$D(\mu_i) a_i D^\dagger(\mu_i) = a_i - \mu_i, \tag{B.2a}$$
$$D(\mu_i) a_i^\dagger D^\dagger(\mu_i) = a_i^\dagger - \mu_i^*. \tag{B.2b}$$

This seems to be be a seemingly minor intervention, however, the effect on the full Hamiltonian given by Eq. (5.1) is much more extensive. On the one hand, the terms that pump the qubits are eliminated. On the other hand, new terms proportional to $a_i^\dagger$ and a_i and some negligible constant terms are generated. Since dissipation processes are part of the whole system, we also have to transform the cavity decay described by the Lindblad dissipator $\mathcal{D}[\sqrt{\kappa} a_i]\rho$. Its transformation reads

$$D(\mu_i)\mathcal{D}[\sqrt{\kappa} a_i]\rho D^\dagger(\mu_i) = \mathcal{D}[\sqrt{\kappa} a_i]\rho + \frac{\kappa}{2}\left[\mu_i a_i^\dagger - \mu_i^* a_i, \rho\right]. \tag{B.3}$$

The last term can be seen as a new contribution to the von Neumann part of the Lindblad master equation, which describes direct cavity pumping with the imaginary strength $\mathrm{i}\kappa\mu_i/2$. Considering this, the transformed full Hamiltonian can be divided into three parts that assume the form

$$H'_\mathrm{q} = \sum_i \Delta_\mathrm{qd} \sigma_i^\dagger \sigma_i, \tag{B.4}$$

$$H'_\mathrm{c} = \sum_i \Delta_\mathrm{cd} b_i^\dagger b_i - \sum_{i,j} J_{ij} b_i^\dagger b_j + \sum_i \left(\varepsilon_{\mathrm{c},i} b_i^\dagger + \varepsilon_{\mathrm{c},i}^* b_i\right), \tag{B.5}$$

$$H'_\mathrm{c,q} = \sum_i g\left(a_i^\dagger \sigma_i^- + a_i \sigma_i^+\right), \tag{B.6}$$

where we used $J_{ij} = J_{ji}$. The new non-constant term describes direct pumping of photons into the cavity with the complex strength

$$\varepsilon_{\mathrm{c},i} = \mu_i \left(\sum_j J_{ij} \mathrm{e}^{\mathrm{i}(\phi_i - \phi_j)} - \Delta_{\mathrm{cd}} + \mathrm{i}\frac{\kappa}{2} \right). \tag{B.7}$$

By a unitary transformation of the form $a_i \mapsto a_i \exp(\mathrm{i}\varphi)$, $\sigma_i \mapsto \sigma_i \exp(\mathrm{i}\varphi)$ one finds that the complex value λ gets a phase factor, i.e., $\lambda \mapsto \lambda \exp(-\mathrm{i}\varphi)$, which can be chosen such that the strength becomes real. This number is the strength of the drive which acts on the photons in the cavity.

As we can see, driving the qubits and driving the cavities are mathematically equivalent up to a constant factor in the strength of the respective drive. Finally, we have seen that the dynamics of Eq. (5.18) remains unchanged regardless of whether one drives the qubits or cavities.

Appendix C

Number of states of the excitation basis

When we work with systems with different numbers of cavities, we will have correspondingly different numbers of basis states for each excitation basis. A system of N cavities with one qubit each has

$$n_{\mathrm{q}}(N,m) = \frac{N!}{m! \cdot (N-m)!} \equiv \binom{N}{m} \tag{C.1}$$

qubit states with $m \leq N$ excitations. By summing up $n_{\mathrm{q}}(N,m)$ for all excitations m, one finds that the system consists of overall 2^N qubit states. Since photons are bosons, the total number of photon states is infinite. However, the number of photon states with m excitations (photons) is given by

$$n_{\mathrm{p}}(N,m) = \frac{1}{(N-1)!} \prod_{k=1}^{N-1} (m+k). \tag{C.2}$$

The excitation basis of the whole system with $m > 0$ excitations will have

$$\begin{aligned} n(N,m) &= \sum_{l=0}^{N} n_{\mathrm{q}}(N,l) n_{\mathrm{p}}(N,m-l) \\ &= \frac{1}{(N-1)!} \sum_{l=0}^{N} \binom{N}{l} \prod_{k=1}^{N-1} (m-l+k). \end{aligned} \tag{C.3}$$

basis states, i.e., product states of qubit and photon states. For $m = 0$, there is only one product state namely the ground state $|g\rangle^{\otimes N} \otimes |0\rangle^{\otimes N}$.

Table C.1 shows examples for different values of N and m. As we can see, the number of photon states with m excitations grows with the power of $N-1$. Therefore, the number of basis states with m excitations grows with the power of $N-1$ as well.

Table C.1: Number of basis states for a system with N cavities with m excitations.

m	$n_{\mathrm{q}}(1,m)$	$n_{\mathrm{p}}(1,m)$	$n(1,m)$	$n_{\mathrm{q}}(2,m)$	$n_{\mathrm{p}}(2,m)$	$n(2,m)$	$n_{\mathrm{q}}(3,m)$	$n_{\mathrm{p}}(3,m)$	$n(3,m)$
0	1	1	1	1	1	1	1	1	1
1	1	1	2	2	2	4	3	3	6
2	-	1	2	1	3	8	3	6	18
3	-	1	2	-	4	12	1	10	38
4	-	1	2	-	5	16	-	15	66
5	-	1	2	-	6	20	-	21	102
⋮	⋮	⋮	⋮	⋮	⋮	⋮	⋮	⋮	⋮
m	$\binom{1}{m}$	1	2	$\binom{2}{m}$	$m+1$	$4m$	$\binom{3}{m}$	$\frac{m^2+3m+2}{2}$	$4m^2+2$
⋮	⋮	⋮	⋮	⋮	⋮	⋮	⋮	⋮	⋮

Appendix D

Baker–Campbell–Hausdorff formula

The Baker–Campbell–Hausdorff formula (BCH formula) is the solution for Z to the equation

$$\mathrm{e}^{Z} = \mathrm{e}^{X}\mathrm{e}^{Y}, \tag{D.1}$$

where X and Y are linear operators. With e^{A} (or $\exp A$), we define the exponential map of a linear operator A by

$$\mathrm{e}^{A} := \sum_{k=0}^{\infty} \frac{1}{k!} A^{k}, \tag{D.2}$$

where $A^0 = I$ (the identity operator). In order to simplify the following equations, we introduce the two linear maps

$$\mathrm{Ad}_A\, X := AXA^{-1} \tag{D.3}$$

and

$$\mathrm{ad}_X\, Y := [X, Y], \tag{D.4}$$

where $[X, Y] := XY - YX$ defines the commutator of X and Y [108]. The definition of ad_X allows to write iterative commutators in a short way [109]:

$$(\mathrm{ad}_X)^m Y = \underbrace{[X, \ldots [X, [X}_{m \text{ times}}, Y]] \ldots], \tag{D.5}$$

with $(\mathrm{ad}_X)^0 Y = Y$. The BCH formula for $Z = \log(\mathrm{e}^{X}\mathrm{e}^{Y})$ can be expressed in the integral form

$$\log(\mathrm{e}^{X}\mathrm{e}^{Y}) = X + \int_0^1 g(\mathrm{e}^{\mathrm{ad}_X}\mathrm{e}^{t\,\mathrm{ad}_Y}) Y \mathrm{d}t, \tag{D.6}$$

where $g(z) = z \log z/(z-1)$ [108, 109]. From the series expansion of the logarithmic and the exponential function of Z we get the sum of iterated commutators of X and Y, which is given by

$$\log(\mathrm{e}^{X}\mathrm{e}^{Y}) = X + Y + \frac{1}{2}[X, Y] + \frac{1}{12}[X, [X, Y]] + \frac{1}{12}[Y, [Y, X]] + \ldots, \tag{D.7}$$

where "..." indicate higher order terms [110]. For proving the BCH formula, the following proposition is used [108, 109, 110]:

$$\mathrm{Ad}_{\mathrm{e}^X} = \mathrm{e}^{\mathrm{ad}_X}, \tag{D.8}$$

or written out explicitly

$$\begin{aligned} \mathrm{e}^X Y \mathrm{e}^{-X} &= \sum_{k=0}^{\infty} \frac{1}{k!} (\mathrm{ad}_X)^k Y \\ &= Y + [X,Y] + \frac{1}{2}[X,[X,Y]] + \dots \end{aligned} \tag{D.9}$$

This proposition can be proved as follows [110]: Let $f(t) = \mathrm{Ad}_{\mathrm{e}^{tX}}$ for $t \in \mathbb{R}$. Calculate its derivative:

$$\begin{aligned} f'(t)Y &= \frac{\mathrm{d}}{\mathrm{d}t} f(t) Y \\ &= \frac{\mathrm{d}}{\mathrm{d}t} \mathrm{e}^{tX} Y \mathrm{e}^{-tX} \\ &= X \mathrm{e}^{tX} Y \mathrm{e}^{-tX} - \mathrm{e}^{tX} Y \mathrm{e}^{-tX} X \\ &= X(\mathrm{Ad}_{\mathrm{e}^{tX}} Y) - (\mathrm{Ad}_{\mathrm{e}^{tX}} Y) X \\ &= \mathrm{ad}_X \, \mathrm{Ad}_{\mathrm{e}^{tX}} Y. \end{aligned}$$

Thus,

$$f'(t) = \mathrm{ad}_X \, f(t), \quad \text{and} \quad f(0) = 1.$$

The only solution of these equations is $f(t) = \exp(t \, \mathrm{ad}_X)$. Finally, $f(1)$ gives the desired result, q.e.d. Equation (D.9) is widely used in physics for unitary transformations of the form

$$A \mapsto \mathrm{e}^{\mathrm{i}X} A \mathrm{e}^{-\mathrm{i}X}. \tag{D.10}$$

That is why the explicit form in Eq. (D.9) of the above proposition is often erroneously called BCH formula.

Bibliography

[1] Johnny Moughames, Xavier Porte, Michael Thiel, Gwenn Ulliac, Laurent Larger, Maxime Jacquot, Muamer Kadic, and Daniel Brunner. Three-dimensional waveguide interconnects for scalable integration of photonic neural networks. Optica, 7(6):640, June 2020.

[2] Guy Van der Sande, Daniel Brunner, and Miguel C. Soriano. Advances in photonic reservoir computing. Nanophotonics, 6(3):561–576, May 2017.

[3] Tobias Heuser, Jan Grose, Steffen Holzinger, Maximilian M. Sommer, and Stephan Reitzenstein. Development of Highly Homogenous Quantum Dot Micropillar Arrays for Optical Reservoir Computing. IEEE Journal of Selected Topics in Quantum Electronics, 26(1):1–9, January 2020.

[4] A. Einstein, B. Podolsky, and N. Rosen. Can Quantum-Mechanical Description of Physical Reality Be Considered Complete? Physical Review, 47(10):777–780, May 1935.

[5] David P. DiVincenzo. The Physical Implementation of Quantum Computation. Fortschritte der Physik, 48(9-11):771–783, September 2000.

[6] Michael A. Nielsen and Isaac L. Chuang. Quantum computation and quantum information. Cambridge University Press, Cambridge ; New York, 2000.

[7] Charles H. Bennett, Gilles Brassard, Claude Crépeau, Richard Jozsa, Asher Peres, and William K. Wootters. Teleporting an unknown quantum state via dual classical and Einstein-Podolsky-Rosen channels. Physical Review Letters, 70(13):1895–1899, March 1993.

[8] Dik Bouwmeester, Jian-Wei Pan, Klaus Mattle, Manfred Eibl, Harald Weinfurter, and Anton Zeilinger. Experimental quantum teleportation. Nature, 390(6660):575–579, December 1997.

[9] John Preskill. Quantum computing and the entanglement frontier, 2012.

[10] Lov K. Grover. A fast quantum mechanical algorithm for database search. In Proceedings of the twenty-eighth annual ACM symposium on Theory of computing - STOC '96, pages 212–219, Philadelphia, Pennsylvania, United States, 1996. ACM Press.

[11] Peter W. Shor. Algorithms for quantum computation: discrete logarithms and factoring. In Proceedings 35th Annual Symposium on Foundations of ComputerScience, pages 124–134, Santa Fe, NM, USA, 1994. IEEE Comput. Soc. Press.

[12] Frank Arute, Kunal Arya, Ryan Babbush, Dave Bacon, Joseph C. Bardin, Rami Barends, Rupak Biswas, Sergio Boixo, Fernando G. S. L. Brandao, David A. Buell, Brian Burkett, Yu Chen, Zijun Chen, Ben Chiaro, Roberto Collins, William Courtney, Andrew Dunsworth, Edward Farhi, Brooks Foxen, Austin Fowler, Craig Gidney, Marissa Giustina, Rob Graff, Keith Guerin, Steve Habegger, Matthew P. Harrigan, Michael J. Hartmann, Alan Ho, Markus Hoffmann, Trent Huang, Travis S. Humble, Sergei V. Isakov, Evan Jeffrey, Zhang Jiang, Dvir Kafri, Kostyantyn Kechedzhi, Julian Kelly, Paul V. Klimov, Sergey Knysh, Alexander Korotkov, Fedor Kostritsa, David Landhuis, Mike Lindmark, Erik Lucero, Dmitry Lyakh, Salvatore Mandrà, Jarrod R. McClean, Matthew McEwen, Anthony Megrant, Xiao Mi, Kristel Michielsen, Masoud Mohseni, Josh Mutus, Ofer Naaman, Matthew Neeley, Charles Neill, Murphy Yuezhen Niu, Eric Ostby, Andre Petukhov, John C. Platt, Chris Quintana, Eleanor G. Rieffel, Pedram Roushan, Nicholas C. Rubin, Daniel Sank, Kevin J. Satzinger, Vadim Smelyanskiy, Kevin J. Sung, Matthew D. Trevithick, Amit Vainsencher, Benjamin Villalonga, Theodore White, Z. Jamie Yao, Ping Yeh, Adam Zalcman, Hartmut Neven, and John M. Martinis. Quantum supremacy using a programmable superconducting processor. Nature, 574(7779):505–510, October 2019.

[13] Han-Sen Zhong, Hui Wang, Yu-Hao Deng, Ming-Cheng Chen, Li-Chao Peng, Yi-Han Luo, Jian Qin, Dian Wu, Xing Ding, Yi Hu, Peng Hu, Xiao-Yan Yang, Wei-Jun Zhang, Hao Li, Yuxuan Li, Xiao Jiang, Lin Gan, Guangwen Yang, Lixing You, Zhen Wang, Li Li, Nai-Le Liu, Chao-Yang Lu, and Jian-Wei Pan. Quantum computational advantage using photons. Science, 370(6523):1460–1463, December 2020.

[14] Han-Sen Zhong, Yu-Hao Deng, Jian Qin, Hui Wang, Ming-Cheng Chen, Li-Chao Peng, Yi-Han Luo, Dian Wu, Si-Qiu Gong, Hao Su, Yi Hu, Peng Hu, Xiao-Yan Yang, Wei-Jun Zhang, Hao Li, Yuxuan Li, Xiao Jiang, Lin Gan, Guangwen Yang, Lixing You, Zhen Wang, Li Li, Nai-Le Liu, Jelmer J. Renema, Chao-Yang Lu, and Jian-Wei Pan. Phase-Programmable Gaussian Boson Sampling Using Stimulated Squeezed Light. Physical Review Letters, 127(18):180502, October 2021.

[15] Yulin Wu, Wan-Su Bao, Sirui Cao, Fusheng Chen, Ming-Cheng Chen, Xiawei Chen, Tung-Hsun Chung, Hui Deng, Yajie Du, Daojin Fan, Ming Gong, Cheng Guo, Chu Guo, Shaojun Guo, Lianchen Han, Linyin Hong, He-Liang Huang, Yong-Heng Huo, Liping Li, Na Li, Shaowei Li, Yuan Li, Futian Liang, Chun Lin, Jin Lin, Haoran Qian, Dan Qiao, Hao Rong, Hong Su, Lihua Sun, Liangyuan Wang, Shiyu Wang, Dachao Wu, Yu Xu, Kai Yan, Weifeng Yang, Yang Yang, Yangsen Ye, Jianghan Yin, Chong Ying, Jiale Yu, Chen Zha, Cha Zhang, Haibin Zhang, Kaili Zhang, Yiming Zhang, Han Zhao, Youwei Zhao, Liang Zhou, Qingling Zhu, Chao-Yang Lu, Cheng-Zhi Peng, Xiaobo Zhu, and Jian-Wei Pan. Strong Quantum Computational Advantage Using a Superconducting Quantum Processor. Physical Review Letters, 127(18), October 2021.

[16] Qingling Zhu, Sirui Cao, Fusheng Chen, Ming-Cheng Chen, Xiawei Chen, Tung-Hsun Chung, Hui Deng, Yajie Du, Daojin Fan, Ming Gong, Cheng Guo, Chu Guo, Shaojun Guo, Lianchen Han, Linyin Hong, He-Liang Huang, Yong-

Heng Huo, Liping Li, Na Li, Shaowei Li, Yuan Li, Futian Liang, Chun Lin, Jin Lin, Haoran Qian, Dan Qiao, Hao Rong, Hong Su, Lihua Sun, Liangyuan Wang, Shiyu Wang, Dachao Wu, Yulin Wu, Yu Xu, Kai Yan, Weifeng Yang, Yang Yang, Yangsen Ye, Jianghan Yin, Chong Ying, Jiale Yu, Chen Zha, Cha Zhang, Haibin Zhang, Kaili Zhang, Yiming Zhang, Han Zhao, Youwei Zhao, Liang Zhou, Chao-Yang Lu, Cheng-Zhi Peng, Xiaobo Zhu, and Jian-Wei Pan. Quantum computational advantage via 60-qubit 24-cycle random circuit sampling. Science Bulletin, 67(3):240–245, February 2022.

[17] Lars S. Madsen, Fabian Laudenbach, Mohsen Falamarzi. Askarani, Fabien Rortais, Trevor Vincent, Jacob F. F. Bulmer, Filippo M. Miatto, Leonhard Neuhaus, Lukas G. Helt, Matthew J. Collins, Adriana E. Lita, Thomas Gerrits, Sae Woo Nam, Varun D. Vaidya, Matteo Menotti, Ish Dhand, Zachary Vernon, Nicolás Quesada, and Jonathan Lavoie. Quantum computational advantage with a programmable photonic processor. Nature, 606(7912):75–81, June 2022.

[18] John Preskill. Quantum Computing in the NISQ era and beyond. Quantum, 2:79, August 2018.

[19] Sonia Buckley, Kelley Rivoire, and Jelena Vučković. Engineered quantum dot single-photon sources. Reports on Progress in Physics, 75(12):126503, December 2012.

[20] Barbara Goss Levi. Two-ion logic gates open the way to further advances in quantum computing. Physics Today, 56(5):17–19, May 2003.

[21] J. J. García-Ripoll, P. Zoller, and J. I. Cirac. Speed Optimized Two-Qubit Gates with Laser Coherent Control Techniques for Ion Trap Quantum Computing. Physical Review Letters, 91(15), October 2003.

[22] V. M. Schäfer, C. J. Ballance, K. Thirumalai, L. J. Stephenson, T. G. Ballance, A. M. Steane, and D. M. Lucas. Fast quantum logic gates with trapped-ion qubits. Nature, 555(7694):75–78, March 2018.

[23] John Clarke and Frank K. Wilhelm. Superconducting quantum bits. Nature, 453(7198):1031–1042, June 2008.

[24] L. DiCarlo, J. M. Chow, J. M. Gambetta, Lev S. Bishop, B. R. Johnson, D. I. Schuster, J. Majer, A. Blais, L. Frunzio, S. M. Girvin, and R. J. Schoelkopf. Demonstration of two-qubit algorithms with a superconducting quantum processor. Nature, 460(7252):240–244, July 2009.

[25] Morten Kjaergaard, Mollie E. Schwartz, Jochen Braumüller, Philip Krantz, Joel I.-Jan Wang, Simon Gustavsson, and William D. Oliver. Superconducting Qubits: Current State of Play. arXiv:1905.13641 [cond-mat, physics:physics, physics:quant-ph], July 2019. arXiv: 1905.13641.

[26] Y.-Y. Huang, Y.-K. Wu, F. Wang, P.-Y. Hou, W.-B. Wang, W.-G. Zhang, W.-Q. Lian, Y.-Q. Liu, H.-Y. Wang, H.-Y. Zhang, L. He, X.-Y. Chang, Y. Xu, and L.-M. Duan. Experimental Realization of Robust Geometric Quantum Gates with Solid-State Spins. Physical Review Letters, 122(1), January 2019.

[27] Daniel Loss and David P. DiVincenzo. Quantum computation with quantum dots. Physical Review A, 57(1):120–126, January 1998.

[28] Herbert Walther, Benjamin T H Varcoe, Berthold-Georg Englert, and Thomas Becker. Cavity quantum electrodynamics. Reports on Progress in Physics, 69(5):1325–1382, May 2006.

[29] E. T. Jaynes and F. W. Cummings. Comparison of quantum and semiclassical radiation theories with application to the beam maser. Proceedings of the IEEE, 51(1):89–109, 1963.

[30] Camille Aron, Manas Kulkarni, and Hakan E. Türeci. Steady-state entanglement of spatially separated qubits via quantum bath engineering. Physical Review A, 90(6), December 2014.

[31] M. E. Kimchi-Schwartz, L. Martin, E. Flurin, C. Aron, M. Kulkarni, H. E. Tureci, and I. Siddiqi. Stabilizing Entanglement via Symmetry-Selective Bath Engineering in Superconducting Qubits. Physical Review Letters, 116(24):240503, June 2016.

[32] C. Sánchez Muñoz, E. del Valle, A. González Tudela, K. Müller, S. Lichtmannecker, M. Kaniber, C. Tejedor, J. J. Finley, and F. P. Laussy. Emitters of N-photon bundles. Nature Photonics, 8(7):550–555, July 2014.

[33] Marc Bostelmann, Steffen Wilksen, Frederik Lohof, and Christopher Gies. Multipartite-entanglement generation in coupled microcavity arrays. Physical Review A, 107(3):032417, March 2023.

[34] Artur K. Ekert. Quantum cryptography based on Bell's theorem. Physical Review Letters, 67(6):661–663, August 1991.

[35] H.-J. Briegel, W. Dür, J. I. Cirac, and P. Zoller. Quantum Repeaters: The Role of Imperfect Local Operations in Quantum Communication. Physical Review Letters, 81(26):5932–5935, December 1998.

[36] R. L. Rivest, A. Shamir, and L. Adleman. A method for obtaining digital signatures and public-key cryptosystems. Communications of the ACM, 21(2):120–126, February 1978.

[37] Hans J. Briegel and Robert Raussendorf. Persistent Entanglement in Arrays of Interacting Particles. Physical Review Letters, 86(5):910–913, January 2001.

[38] Hui Deng, Gian Luca Lippi, Jesper Mørk, Jan Wiersig, and Stephan Reitzenstein. Physics and Applications of High-β Micro- and Nanolasers. Advanced Optical Materials, 9(19):2100415, October 2021.

[39] Pascale Senellart, Glenn Solomon, and Andrew White. High-performance semiconductor quantum-dot single-photon sources. Nature Nanotechnology, 12(11):1026–1039, November 2017.

[40] Tomoyuki Yoshie, Lingling Tang, and Shu-Yu Su. Correction: Yoshie, T. *et al.* Optical Microcavity: Sensing down to Single Molecules and Atoms. *Sensors* 2011, *11*, 1972-1991. Sensors, 11(6):6493–6493, June 2011.

[41] T. Heuser, M. Pflüger, I. Fischer, J. A. Lott, D. Brunner, and S. Reitzenstein. Developing a photonic hardware platform for brain-inspired computing based on 5×5 VCSEL arrays. Journal of Physics: Photonics, 2(4):044002, October 2020.

[42] Lewis Reeves, Yue Wang, and Thomas F. Krauss. 2D Material Microcavity Light Emitters: To Lase or Not to Lase? Advanced Optical Materials, 6(19):1800272, October 2018.

[43] Bruno Romeira and Andrea Fiore. Purcell Effect in the Stimulated and Spontaneous Emission Rates of Nanoscale Semiconductor Lasers. IEEE Journal of Quantum Electronics, 54(2):1–12, April 2018.

[44] A. K. Nowak, S. L. Portalupi, V. Giesz, O. Gazzano, C. Dal Savio, P.-F. Braun, K. Karrai, C. Arnold, L. Lanco, I. Sagnes, A. Lemaître, and P. Senellart. Deterministic and electrically tunable bright single-photon source. Nature Communications, 5(1):3240, May 2014.

[45] Magdalena Moczała-Dusanowska, Łukasz Dusanowski, Stefan Gerhardt, Yu Ming He, Marcus Reindl, Armando Rastelli, Rinaldo Trotta, Niels Gregersen, Sven Höfling, and Christian Schneider. Strain-Tunable Single-Photon Source Based on a Quantum Dot–Micropillar system. ACS Photonics, 6(8):2025–2031, August 2019.

[46] Marco Schmidt, Martin V. Helversen, Sarah Fischbach, Arsenty Kaganskiy, Ronny Schmidt, Andrei Schliwa, Tobias Heindel, Sven Rodt, and Stephan Reitzenstein. Deterministically fabricated spectrally-tunable quantum dot based single-photon source. Optical Materials Express, 10(1):76, January 2020.

[47] Y. L. Delley, M. Kroner, S. Faelt, W. Wegscheider, and A. İmamoğlu. Deterministic entanglement between a propagating photon and a singlet-triplet qubit in an optically active quantum dot molecule. Physical Review B, 96(24), December 2017.

[48] T. Grujic, S. R. Clark, D. Jaksch, and D. G. Angelakis. Non-equilibrium many-body effects in driven nonlinear resonator arrays. New Journal of Physics, 14(10):103025, October 2012.

[49] Michael J. Hartmann and Martin B. Plenio. Strong Photon Nonlinearities and Photonic Mott Insulators. Physical Review Letters, 99(10):103601, September 2007.

[50] Michael J. Hartmann, Fernando G. S. L. Brandão, and Martin B. Plenio. Quantum many-body phenomena in coupled cavity arrays. Laser & Photonics Reviews, 2(6):527–556, December 2008.

[51] Daniel Brunner and Ingo Fischer. Reconfigurable semiconductor laser networks based on diffractive coupling. Optics Letters, 40(16):3854, August 2015.

[52] J. Ruiz-Rivas, E. del Valle, C. Gies, P. Gartner, and M. J. Hartmann. Spontaneous collective coherence in driven dissipative cavity arrays. Physical Review A, 90(3), September 2014.

[53] Eduardo Mascarenhas, Dario Gerace, Hugo Flayac, Marcelo F. Santos, Alexia Auffèves, and Vincenzo Savona. Laser from a many-body correlated medium. Physical Review B, 93(20):205148, May 2016.

[54] Li-hui Sun, Sujuan Wei, Wenju Gu, and Gao-xiang Li. Generation of six-mode cluster states in a coupled cavity array. Journal of the Optical Society of America B, 33(9):1865, September 2016.

[55] Keisuke Fujii and Kohei Nakajima. Harnessing Disordered-Ensemble Quantum Dynamics for Machine Learning. Physical Review Applied, 8(2), August 2017.

[56] Sven M. Hein, Camille Aron, and Hakan E. Türeci. Purification and switching protocols for dissipatively stabilized entangled qubit states. Physical Review A, 93(6):062331, June 2016.

[57] Camille Aron, Manas Kulkarni, and Hakan E. Türeci. Photon-Mediated Interactions: A Scalable Tool to Create and Sustain Entangled States of N Atoms. Physical Review X, 6(1):011032, March 2016.

[58] Bruno Bellomo, Rosario Lo Franco, and Giuseppe Compagno. n identical particles and one particle to entangle them all. Physical Review A, 96(2):022319, August 2017.

[59] Hayata Yamasaki, Alexander Pirker, Mio Murao, Wolfgang Dür, and Barbara Kraus. Multipartite entanglement outperforming bipartite entanglement under limited quantum system sizes. Physical Review A, 98(5):052313, November 2018.

[60] Manfred Eibl, Nikolai Kiesel, Mohamed Bourennane, Christian Kurtsiefer, and Harald Weinfurter. Experimental Realization of a Three-Qubit Entangled W State. Physical Review Letters, 92(7):077901, February 2004.

[61] Ming Gong, Ming-Cheng Chen, Yarui Zheng, Shiyu Wang, Chen Zha, Hui Deng, Zhiguang Yan, Hao Rong, Yulin Wu, Shaowei Li, Fusheng Chen, Youwei Zhao, Futian Liang, Jin Lin, Yu Xu, Cheng Guo, Lihua Sun, Anthony D. Castellano, Haohua Wang, Chengzhi Peng, Chao-Yang Lu, Xiaobo Zhu, and Jian-Wei Pan. Genuine 12-Qubit Entanglement on a Superconducting Quantum Processor. Physical Review Letters, 122(11):110501, March 2019.

[62] H. Häffner, W. Hänsel, C. F. Roos, J. Benhelm, D. Chek-al kar, M. Chwalla, T. Körber, U. D. Rapol, M. Riebe, P. O. Schmidt, C. Becher, O. Gühne, W. Dür, and R. Blatt. Scalable multiparticle entanglement of trapped ions. Nature, 438(7068):643–646, December 2005.

[63] Dagmar Bruß, Nilanjana Datta, Artur Ekert, Leong Chuan Kwek, and Chiara Macchiavello. Multipartite entanglement in quantum spin chains. Physical Review A, 72(1):014301, July 2005.

[64] Dong Wang, You-Di Hu, Zhe-Qiang Wang, and Liu Ye. Efficient and faithful remote preparation of arbitrary three- and four-particle w-class entangled states. Quantum Information Processing, 14(6):2135–2151, June 2015.

[65] Na-Na Wu and Min Jiang. A highly efficient scheme for joint remote preparation of multi-qubit W state with minimum quantum resource. Quantum Information Processing, 17(12):340, December 2018.

[66] Yong-Su Kim, Young-Wook Cho, Hyang-Tag Lim, and Sang-Wook Han. Efficient linear optical generation of a multipartite W state via a quantum eraser. Physical Review A, 101(2):022337, February 2020.

[67] Guo-Zhu Song, Ming-Jie Tao, Jing Qiu, and Hai-Rui Wei. Quantum entanglement creation based on quantum scattering in one-dimensional waveguides. Physical Review A, 106(3):032416, September 2022.

[68] Stephan Ritter, Christian Nölleke, Carolin Hahn, Andreas Reiserer, Andreas Neuzner, Manuel Uphoff, Martin Mücke, Eden Figueroa, Joerg Bochmann, and Gerhard Rempe. An elementary quantum network of single atoms in optical cavities. Nature, 484(7393):195–200, April 2012.

[69] D. Hucul, I. V. Inlek, G. Vittorini, C. Crocker, S. Debnath, S. M. Clark, and C. Monroe. Modular entanglement of atomic qubits using photons and phonons. Nature Physics, 11(1):37–42, January 2015.

[70] Severin Daiss, Stefan Langenfeld, Stephan Welte, Emanuele Distante, Philip Thomas, Lukas Hartung, Olivier Morin, and Gerhard Rempe. A quantum-logic gate between distant quantum-network modules. Science, 371(6529):614–617, February 2021.

[71] Peter C. Humphreys, Norbert Kalb, Jaco P. J. Morits, Raymond N. Schouten, Raymond F. L. Vermeulen, Daniel J. Twitchen, Matthew Markham, and Ronald Hanson. Deterministic delivery of remote entanglement on a quantum network. Nature, 558(7709):268–273, June 2018.

[72] R. Stockill, M. J. Stanley, L. Huthmacher, E. Clarke, M. Hugues, A. J. Miller, C. Matthiesen, C. Le Gall, and M. Atatüre. Phase-Tuned Entangled State Generation between Distant Spin Qubits. Physical Review Letters, 119(1):010503, July 2017.

[73] L. J. Stephenson, D. P. Nadlinger, B. C. Nichol, S. An, P. Drmota, T. G. Ballance, K. Thirumalai, J. F. Goodwin, D. M. Lucas, and C. J. Ballance. High-Rate, High-Fidelity Entanglement of Qubits Across an Elementary Quantum Network. Physical Review Letters, 124(11), March 2020.

[74] Ryszard Horodecki, Paweł Horodecki, Michał Horodecki, and Karol Horodecki. Quantum entanglement. Reviews of Modern Physics, 81(2):865–942, June 2009.

[75] Otfried Gühne and Géza Tóth. Entanglement detection. Physics Reports, 474(1-6):1–75, April 2009.

[76] Daniel M. Greenberger, Michael A. Horne, Abner Shimony, and Anton Zeilinger. Bell's theorem without inequalities. American Journal of Physics, 58(12):1131–1143, December 1990.

[77] Mark Hillery, Vladimír Bužek, and André Berthiaume. Quantum secret sharing. Physical Review A, 59(3):1829–1834, March 1999.

[78] Shamminuj Aktar, Andreas Bartschi, Abdel-Hameed A. Badawy, and Stephan Eidenbenz. A Divide-and-Conquer Approach to Dicke State Preparation. IEEE Transactions on Quantum Engineering, 3:1–16, 2022.

[79] W. Dür, G. Vidal, and J. I. Cirac. Three qubits can be entangled in two inequivalent ways. Physical Review A, 62(6), November 2000.

[80] Brian C. Hall. Quantum theory for mathematicians. Number 267 in Graduate texts in mathematics. Springer, New York, 2013. OCLC: ocn828487961.

[81] Reinhard F. Werner. Quantum states with Einstein-Podolsky-Rosen correlations admitting a hidden-variable model. Physical Review A, 40(8):4277–4281, October 1989.

[82] Asher Peres. Separability Criterion for Density Matrices. Physical Review Letters, 77(8):1413–1415, August 1996.

[83] Michał Horodecki, Paweł Horodecki, and Ryszard Horodecki. Separability of mixed states: necessary and sufficient conditions. Physics Letters A, 223(1-2):1–8, November 1996.

[84] V. Vedral, M. B. Plenio, M. A. Rippin, and P. L. Knight. Quantifying Entanglement. Physical Review Letters, 78(12):2275–2279, March 1997.

[85] Charles H. Bennett, David P. DiVincenzo, John A. Smolin, and William K. Wootters. Mixed-state entanglement and quantum error correction. Physical Review A, 54(5):3824–3851, November 1996.

[86] G. Vidal and R. F. Werner. Computable measure of entanglement. Physical Review A, 65(3):032314, February 2002.

[87] M. Barbieri, F. De Martini, G. Di Nepi, P. Mataloni, G. M. D'Ariano, and C. Macchiavello. Detection of Entanglement with Polarized Photons: Experimental Realization of an Entanglement Witness. Physical Review Letters, 91(22):227901, November 2003.

[88] Mohamed Bourennane, Manfred Eibl, Christian Kurtsiefer, Sascha Gaertner, Harald Weinfurter, Otfried Gühne, Philipp Hyllus, Dagmar Bruß, Maciej Lewenstein, and Anna Sanpera. Experimental Detection of Multipartite Entanglement using Witness Operators. Physical Review Letters, 92(8):087902, February 2004.

[89] Thomas Guff, Nicolas Boulle, and Igor Pikovski. Optimal fidelity witnesses for gravitational entanglement. Physical Review A, 105(2):022444, February 2022.

[90] Richard Jozsa. Fidelity for Mixed Quantum States. Journal of Modern Optics, 41(12):2315–2323, December 1994.

[91] Marlan O. Scully and M. Suhail Zubairy. Quantum Optics. Cambridge University Press, 1 edition, September 1997.

[92] Rodney Loudon. The quantum theory of light. Oxford science publications. Oxford University Press, Oxford ; New York, 3rd ed edition, 2000.

[93] D. F. Walls and G. J. Milburn. Quantum optics. Springer, Berlin, 2nd ed edition, 2008.

[94] Mark Fox. Quantum optics: an introduction. Number 15 in Oxford master series in physics. Oxford University Press, Oxford ; New York, 2006.

[95] C. W. Gardiner and P. Zoller. The quantum world of ultra-cold atoms and light. Number volume 2 in Cold atoms. Imperial College Press, London, 2014. OCLC: ocn877368191.

[96] A V Dodonov. Errors in zero-excitation state preparation due to anti-rotating terms in two-atom Markovian cavity QED. Physica Scripta, 82(5):055401, November 2010.

[97] Stephen M. Barnett and Paul M. Radmore. Methods in Theoretical Quantum Optics. Oxford University PressOxford, 1 edition, November 2002.

[98] Antonio de Freitas, L. Sanz, and José M. Villas-Bôas. Coherent control of the dynamics of a single quantum-dot exciton qubit in a cavity. Physical Review B, 95(11):115110, March 2017.

[99] Howard Carmichael. An Open Systems Approach to Quantum Optics: Lectures Presented at the Université Libre de Bruxelles, October 28 to November 4, 1991. Springer Berlin Heidelberg, Berlin, Heidelberg, 1993. OCLC: 851754522.

[100] Heinz-Peter Breuer and F. Petruccione. The theory of open quantum systems. Oxford University Press, Oxford ; New York, 2002. OCLC: ocm49872077.

[101] Maximilian A. Schlosshauer. Decoherence and the quantum-to-classical transition. The frontiers collection. Springer, Berlin ; London, 2007. OCLC: ocn124026662.

[102] Alberto Mercurio, Shilan Abo, Fabio Mauceri, Enrico Russo, Vincenzo Macrì, Adam Miranowicz, Salvatore Savasta, and Omar Di Stefano. Pure Dephasing of Light-Matter Systems in the Ultrastrong and Deep-Strong Coupling Regimes. Physical Review Letters, 130(12):123601, March 2023.

[103] Adria Grabulosa, Johnny Moughames, Xavier Porte, Muamer Kadic, and Daniel Brunner. Additive 3D photonic integration that is CMOS compatible, 2023.

[104] Tobias Heuser, Jan Große, Arsenty Kaganskiy, Daniel Brunner, and Stephan Reitzenstein. Fabrication of dense diameter-tuned quantum dot micropillar arrays for applications in photonic information processing. APL Photonics, 3(11):116103, November 2018.

[105] R. H. Dicke. Coherence in Spontaneous Radiation Processes. Physical Review, 93(1):99–110, January 1954.

[106] Pierre Meystre and Murray Sargent. Elements of quantum optics: with 218 problems. Springer, Berlin, 3. ed edition, 1999. OCLC: 845092173.

[107] E Brion, L H Pedersen, and K Mølmer. Adiabatic elimination in a lambda system. Journal of Physics A: Mathematical and Theoretical, 40(5):1033–1043, February 2007.

[108] Brian C. Hall. Lie groups, Lie algebras, and representations: an elementary introduction. Number 222 in Graduate texts in mathematics. Springer, Cham ; New York, second edition edition, 2015. OCLC: ocn910324548.

[109] Willard Miller. Symmetry groups and their applications. Number v. 50 in Pure and applied mathematics; a series of monographs and textbooks. Academic Press, New York, 1972.

[110] Wulf Rossmann. Lie groups: an introduction through linear groups. Number 5 in Oxford graduate texts in mathematics. Oxford University Press, Oxford ; New York, 2002.

List of Publications

1. *Multipartite-entanglement generation in coupled microcavity arrays*, M. Bostelmann, S. Wilksen, F. Lohof, and C. Gies, Phys. Rev. A **107**, 032417, (2023).

University of Bremen
Institute for Theoretical Physics
Faculty 01
Physics / Electrical Engineering
Otto-Hahn-Allee 1
28359 Bremen, Germany

Phone +49 421 218-62035
bostelmann@uni-bremen.de
www.itp.uni-bremen.de/ag-gies

October 12, 2023